A study of hybrid ventilation in an institutional building: Modeling and predictive control

Charalampos Vallianos

A Thesis in the Department of
Building, Civil and Environmental Engineering

Presented in the Partial Fulfillment of the Requirements
for the Degree of Master of Applied Science (Building Engineering) at
Concordia University
Montréal, Québec, Canada

November 13, 2017

CONCORDIA UNIVERSITY

CONCORDIA UNIVERSITY
School of Graduate Studies

This is to certify that the thesis prepared

By: Charalampos Vallianos

Entitled: A study of hybrid ventilation in an institutional building: Modeling and predictive control

and submitted in partial fulfillment of the requirements for the degree of

Master of Applied Science (Building Engineering)

complies with the regulations of the University and meets the accepted standards with respect to originality and quality.

Signed by the final examining committee:

Dr. L. Wang Chair

Dr. G. Vatistas Examiner

Dr. F. Nasiri Examiner

Dr. A. Athienitis Supervisor

Approved by _____
Chair of Department or Graduate Program Director

_____
Dean of Faculty

Date _____

ABSTRACT

A study of hybrid ventilation in an institutional building: Modeling and predictive control

Charalampos Vallianos

This thesis presents a numerical and experimental study of a hybrid ventilation system of an institutional building with emphasis on thermal comfort. Hybrid ventilation can improve thermal comfort and at the same time reduce energy consumption and peak power demand. By precooling the thermal mass of the building the energy consumption of the following day can also be reduced. A 17–story high institutional building is used as a case study to test different control strategies and to define the temperature low limit for admitting exterior air into the building through a transition space (a corridor), in order to ensure thermal comfort. A developed model, calibrated from full–scale tests, estimates the heat removed from the concrete and the impact on thermal comfort. It is used to test and compare the existing control strategy to different ones of both reactive and predictive nature. 12 typical days are used to compare different control strategies. The system is currently operating based on heuristic control, with an exterior air temperature setpoint above which the air is allowed into the corridors. A control strategy based on data of the previous hour (reactive) is expected to triple the energy savings potential, but not guarantee satisfactory thermal comfort. A predictive control strategy provides thermal comfort, but also energy savings potential of the same magnitude as the reactive. Energy savings potential is increased even more if it is

weighted more against discomfort when the building is unoccupied. In general the predictive control strategy opens the motorized dampers as much as possible during the cold days – without compromising thermal comfort – to precool the concrete floor so that it can reduce the cooling load of the next day.

ACKNOWLEDGEMENTS

I would like to thank my supervisor, Professor Andreas Athienitis for his support and guidance. You gave me the opportunity to work on a case study and study the implementation of control strategy on a real building. You always helped me look at the bigger picture and because of you I participated in a lot of meetings and projects that broadened my engineering horizons.

This work is part of a broader ongoing research project under the Centre for net-Zeros Energy Buildings. I would like to thank Professor Wang and his students, Dahai Qi, Ali Katal and Jun Cheng for our collaboration during these years. All these data measurements and control strategies would have never been implemented without the support of Concordia Facilities management, and specifically of Daniel Gauthier. Thank you, Daniel, for teaching us so much and giving us a small share of your vast knowledge and experience.

From the administrative team I would like to thank Gerald Parnis, Jacques Payer, Lyne Dee, Jenny Drapeau and Olga Soares. I would like to thank Jiwu Rao for all his help and support on anything related to sensors and experimental procedures.

I would like to acknowledge the financial support through the Concordia Graduate Scholarship in Natural Sciences and Engineering Research and the financial support from Professor Athienitis. This work is part of the "living labs" project, which aims to supply the existing building with a minimum amount of sensors and maximize their energy efficiency and thermal comfort without interrupting their operation. Parts of the work are funded by a Hydro Quebec Industrial Research Chair, which benefits from a partnership of Hydro–Quebec, Reg-

ulvar and Natural Resources Canada CanmetEnergy. I would like to thank Ahmed Daoud and Jocelyn Milette from Hydro–Quebec, Jose Candanedo from NRC CanmetEnergy and Gabrielle Mainville from Regulvar.

Working at the office taught me a lot and helped me progress as student, as a professional and as a scientist. This, of course, would not have been possible without my colleagues within the Centre for Net-Zero Energy Buildings. Whether it was during a meeting, at a conference or at a pub drinking beer and having a burger, our conversations were always instructive and helpful. More specifically, thank you, Sophie Yuan; you were working on this project when I started my degree and you taught me a lot during the experiments. Thank you for sharing your experiences with me. Thank you, Costa Kapsis, for helping me integrate smoothly into the team and Canada in general. Thank you, Vasken Dermardiros, for everything. From simple things, like proof–reading some of my articles, to working with me on all those little projects, to sharing my passion for artificial intelligence and machine learning, and always doing so in such a pleasant and funny manner. Thank you Sam Yip, Tassos Papachristou, Camille John, Jennifer Date, Zissis Ioannidis, Olesia Kruglov, David Sun, Shahriar Hossain, Katherine D'Avignon, Bruno Marcotte, Ali Saberi, Edvinas Bigaila, Statos Rounis, Remi Dumoulin, Sormin Sultana, Mathieu Le Cam and Nunzio Cotrufo.

Last but not least I would like to thank all the people who were there for me during those two years, both those in Canada and my friends and family who still live in Greece. I would like to thank my girlfriend Tatianna for her patience and her support when it was most needed. I would like to thank my parents, Antonis and Eleni, and my sister Calliope, because to them I owe a large portion of the person I am today.

TABLE OF CONTENTS

LIST OF FIGURES

LIST OF TABLES

CHAPTER 1

INTRODUCTION

This first chapter explains the motivation behind this thesis, explains what the final objective is and presents a short outline of the next chapters.

1.1 Motivation

In Canada, the total energy use for space cooling of the commercial and industrial sector has increased by 25.9 % from 1990 to 2014 [2]. Quebec's climate makes cooling from natural and hybrid ventilation systems an ideal solution, because of the high diurnal temperature differences [3].

In most cases of institutional buildings, the cooling loads are high because of a high window–to–wall ratio and internal heat gains due to occupants and plug loads. As a result the buildings needs cooling during a large portion of the shoulder seasons. It is not uncommon to cool the core of the building because of the internal gains, and at the same time heat the perimeter of the building because of the low weather temperature and low glass insulation.

Using natural or hybrid ventilation instead of mechanical can decrease the growth of energy consumption for space cooling, especially if buildings are designed with the coupling of a natural or hybrid ventilation system with the appropriate amount of thermal mass. Using night ventilation the buildings will be able to take advantage of high diurnal temperature differences, precool the building during the night and prepare it for the high cooling loads of

the following day.

An important aspect of the control of natural or hybrid ventilation systems is determining the weather conditions to allow the exterior air into the space, so that the thermal comfort of the occupants is not compromised. During night cooling institutional buildings are unoccupied and therefore the energy savings potential can be weighted more, reducing the low air inlet temperature limit without fear of creating a thermally uncomfortable environment.

1.2 Background

A representative building using a hybrid ventilation system is one of Concordia University buildings, the EV building. It is a typical high-rise institutional office building, located in downtown Montreal. It consists of five three–story high atria. A seventeenth floor serves as the mechanical room. Each floor has two motorized, insulated inlet dampers, on the southeast and northwest façade of the building. A schematic of the air flow is shown in Figure 1.1. The exterior air enters the building through these dampers and then flows along the corridor on each floor, cooling the building, until it reaches the atrium. The atria are interconnected with motorized grilles, allowing the air to pass through. The atria function as a solar chimney, driving the air through the whole building and exhausting it from the roof. When the stack effect is not strong enough the pressure difference can be enhanced by variable speed fans, installed on the roof in 2015, where the outlet of the air is.

The building benefits from a significant buoyancy effect due to its height, fan assistance when necessary and motorized inlet dampers that can be modulated individually. It is equipped with 40-centimeter thick exposed concrete floor, which can reduce the indoor temperature fluctuations by retaining heat during the day when cooling loads are highest, and cooling down at night through hybrid ventilation when outdoor temperatures are at its lowest.

There are various studies conducted on this system, both during the design and the operation stage. The studies during the design stage ensured that the building would be ready to incorporate the different technologies associated with such a complex system as well as to control all the different components through the Building Automation System.

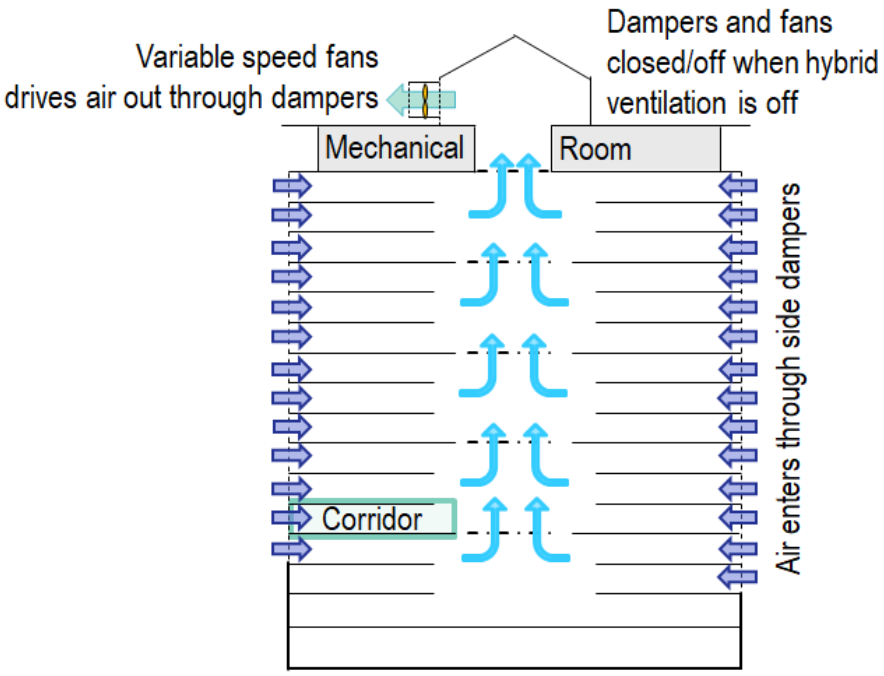

Figure 1.1: Schematic of air flow through Concordia EV building due to hybrid ventilation. Courtesy of Sophie Yuan

On the other hand, the building is constantly being monitored and studies use these measurements and explore ways to enhance the cooling potential of the fans, without compromising thermal comfort.

1.3 Objectives

The objective of this study is to model the corridors right after the inlet of the exterior air to the buildings, because this is where thermal comfort will be most easily compromised. Based on this model different control strategies will be evaluated. Eventually the most promising strategies will be implemented for the hybrid ventilation case of the EV building at Concordia university, which serves as the case study.

This work is part of a broader on–going research project under the Centre for net-Zero Energy Building Studies (CZEBS). There are projects studying the thermal effect of the hybrid ventilation system and its resulting air flow throughout the whole building in more

detail . These studies can be coupled with the one presented in this thesis to operate the hybrid ventilation system as efficiently as possible. Using the whole–building simulations, the total energy savings potential of the building can be found, and then using the model presented in this thesis the thermal comfort can evaluated. If the two models run iteratively, the best ratio of energy savings and thermal comfort can be achieved.

1.4 Outline

The contents of this thesis can be summarized as follows:

Chapter 1 provides an introduction to the topic, some insight to the motivation behind the work and sets the objectives.

Chapter 2 presents a literature review of the modeling techniques and the control strategies used in hybrid and natural ventilation systems. Since modeling such a system touches on many different modeling aspects, only those of interest to this thesis are mentioned. The reader is encouraged to research the topics of their interest in depth using the review articles referenced in the thesis.

Chapter 3 presents the EV building, which is used as case study for this work. It explains the hybrid ventilation system of the building, discusses the previous studies on the building and their conclusions and describes the experimental set-up. In the end, it discusses some observations that are key to the development of the model.

Chapter 4 describes the development of the model. It presents the equations and the thermal network, explains various assumptions and evaluates the model with the measurements from the experiments.

Chapter 5 presents different control strategies and their performance. It compares the control strategies to each other and discusses their advantages and disadvantages.

Chapter 6 concludes the work, mentioning some key aspects of the analysis performed in the thesis. It explains the limitations and sets some objectives for future work.

CHAPTER 2

LITERATURE REVIEW

This chapter focuses on previous studies and state-of-the-art knowledge of thermal models for buildings with a natural or hybrid ventilation system, the controls of such systems and the thermal comfort associated with them.

2.1 Modeling buildings with a natural or hybrid ventilation system

Thermal models predict the thermal response of a building. They are used in building design to simulate the behavior of the building for different situations and design parameters and observe their effect on energy demand, thermal comfort and control strategies [4]. Depending on the objective and the problem at hand, the whole building may be modeled, or just the section of interest. Thermal models (like all models) vary in complexity, accuracy and computational demand.

The modeling of the effects of natural or hybrid ventilation on a building can be divided into three parts: the modeling of air flow, the modeling of thermal mass and the modeling of thermal comfort.

2.1.1 Modeling of air flow

The methods used for natural ventilation can be divided into the following main categories [5]: Analytical models, empirical models and computational simulations. Airflow models of natural ventilation are usually solved along with thermal models, because of the effect of temperature on stack-driven flow. These categories can be further subdivided and are often used in combination. In this section the role of experimental methods is also discussed. Extensive information on performance of prediction in ventilation is presented by Chen [6] and Omrani et al. [5].

Analytical and empirical methods

Analytical models are also called white-box or glass-box models, because the principles defining them and the structure are clear. They are based on physics (like mass and energy conservation equations, etc.) and are usually verified experimentally [7]. Although they can be quite detailed, they are often easy to understand. The limitations of these models are the simplifications and the assumptions that are required. They need to be case specific and many times result in inaccurate predictions. They are useful as design tools for the early stages of design, when many details are not known anyway and a fast, rough approximation is required.

Analytical and empirical methods are used mostly on simple problems, without many uknown parameters, because of the high number of simplifications needed if the system is too complex. For example, a number of analytical and empirical models of single–sided natural ventilation in literature [8–13] are based on Equation (2.1), which is called the orifice equation. Q_v is the ventilation rate (m/s^3), C_d is the dimensionless discharge coefficient, A is the opening area (m^3), ρ is the density (kg/m^3) and ΔP is the pressure difference (Pa). This equation can be used for natural ventilation driven by wind, stack and pressure differences.

$$Q_v = C_d A \sqrt{\frac{2|\Delta P|}{\rho}} \tag{2.1}$$

The difference between single-sided ventilation and cross ventilation is that the air flow through an opening in single sided-ventilation is affected more by wind-driven turbulence and

the variation of the pressure gradients by external sources. These effects make single-sided ventilation hard to predict [14].

On the other hand, there are studies that show the difficulties that arise when analytical and empirical models are used on systems with many zones or unusual geometry. The resulting equations are non-linear and are usually solved numerically. Li [15] has presented the governing equations for stack, wind-assisted and wind-opposed natural ventilation. Although analytical solutions to these equations exist, it is hard to extract useful information from them. Holford and Hunt [16] presented a set of 6 non-linear and one integral equations to describe the natural ventilation phenomena between a single–story zone and an atrium. Freire et al. [17] ran several cross and single-sided natural ventilation simulations in order to compare three models to each other. They compared their results with experimental data taken from a full-scale wind tunnel and from a three-story high office building. The empirical models they used predicted the trends of the natural ventilation phenomena, but the difference between the predictions and the actual results was about 30 %. Ai and Mark [18] investigated the applicability of empirical models on accurately predicting ventilation rates in multi-story buildings. They concluded that empirical models cannot accurately predict the ventilation rate differences in different zones.

Computational simulation

Most of the reviewed papers used computational simulations to predict and simulate natural and hybrid ventilation systems. These models are usually used in combination with experimental data, either to investigate the effect of some parameters, or to be experimentally validated and then used to accurately simulate natural ventilation for future studies.

The first type of computational simulation studies is using Computational Fluid Dynamics (CFD) techniques to solve the Navier-Stokes equations for the specific geometry and boundary conditions. They are computationally demanding, especially for complex systems and geometries. The result is a detailed description of the air flow that can provide information on temperature and velocity, particle concentration distribution, etc.

The usual procedure is as follows [19]: at first the geometry of the problem is defined. The different domains (fluid, solid, etc.) are specified. The design is often done with sepa-

rate computer-aided design programs. Then the domains are divided into discrete volumes or cells, which form the mesh. Depending on the problem and the geometry the mesh can consist of cells of different shapes, like tetrahedra, polyhedra, prisms, etc., can be structured or unstructured, uniform or non-uniform. Then the physics of the problem is defined (the equations describing the problem), as well as the boundary conditions and the initial conditions for the transient problems. The equations are solved iteratively for the problem (steady-state or transient), and the results are visualized. The visualization can be done on a separate computer program.

The model needs to be tested for mesh independence. This means that several simulations with different qualities of spatial and time discretizations need to be tested to make sure that the result remains the same. Lower quality of the mesh means lower computational resources, but lower accuracy. The ability to properly predict the air flow depends also on the boundary conditions and the assumptions of the model [5].

There is a big number of studies using CFD [20–27]. It is out of the scope of this thesis to go in depth and present all of them, but some related to the topic of this thesis will be discussed. There are numerous review articles on the subject; for example, more information on the application of CFD for models of wind-induced natural ventilation in buildings can be found in [28]. Wang and Chen [29] investigated the impact of window types on single-sided natural ventilation. They concluded that the different types of windows had a different effect on the ventilation rate for different wind directions. The reason is the change of flow pattern because of the windows and the turbulence. Ding et al. [30] created a 3D isothermal flow transfer model of a high-rise building with cross ventilation and used scSTREAM to simulate the effect of different parameters on steady-state conditions. They found that the area-weighted average indoor air speed increases with increased opening sizes and decreased surrounding building heights, with the latter being the most influential. Song and Meng [31] used Fluent CFD simulations to investigate the efficiency of ventilation design in schools in China. They conducted a questionnaire survey for three weeks and found that the kids were feeling comfortable at the places that the simulation indicated a high ventilation rate. According to the simulation, double rows of windows, exhaust and ceiling fans can improve the thermal comfort conditions.

The second type of computational simulation studies is the "airflow network model", or multi-zone models. In these models the air flow is divided into zones and each one is considered to be well-mixed. The characteristics (temperature, air speed, humidity, etc.) are assumed to be uniform for the whole zone. Each zone is represented with one node. Most solvers compute the characteristics of each node based on the pressure difference [32]. Many commonly used models are multi-zone, like the ones used by CONTAM, COMIS and ESP-r. These models are useful for whole building simulations, since they reduce the number of the nodes and equations to a minimum. This is their disadvantage as well, since they cannot provide detailed information on the behavior of the flow in each zone. It should be noted that they are only accurate for indoor spaces, because outdoor airflows cannot be assumed to be uniform. An extensive review on how these models and some of their applications can be found in [33].

To increase the accuracy and detail of the results, a common technique is to couple CFD to building energy simulation software (which use airflow network models). Building energy simulation software tools perform a heat transfer simulation for the whole building, which can be used for energy savings prediction and thermal discomfort estimation. The coupling of airflow and heat transfer modeling is further discussed in section Section 2.1.4. In some cases, when heat transfer is not of concern, just the CFD and air flow network models are coupled. In this case the results are more accurate than the ones from the network model and they are produced faster than using CFD [34, 35].

Role of experimental methods

All the aforementioned models have uncertainties, which derive from approximations and simplifications. Most of the models are validated experimentally to test how accurately they can predict the flow. Then the model is used to analyze the whole space (and not just the points where the sensors are in experiments), and to investigate the effect of various design parameters on the flow. It is not always easy, or even possible, to conduct an experiment. There are many factors associated: specialized equipment (sensors), access to case study buildings, ideal weather conditions, time, money. A lot of the studies already presented are studies of models validated with experimental data.

Experimental methods can be broken down to full-scale and reduced-scale experiments. Full-scale experiments can be classified into two categories: laboratory experiments and on-site measurements [6]. There are practical obstacles for laboratory experiments when the building is bigger than a couple of rooms, because the whole building has to be into an environmental chamber or a wind tunnel to simulate the weather conditions. Alternatively, on-site measurements from a similar building can be used to predict the natural ventilation. Tracer gas techniques are widely used in full-scale experimental studies [9, 36–38].

Recently many studies have been published about full-scale experiments of natural ventilation. Stathopoulou et al. [39] investigated the effect of outdoor pollution and meteorogical conditions on air quality of two large athletic halls with natural and mechanical ventilation. Wang et al. [40] evaluated ventilation effectiveness conducting a full-scale experiment in a section of a Boeing 767 containing thirty five mannequins. Omnari et al. [41] predicted indoor air inlet velocity by correlating it to wind speed available from weather stations close to the building. Xu and Ojima [42] quantified energy demand reduction in a house with a double skin façade by measuring ventilation.

An extensive review on experimental techniques for natural ventilated buildings can be found in [43], on room air measurement and the equipment used for measuring air velocity in [44]. Information on particle velocimetry is presented in [45].

However, if placing sensors to measure the air flow in a building is not possible, reduces-scale experiments can be conducted. Rooms or even buildings of reduced size can be used as models. In order to have similarity between the reduced-size model and the actual building certain dimensionless numbers have to be the same (Reynolds number, Prandtl number, Grashof number, etc.). Difficulties arise when heat transfer is considered in a room with ventilation, because it is hard to achieve similarity using Reynolds and Grashof numbers [6].

Gao and Lee [46] used CFD simulation, validated with experimental data from tracer gas decay to evaluate the influence of window types on natural ventilation performance of residential buildings in Hong Kong. The same authors [47] used the same method to evaluate the influence of opening configuration on the same buildings. Zhou et al. [48] proposed an optimized design strategy for high-rise residential buildings, which they evaluated with CFD validated with experimental data. Jiang et al. [49] used large-eddy simulation, validated

with experimental data, to study different types of natural ventilation configurations. Ding et al. [50] created a reduced-scale model to gather experimental data, which they used to validate a CFD model, to investigate natural ventilation in a building with a double-skin façade connected with a solar chimney.

2.1.2 Modeling of transient heat diffusion

There are four main approaches regarding modeling the heat transfer through thermal mass: lumped system approximation, conduction transfer functions, control volume finite difference methods and black-box models. Black-box models, in contrast to white-box models, are the models which connect inputs and outputs in a way that is not physics-based. It is usually based on statistical methods and machine learning techniques.

Equation (2.2) shows the general equation of the transient heat conduction. In addition to this equation the boundary conditions and the initial condition have to be defined.

$$\frac{\partial}{\partial x}\Big(k\frac{\partial T}{\partial x}\Big) + \frac{\partial}{\partial y}\Big(k\frac{\partial T}{\partial y}\Big) + \frac{\partial}{\partial z}\Big(k\frac{\partial T}{\partial z}\Big) + \dot{q} = \rho c_p \frac{\partial T}{\partial t} \tag{2.2}$$

where

T (K), temperature;

k (W/mK), thermal conductivity;

$\dot{q}$ (W/m^3), heat generation;

ρ (kg/m^3), density; and

c_p (J/kgK), specific heat capacity.

There are many simplifications that can apply to this equation depending on the situation. In most cases the heat transfer can be assumed to be one-dimensional and an exact solution to the differential equation can be found. In many situations, though, it is too complex to derive an exact solution.

A common boundary condition, especially in buildings, involves heat convection, which means that the thermal mass exchanging heat with a fluid (with air when it comes to buildings). Equation (2.3) describes a heat convection boundary condition between a wall and the air, at the surface of the wall.

$$-k\frac{\partial T}{\partial y} = h(T_f - T) \tag{2.3}$$

where

T (K), temperature of wall;

k (W/mK), thermal conductivity;

h (W/m^{2}K), convective heat transfer coefficient;

T_f (K), temperature of the fluid.

The wall surfaces also radiate towards each other, if their temperatures are different. Both the radiative and the convective heat exchange are processes that are non-linear. Their respective coefficients are often linearized and combined, introducing some error, but allowing the usage of methods that require linear algebra [51].

Conduction transfer functions

Conduction transfer functions (CTF) provide a set of coefficients that correlate the current conductive heat fluxes to past surface temperatures and past heat fluxes [51]. This is the model recommended by ASHRAE [52]. Once the coefficients are determined, they are independent of the excitation variables [53]. This is a big advantage for computational time, since they do not need to be derived every time e.g. the exterior temperature changes.

A lot of building simulation software tools use this method (EnergyPlus [54], TRNSYS [55], etc.). There are three popular methods to obtain the coefficients: direct root-finding (DRF) method, state-space (SS) method and frequency-domain regression (FDR) method [53].

The direct root-finding method was first introduced by Hittle [56]. In the beginning a unit triangular temperature is applied to the inside and outside surfaces. The fluxes on

each surface due to each one of the pulses are infinite series and define the response factors, or conduction transfer functions. The roots to a nonlinear equation are found numerically, which is a source of inaccuracy and sometimes a root may be missed, especially if there are two consecutive roots really close to each other. This has been demonstrated by many studies [57–59]. Hittle and Bishop [60] developed an improved numerical technique for calculating these roots. The direct root-finding method is computationally inefficient.

The state-space method has the advantage that there is no need to find the roots of the system, and therefore the problem of missing a root is avoided. At first the rational fraction of an s-transfer function is obtained from series expansion. Then the state space equation is established and the state matrix calculated. The system is discretized and the the response factors are obtained by matrix multiplication [61]. The discretization is done with finite difference or finite element methods.

Frequency-domain regression method has been developed to perform transient heat conduction analysis including the calculation of the response factors and conduction transfer functions. A set of linear equations is solved to get a simple polynomial s-transfer function for internal, cross and external heat conduction. Then, using inverse Laplace transform or Z-transforms on those polynomials, the response factors or the conduction transfer functions are calculated [62]. This method, like the state-space method, does not involve the numerical solving of an equation and therefore avoids miscalculations. FDR has been used my many studies that report high accuracy [63–66]

Li et al. [67] performed a comparison analysis of the three methods (DRF, SS and FDR methods) using the heat flux comparison method. They concluded that for SS and DRF the error can be up to 100 %, depending on the conditions, but the FDR method can calculate the CTFs with very good accuracy. FDR is more robust and reliable and a more practical way to calculate CTFs.

Zhou et al. [68] used the harmonic response method, a frequency domain method, to model thermal mass and couple it with natural ventilation. They estimated the average indoor air temperature and the time constant for different configurations of walls with and without insulation.

Control volume finite difference methods

This method spatially discretizes the solid into many control volumes. Each one is assumed to describe a layer with uniform characteristics (temperature, density, specific heat capacity, etc.). A node is located at the center of each control volume. The heat flux between two nodes is proportional to the difference between the temperature of the two nodes. The conductance between two nodes is calculated as kA/L, where k is the thermal conductivity (W/mK), A is the area of the surface of contact and L is the distance between the two nodes. The thermal mass of the control volume is modeled as a capacitance attached to the node. A heat balance analysis on the control volume results in Equation (2.4) [69]:

$$C_i \frac{dT_i}{dt} = Q_i + \sum_{j=i}^{n} U_{i,j}(T_j - T_i) \tag{2.4}$$

There are three approaches to discretize Equation (2.4) in the time domain: the implicit method, the explicit method and Crank-Nicholson method. The explicit method only relies on the values of previous timesteps to estimate the temperature of a node. The implicit method correlates the temperature of the node to the ones of nearby nodes at the same timstep. That results to a system of equations that are solved simultaneously. The explicit method has a critical timestep to ensure convergence, but is less computationally demanding than the implicit. Crank-Nicholson is a method that combines the two previous ones, ensuring convergence, but achieving higher accuracy on time discretization (accuracy of Δt^2).

Mazzarella and Pasini [70] compared Conduction Transfer functions and Finite Difference methods implemented in building simulation software tools. They concluded that CTF methods require less computational resources, but have lower accuracy. They did not test Frequency Domain methods, because they were not implemented in any available tool at the time.

Lumped system approximation

In order to simulate a transient heat conduction problem the "lumped capacitance method" can be used. This method assumes that the temperature of the solid is spatially uniform at any instant during the transient process. Although this is impossible, it is a good ap-

proximation when the resistance to conduction within the solid is small compared to the resistance to heat transfer between the solid and its surroundings. To check the validity of this assumption, the dimensionless number Biot is defined in Equation (2.5):

$$Bi \equiv \frac{R_{cond}}{R_{conv}} = \frac{L/kA}{1/hA} = \frac{hL}{k} \tag{2.5}$$

If $Bi \ll 1$ then the resistance to conduction within the solid is much less than the resistance to convection across the fluid boundary layer, and the assumption is reasonable. Typically, a value $Bi \ll 0.1$ ensures results in error of less than 5 % [71].

A system can get modeled as an electrical circuit equivalent, called thermal network. This is the most commonly used method. Figure 2.1 shows a multi-layered wall consisting of a layer of insulation and a layer of concrete. The insulation is assumed to have no thermal mass, whereas concrete is represented with a thermal capacitance. The heat source is the exterior temperature. The convection between the exterior air and the exterior surface of the wall is between nodes 1 and 2, the conduction in the insulation is between nodes 2 and 3, the conduction in the first half of the concrete is between nodes 3 and 4, the conduction in the second half of the concrete is between nodes 4 and 5 and the convection between the interior air and the interior surface of the wall is the last resistance. The last node represents the interior air temperature. The capacitance on node 4 represents the thermal capacitance, or thermal mass of concrete.

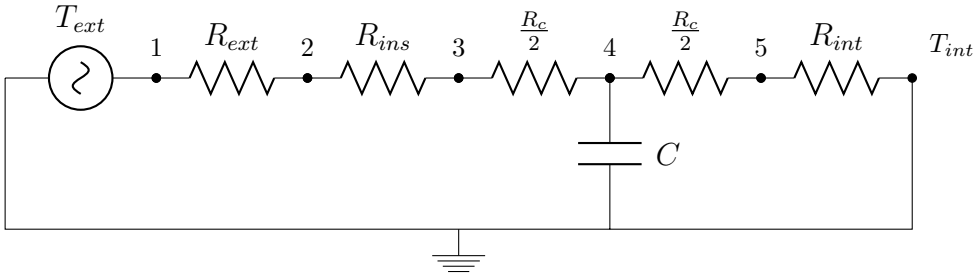

Figure 2.1: Thermal network of a multilayered wall, consisting of one layer of insulation without thermal mass and a layer of concrete, which has thermal mass

Most of the literature in lumped capacitance models is focusing on the required model order or what part of the building should be treated as one effective capacitance [72].

Hudson and Underwood [73] showed that a first-order model (one capacitance) performed well for the short term, but a more detailed model may be needed to be accurate in long–term simulations. They also mention that for short–term simulations the initialization of the model can be a problem. To address this issue many researchers [74–76] simulate more days than they need and use the first days as warm–up days. Usually they just repeat the climate data of the first day or week, depending on the problem at hand. This way no additional weather data are needed.

Many studies of lumped capacitance models have shown good accuracy on predicting the heat loads of a building and the thermal performance in general. These models are either first–order models, with various modifications to the capacitances [77, 78], or second–order [79, 80]. An extensive analysis on the suitability of lumped–capacitance models in calculating energy need and thermal behavior of buildings can be found in [81].

Black-box models

A rising, in both popularity and accuracy, technique is using artificial intelligence and neural networks to model, predict and control the thermal behavior of buildings. Black-box models have the advantage that no information is needed about the physical properties of the buildings [82]. They can also be adaptive and self-learning [83]. Many different types of neural networks have been tried: simple multi-layer perceptrons [83–85], Radial–Basis Function networks (RBF) [86] and Non–linear AutoRegressive models with eXogenous inputs (NARX) [87, 88]. The parameter that has to be defined is the number of neurons for each network. In most cases this number results either from heuristics or from a self adjusting mechanism implemented in the algorithm.

Data–driven models represent a correlation, a mapping of sorts between the inputs and the outputs. To establish this mapping the model is trained on data (called the training set). When the number of neurons and layers increases, so does its capacity to capture the various factors correlating the inputs to the outputs and also the training set needed. Since this mapping is established using the training set, the ability of the model to extrapolate is limited.

A second problem is overfitting. That means that the network yields good results during

the training phase, but it is trained well to predict the data available and only that. That results in lower accuracy when new data are presented, and under circumstances may lead to poor generalization ability. There are many techniques to avoid that. In some cases the available training set is divided into two batches. One is used to train the data and the other one is used to validate the generalization ability of the network. Another method is to apply some kind of pruning and/or growing mechanism to determine the proper size of the network [88].

Importance of modeling thermal mass

As mentioned, modeling gives insight into alternate design options and how they affect the performance of a building. That is the case with thermal mass especially, because of the large time difference between the storing of thermal energy in the mass and its realeasing [89]. Thermal mass acts as a thermal buffer, and can help to reduce the heating or cooling load of the building [90]. Especially if the amount of thermal mass and the coupling with the thermal zone are done properly, it can help maintain thermal comfort by avoiding large temperature fluctuations [91].

Thermal mass offers the option to heat or cool the space during unoccupied hours, or during times that off peak tariffs apply. Pre-cooling or pre-heating the space during these hours reduces the peak demand. This is especially beneficial in many countries, like Canada, where the highest peak of the month defines the tariff. Moreover, the mechanical system will work at a maximum efficiency for a longer time [92].

An extensive review on abilities and limitations of thermal mass activation for thermal comfort, peak shifting and shaving can be found in [93] and on the impact of thermal mass on building energy consumption in [94].

2.1.3 Modeling of thermal comfort

Thermal comfort is one of the most important aspects when it comes to building design. For this reason many studies have tried to define it and model it. ASHRAE issued Standard 55, where thermal comfort is defined as “that condition of mind which expresses satisfaction with the thermal environment and is assessed by subjective evaluation” [95].

There are 6 main factors that affect thermal comfort, the first four are environmental and the last two personal: air temperature, mean radiant temperature, relative humidity, air speed, metabolic activity and clothing level. There is a new approach, called adaptive thermal comfort, that takes into account the efforts occupants make to restore thermal comfort by controlling the environment [96].

An extensive review on thermal comfort models and indicators for indoor environments can be found in [97] and on theory and practice of assessing thermal comfort in [98].

The PMV model (Predicted Mean Vote)

The PMV index is derived from the thermal comfort equation (heat balance equation on a human body) and tuned using approximately 1300 surveys [99]. It treats the body like a whole being. It consists of a 7-points scale from -3 (cold) to 3 (hot). It estimates the mean value of thermal sensation votes of a large group of people.

There are many studies supporting or proposing modifications to Fanger's model [100–102] and many highlighting its limitations [103–105]. According to ASHRAE Standard 55 [95] the acceptable range of PMV is [-0.5,+0.5].

The main arguments against Fanger's model, as explained in [96] are:

- People are considered passive sensors, so the fact that, if they feel uncomfortable, they will change their activity, clothing, etc. to adapt to the situation is not considered.
- It is the same throughout the world. Different climates and types of buildings affect thermal comfort in a different way.
- Thermal neutrality is not objective or the same for all people. Psychological and cultural aspects affect the optimum conditions for different people.
- Thermal preferences are asymmetrical around neutrality and that's why the assumption that the interval [-1,+1] represents comfortable conditions may not be always the case.

PMV for natural ventilation

The PMV model was developed for air-conditioned spaces. Studies [106, 107] have shown that there is a difference between the PMV and the thermal sensation declared by the oc-

cupants in naturally ventilated buildings. Yao et al. [108] have proposed an adaptive PMV (aPMV) for naturally ventilated buildings, correlating it to Fanger's PMV as shown in Equation (2.6):

$$aPMV = (PMV^{-1} + \beta)^{-1} \tag{2.6}$$

The term β is the "adaptive coefficient" and represents the ratio between the psychological and behavioral impact and the physical stimulus. Different values for this coefficient have been proposed by different studies. A summary can be found in Table 2.1.

Table 2.1: Coefficient β for Equation (2.6) based on various studies

Author and reference	β
Yao et al. [108]	0.293 for warm (22–38 °C) -0.125 for cool (8–18 °C)
Gao et al. [109]	0.029 for indoor air velocity 0–0.2 m/s 0.167 for 0.2–0.8 m/s
Xu et al. [110]	0.285 for warm (30–34 °C) and indoor air velocity 0.3–0.6 m/s -0.136 for cool (8–15 °C)and 0.1–0.2 m/s
Kim et al. [111]	-1.40 warm (25–32 °C) -5.74 cool (14–24 °C)
Song et al. [112]	0.64 in HHE, -0.06 in CE and PMV<0 1.07 in CE and PM>0, -0.37 in CDE

In general the PMV is appropriate for steady-state conditions. It can be used for small variations of the variables, by considering the time-weighted averages of the variables during the previous hourly period [113].

Predicted Percentage Dissatisfied (PPD)

PPD estimates the percentage of persons that are thermally dissatisfied. It is directly dependent on PMV and is shown in Equation (2.7). The minimum PPD is 5 %, meaning that 5 % of the people in a big group will always be dissatisfied. For PMV in [-0.5,+0.5], the

corresponding PPD is <10 %.

$$PPD = 100 - 95e^{-0.03353PMV^4 - 0.2179PMV^2} \tag{2.7}$$

Thermal comfort in transition spaces

Transition spaces are spaces that connect occupied spaces or are used as circulation areas. The occupants do not stay there for a long time, they just pass by.

Chun et al. [114] studied the different studies on thermal comfort in transition spaces. They concluded that the term "transition space" involves a large amount of spaces, such as balconies, metro stations, shopping malls, building entrances, atria, corridors. They characterized three different types of transition spaces: Type 1, which is indoor spaces where people frequently enter and exit the building, and thus the conditions are mixed constantly, Type 2, which is attached, covered spaces connected to buildings, and Type 3, which is spaces that are essentially outside rooms. They report that in Type 1 spaces the PMV index was predicted warm by people because of the higher than usual metabolic rate.

Although there are some empirical approaches to assess thermal comfort in transition spaces [115, 116], this is much harder when it comes to modeling approaches. Ghaddar et al. [117] developed a model based on bioheat model, integrated with thermal comfort and sensation models to predict comfort in transition spaces with air movement. After validating their model, they used it to perform a parametric study on the effect of clothing material on thermal comfort. Wu and Mahdavi [118] studied the transition between rooms with different temperatures. They found that the participants' Thermal Sensation Vote (TSV) matched adequately the PMV calculations. They explained that in winter the participants' tolerance range of comfortable indoor conditions was narrower. Pitts [119] separated transition spaces into entrances, circulation and longer-term occupancy zones. The circulation zones are defined as spaces where occupants are expected to be walking by or standing in for 5–10 minutes. He concludes that in these zones the PMV can be used, but it can be increased from the range of [-0.5,+0.5] to [-1.5,+1.5]. For the rest of the transition spaces they proposed the increase to [-0.7,+0.7].

2.1.4 Coupling of air flow, heat transfer and thermal comfort modeling

As discussed, natural and hybrid ventilation are highly dependent on temperature and heat transfer, due to the stack effect. For this reason, and because it is usually used to predict energy savings, the air flow models are used in conjunction with the heat transfer and thermal mass models. The two main methods for coupling are the "ping-pong" and the "onion" method. In the former both models are solved for each time step and in the latter one of the models is solved and the result is used as input for the other model at the next time step [120]. Most of the studies on the two methods show that the "ping-pong" method can be inaccurate, especially for longer time steps, whereas the "onion" method is computationally demanding, especially for smaller time steps and some times the non-linearity of the equations must be simplified just to get a solution [121–123]. More information on the techniques and strategies for coupling energy simulation programs and CFD programs can be found in [124].

Carrilho de Graça et al. [125] used CFD simulation to predict airflow. The results were used as boundary conditions for thermal analysis of the building. The results from the thermal analysis were used as inputs to Fanger's comfort model. Wang et al. [126] studied the effect of façade design on natural ventilation in Singapore. Using CFD and thermal analysis they estimated the conditions inside the building. According to those conditions they evaluated thermal comfort inside the space, and hence the effect of the natural ventilation.

Muhsin et al. [127] studied natural ventilation in a multi-story house in Malaysia. They created a CFD model that they validated with experimental data. They concluded that the indoor air velocity did not achieve the levels required for thermal comfort. Vitale and Salerno [128] created a CFD model of a building in Rome, based on the finite element method. The results from the CFD analysis were used as inputs to assess thermal comfort, using both Fanger's model and adaptive model. Fanger's model suggested that cooling was needed to have acceptable thermal comfort levels, but with the adaptive model the same levels were deemed acceptable. Hussain and Oosthuizen [129] created a CFD model that they validated with experimental data of an atrium. They assessed thermal comfort by using an extended version of Fanger's PMV and PPD model.

Boyer et al. [130] present a part of the software CODYRUN, where they couple the airflow simulation with heat flow simulation. At every timestep they compute the air mass flow from the air flow simulation and then they use that to compute the heat flow. They validate the model with other analytical models and experimental measurements.

2.2 Control strategies of natural and hybrid ventilation systems

In this section the different techniques for controlling natural and hybrid ventilation systems and the control and controlled parameters are discussed. More information can be found in IEA-EBC Annex 35 HybVent [131] and IEA-EBC Annex 62 Ventilative Cooling [132].

2.2.1 Control strategies

The most popular strategies that have been used until recently are Rule-Based controls. However, over the last decades there has been a lot of research in two types of control strategies, one based on optimal and predictive control and the other based on computational intelligence. An extensive review can be found in [133] and [134].

Typical strategies

The most typical strategies were developed decades ago and are the ones implemented in most buildings. They are the simple On-Off control, the time schedules and the PI/PID controls. Specific parameters are tuned based on simple rule of thumbs and the knowledge of the engineer designing the system. The disadvantages of these methods are that they have to be tuned for every new building and they do not respond well to sudden changes of exterior conditions, especially in buildings with high thermal mass. Their poor performance is countered with reliability [131].

Computational intelligence

Recent research has been studying the use of intelligent control systems that automatically adjust different modes of hybrid ventilation to the exterior conditions. Most of these studies are focusing on controlling HVAC systems, but they can easily be adapted to control the ventilation system. Some are simple neural networks [135].

Others are based on fuzzy logic [136–138]. That means that a physics–based model is not needed. They can incorporate more than one control variables and take into account uncertainties. The conditions are divided into linguistic labels (like very cold, cold, etc.). Then the controller uses these definitions to apply rules of the type "If A, then B" [131]. Marjanovic and Eftekhari [139] used controllers with fuzzy logic to control a natural ventilation system and reported that they satisfied the security demand due to strong wind and they were capable to respond to the changes in exterior conditions.

Spindler and Norford [140, 141] propose a data driven linear model for buildings with hybrid and natural ventilation. It implements control for different zones and modes. The amount of lag terms can vary. They determined the coefficients to the linear model with a training set and then they tested and validated the model with data for each purpose. They have applied it successfully to two buildings with hybrid ventilation.

Mahdavi and Pröglhöf [142] developed a non-linear data-driven model to predict air-change rates and mean indoor air flow speed based on window opening position, exterior air speed and temperature difference between indoor and outdoor conditions in a natural ventilation system. They suggested that a deviation range for air change rate and air flow speed is practically accurate enough for control purposes of a natural ventilation system if it is less than 40 %.

Model predictive control (MPC)

After the model is created, then the response of the building can be simulated based on the exterior conditions. MPC uses forecasts of the next hours, days or weeks as inputs to a model and simulates the response of the building for future conditions. It minimizes a cost function to evaluate the response of the building and to obtain the optimum (or near-optimum) control. The models on which MPC is based can be anything from white-box to

black-box and data-driven models, or even a combination of those. However, they should have the ability to perform well under all the possible circumstances. A detailed review of energy modeling for control and operation and an overview on application of building energy modeling methods specifically can be found in [143].

MPC is being used on buildings a lot the past years, but the applications focus on HVAC systems control [144, 145]. The applications on natural or hybrid ventilation systems are not many. The OptiControl team from Switzerland has been working on MPC in buildings. Oldewurtel et al. [146] give a short overview of the state-of-the-art research in MPC for buildings. They explain in depth the procedure of MPC, discussing the constraints and the cost functions available. Then they investigate the energy savings potential in Integrated Room Automation of Deterministic and Stochastic MPC. They showed that more than half of the cases achieve 40 % energy savings or more.

They mention that the cost function is chosen to serve two purposes: stability and performance target. To ensure stability a cost function that forms a Lyapunov function needs to be chosen. However, this is generally relaxed in building systems, because of the slow responses. The cost function usually shows the performance targets, it is a combination of performance indexes, weighted according to importance [146].

May-Ostendorp et al. [147] studied a series of MPC techniques on mixed mode buildings using EnergyPlus. Then they created a general multi-regressional model that was able to achieve 70–90 % of the energy savings of MPC techniques in just a small fraction of the computational resources. Prívara et al. [148] argue that most models built for buildings are not suitable to be used in MPC. They explain how to obtain models suitable for MPC, combining building energy simulation tools and statistical identification.

Hu and Karava [149] created MPC strategies for a building with mixed-mode cooling. They developed a transient, multi-zone building energy prediction model, performing optimization with the particle swarm technique. They found that MPC can significantly reduce cooling consumption, in contrast to heuristic control, which has an increased risk of over-cooling and violating the acceptable thermal comfort range. The same authors [150] developed a modeling method for multi-zone buildings with mixed-mode cooling, based on state-space and oriented to controls. They validated their model with experimental data.

They used progressive refinement optimization to find sequences of binary decisions (on/off) for the motorized windows. They found that the algorithm finds similar optima with the particle swarm optimization used before, but reducing the computational time from 48 to 2 hours.

It should be noted that the result of MPC depends highly on the accuracy of the forecast (weather, occupancy, etc.).

2.2.2 Control and controlled variables

Control variables are the parameters that are used as inputs to a control strategy, whereas controlled variables are the parameters that are affected by the control signal from a controller [131]. Which variables will be the control and which the controlled changes and depends on the control strategy and what in general the operator is trying to achieve.

The most important control variable in a building with natural or hybrid ventilation is the comfort of the occupants. As discussed in Section 2.1.3 thermal comfort needs to be in acceptable levels, and there are metrics to estimate how comfortable or uncomfortable the occupants will be. This can be further broken down to indoor/outdoor temperature, humidity level, wind speed, etc.

In some cases, like labs, the indoor air quality controls the ventilation rate. Air pollutants can enter into the space from exterior sources, or be generated into the space itself. Usually the measured and control variable is the CO_2 levels, unless there is a specific substance created in the occupied space. The concentration limit for CO_2 control is 1000 ppm, while the concentration in a rural area is about 300 ppm [131].

Energy can also be used as control variable. In many cases part of the decision for the control strategy is made so that the building is energy efficient. In those cases energy consumption - electrical as well as thermal - can be of significance.

These are the most common control variables, but in special cases others can influence the control strategy as well [131]. Some of them are illuminance levels (daylighting), noise levels, pressure difference between two points of interest, etc.

The controlled variables differ from case to case, but usually are the air flow support provided by fans, the inlet openings to the building, the outlet openings to the building or a

combination of the above.

Table 2.2 shows the different control variables used in some studies of natural ventilation, adjusted from Yuan [1].

Table 2.2: Control variables used in various studies. Adjusted from [1]

Study	Control Variable
Kolokotroni and Aronis [151]	Outdoor temperature
Pfafferott et al. [152]	Air Changes per Hour
Artmann et al. [153]	Outdoor temperature Operative temperature
Spindler and Norford [141]	Indoor temperature
Prajongsan and Sharples [154]	Operative temperature Wind speed / Inlet velocity
Karava et al. [155]	Outdoor temperature Outdoor relative humidity
Schulze and Eicker [134]	Outdoor temperature Indoor temperature Operative temperature CO_2 concentration
Hu and Karava [149]	Outdoor dew-point temperature Indoor temperature Operative temperature Wind speed / Inlet velocity

CHAPTER 3

EV BUILDING: A CASE STUDY OF NATURAL AND HYBRID VENTILATION

3.1 Introduction

One of Concordia University buildings, the EV building, was designed with a hybrid ventilation system. It is a typical high-rise institutional building, located in downtown Montreal. Some classes are being taught there, but mainly the EV building is mostly an office building for professors and graduate students. It has 50% window–to–wall ratio. It is equipped with 40-centimeter thick exposed concrete floor, which can be heated with solar radiation during winter. This large amount of thermal mass helps reduce the fluctuations of indoor air temperature and the cooling peak power demand during the summer and the heating peak power demand during the winter.

The solar gains and internal loads result in the building core needing cooling during the whole year. The perimeter of the building needs cooling during mid-April to mid-October. Using natural or fan-assisted ventilation the thermal mass can be cooled, reducing the cooling load of the building. The large amount of thermal mass means that the building can be precooled during the night, so that it can take handle a bigger load in the morning, without using more energy.

Figure 3.1 shows an overview of the air flow in the EV building. It consists of five three–

story high atria. A seventeenth floor serves as the mechanical room. The atria face 35° west of south (Figure 3.2a). Each floor has two motorized, insulated inlet dampers, on the southeast and northwest façade of the building, as shown in Figure 3.2c. The exterior air enters the building through these dampers and then flows along the corridor on each floor, cooling the building, until it reaches the atrium. The atria are interconnected with motorized grilles (Figure 3.2b), allowing the air to pass through. The atria function as a solar chimney, driving the air through the whole building and exhausting it from the roof. When the stack effect is not strong enough the pressure difference can be enhanced by variable speed fans (Figure 3.2d), installed on the roof in 2015, where the outlet of the air is. The air flow paths are summarized in Figure 3.1 and Figure 3.3.

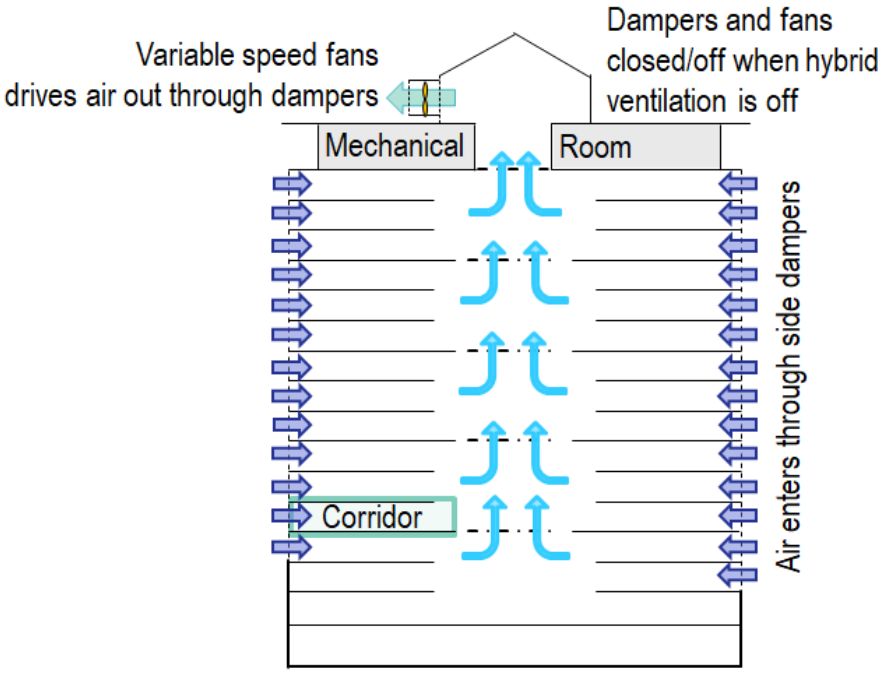

Figure 3.1: Schematic of air flow through Concordia EV building due to hybrid ventilation. Courtesy of Sophie Yuan

When the inlet dampers are open, the mechanical ventilation of the building is still working. The supply rate is lowered to the minimum possible for the corridors and the atria, but it works unchanged for the rest of interior spaces (corridors, washrooms, etc.). When the dampers close, the mechanical ventilation starts conditioning the building right away, which

(a) Concordia EV building

(b) Motorized floor grilles interconnect the atria

(c) Motorized inlet dampers allow the air into the building

(d) Fans on the roof of the building assist ventilation

Figure 3.2: Different components of hybrid ventilation system. Courtesy of Jiwu Rao and Sophie Yuan

to an extent defeats the purpose of the hybrid ventilation. If the system is used to precool the building, then there should be a time difference between the closing of the dampers and the starting of the mechanical ventilation system, to allow the building to heat up passively from the thermal mass and the internal heat gains. Otherwise, the operation of the system may even result in more energy consumption, because the HVAC system immediately tries to get the system close to the setpoint as fast as it can.

After observing the operation of the natural ventilation system, when the fans are not operating, the air movement is affected by wind speed and temperature. In many cases the

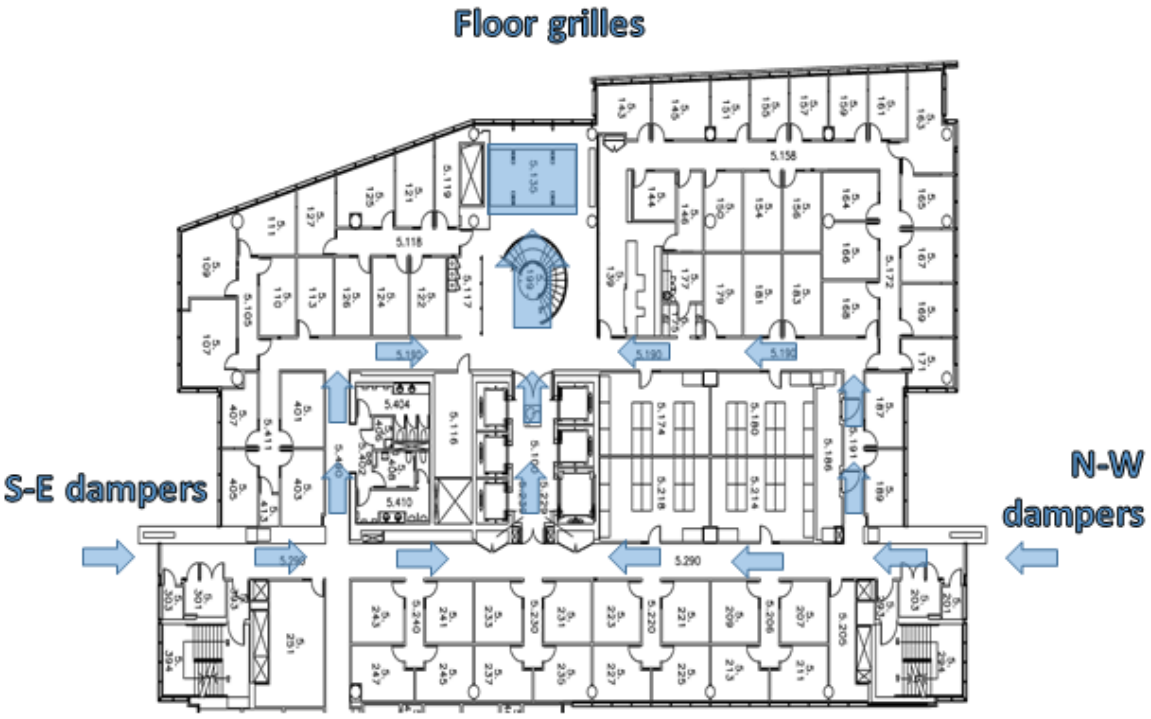

Figure 3.3: Typical floor plan of the EV building and the expected air flow path

result is cross-ventilation, which means that a big portion of the air would enter the building from the south-east façade, travel through the corridor and exit at the north-west façade. A smaller portion of the air would go towards the atrium.

Three sets of two variable speed fans each were installed on the roof to create a bigger pressure difference and assist the air flow. They have a maximum airflow of about 40.000 L/s. As expected, it was observed that the biggest effect was at the top atrium, the one closest to the fans. Unfortunately, the pressure difference created by the fans affected one lab on the fifteenth floor, that had to be under negative pressure for air quality experiments. For this reason, during the operation of the natural or hybrid ventilation system, the inlet dampers of the top atrium (that is fourteenth, fifteenth and sixteenth floor) are kept closed.

Right now the system works based on a simple IF - THEN structure. If the system is closed, it starts when the temperature of exterior air gets above 15°C or below 22°C and the humidity content is lower than 9 grams of water per kilogram of dry air. On the other hand, if it is working, then it stops if the temperature of exterior air gets below 14°C or above 23°C

and the humidity content above 9.5 grams of water per kilogram of dry air. The reason for these setpoints is that, since the building is institutional, the primary objective is thermal comfort of the occupants.

The temperature and relative humidity levels are logged from a weather station installed on the roof of the EV building. It measures air temperature and humidity, wind speed and direction, solar radiation and precipitation (particle size and quantity). As it is common in institutional buildings, the building uses a Building Automation System (BAS) to store, read and distribute data. The weather station sensors, the actuators of the motorized floor grilles and inlet dampers, as well as the motors of the fans, are connected to the BAS. That way the weather data can be accessed by any other controller connected to the BAS and make decisions for the state of setpoint of any other controller.

3.2 Previous studies

Several researchers have studied various subsystems of the EV building, both during the design stage and the operation. Tzempelikos et al. [156] performed a simulation study during the design stage of the building. The analysis includes a study about hybrid ventilation. Carbon dioxide and monoxide were measured at different heights around the building and the air was satisfactory for indoor air quality purposes. They suggested that an acceptable control strategy is exterior air temperature in the range of 12-20°C and not exceeding 70% relative humidity. For night ventilation the temperature range can be extended to 8-22°C.

Karava et al. [155] showed that for a 30-meter long corridor, the heat extracted if the exterior air temperature limit is 12°C can be 2 times higher compared to 15°C and 5 times higher compared to 18°C. They estimate that about 30% of the total cooling load of the atrium and corridors can be covered with hybrid ventilation.

Hu and Karava [149] simulated the building response and applied several control strategies, including MPC, on the ventilation system and the shading devices. Heuristic-based controls resulted in 83% reduced energy consumption, in contrast to 75% of anticipatory controls. However, the heuristic-based control increased thermal discomfort, whereas anticipatory controls maintained operative temperature within range.

Yuan et al. [157] conducted an experimental and simulation study of night ventilation in the EV building. They created a two-dimensional transient finite difference thermal model for a typical corridor on the fifth floor. The model predicts air and floor surface temperature and was validated with experimental data. They also discussed thermal comfort limitations.

Yuan [1] presented a study on the hybrid ventilation system of the same building for a thesis. Extending the work mentioned above, she also suggested thermal comfort guidelines for controlling the hybrid ventilation system. She proposed that the natural ventilation system is controlled with a night ventilation schedule, and based on humidity content, not relative humidity. The estimated cooling potential is shown in Table 3.1. The control is still anticipatory, not predictive.

Table 3.1: Estimated cooling potential of hybrid ventilation system. Adjusted from [1]

Temperature range (°C)	Night ventilation schedule	Relative humidity <70%	Humidity content <11 $g_{water}/kg_{dry\ air}$
15–22	-	Base case	+76% free cooling
12–22 (day) 2–22 (night)	21:00–6:00	+131% free cooling	+447% free cooling
	20:00–8:00	+145% free cooling	+492% free cooling

Vallianos et al. [158] extended this model to simulate the corridor even with the inlet dampers closed. They estimated the discomfort of the occupants, based on Fanger's model, and weigh it against energy savings to decide whether the motorized inlet dampers should be open or closed. They show that the more energy savings is considered, the more time thermal discomfort is above the limit. With this type of control there is always some discomfort of the occupants, which the authors attributed to the reactive nature of control and lack of anticipatory action.

Cheng et al. [159] used measurements from the building to calibrate a simplified and a detailed model in CONTAM. They conclude that the variations of weather conditions and their dynamic interactions with hybrid ventilation systems can be accounted for with flow coefficients. The difference between the results of the simplified model and the detailed model is less than 10%.

3.3 Experimental set-up

The main parameter of the control of the ventilation system is thermal comfort. The place where thermal comfort will be the lowest is close to the inlets, because of the draft and the temperature difference between the interior and exterior air. For this reason a 10-meter long area close to the inlet of the corridor of the fifth floor is studied. It is the same area used in [1, 157, 158]. The specific corridor is chosen, because it is below the neutral plane, which ensures airflow into the building. This way the airflow in the corridor could be detected by the anemometers and a significant change in the indoor environment could be observed.

To investigate the effect of natural ventilation on the building two experiments were conducted. The first one, performed on October 8$^{\text{th}}$–9$^{\text{th}}$, 2015, was set up by Sophie Yuan with the help of the author and used in [1, 157, 158]. It was conducted during the night, when the occupancy of the building is minimal and the temperature difference between the interior and exterior air is high. The dampers were opened at 22:00, when the experiment started. They were kept open for four hours until 02:00. Then they were closed, but the data acquisition system was running for another four hours, until 06:00. The exterior temperature measured at the weather station fluctuated between 7.8°C and 8.9–7.8°C.

The second one was set up by the author and took place during the weekend of September 2$^{\text{nd}}$–3$^{\text{rd}}$, 2017, to avoid high occupancy. During the weekend the exterior conditions would be significantly different from the ones of the previous experiment, giving data for different temperature ranges. The dampers were closed during the night, and then they were let open Saturday 11 am. The system operated based on the existing strategy explained in Section 3.1. The exterior temperature measured at the weather station fluctuated was around 17°C when the dampers opened, raised to 20°C during the day, and then started dropping, reaching 14°C around 1:30 am Sunday. At that point the temperature continued to drop and the dampers closed automatically, because it was too cold. They were open for a total of 14.5 hours. Sunday was a rainy day, and the temperature during the rest of the experiment was low, fluctuating between 13°C and 11°C.

The floor plans of the fifth floor and the position of the sensors are shown in Figure 3.4. Thermocouples placed identically at 1 m, 2.8 m, 5.4 m and 9 m from the façade measure the

temperature of the air and walls. At each position there is a thermocouple placed on each of the two vertical surfaces, one at the suspended ceiling and three thermocouples, suspended at 0.1 m, 1.1 m and 1.7 m off the ground, measuring air temperature. The temperature of the concrete floor is measured by infrared sensors. At the inlet dampers, on the inside of the building, the inlet temperature and wind speed are measured at 0.75 m above the floor, with a thermocouple and a one-directional anemometer. The exterior temperature and the solar radiation on a horizontal surface were measured at the weather station. More information about the sensors and their accuracy is in Appendix A. The solar radiation incident on the façade was computed from the total horizontal solar radiation measured at the weather station. The procedure is explained in Appendix B.

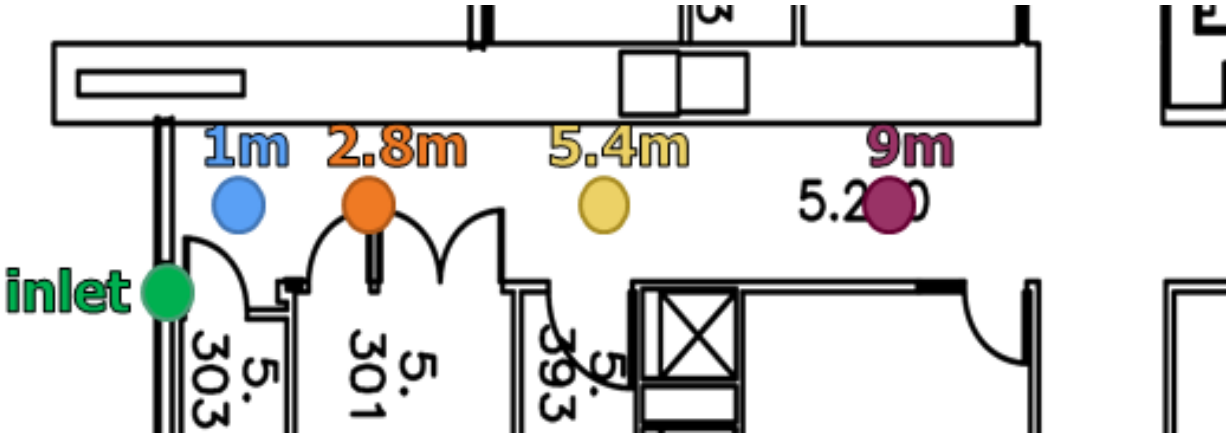

Figure 3.4: Floor plan of fifth floor and position of sensors

3.4 Experimental results

Some results of the two experiments are presented here. These observations led to decisions about the modeling techniques used and discussed in the next chapter.

3.4.1 Air and concrete temperatures

Figure 3.5 and Figure 3.6 show the average air temperature during the experiments of 2015 and 2017 respectively. In both cases the time when the dampers close is obvious, since the temperatures start rising exponentially. The mechanical ventilation starts working as

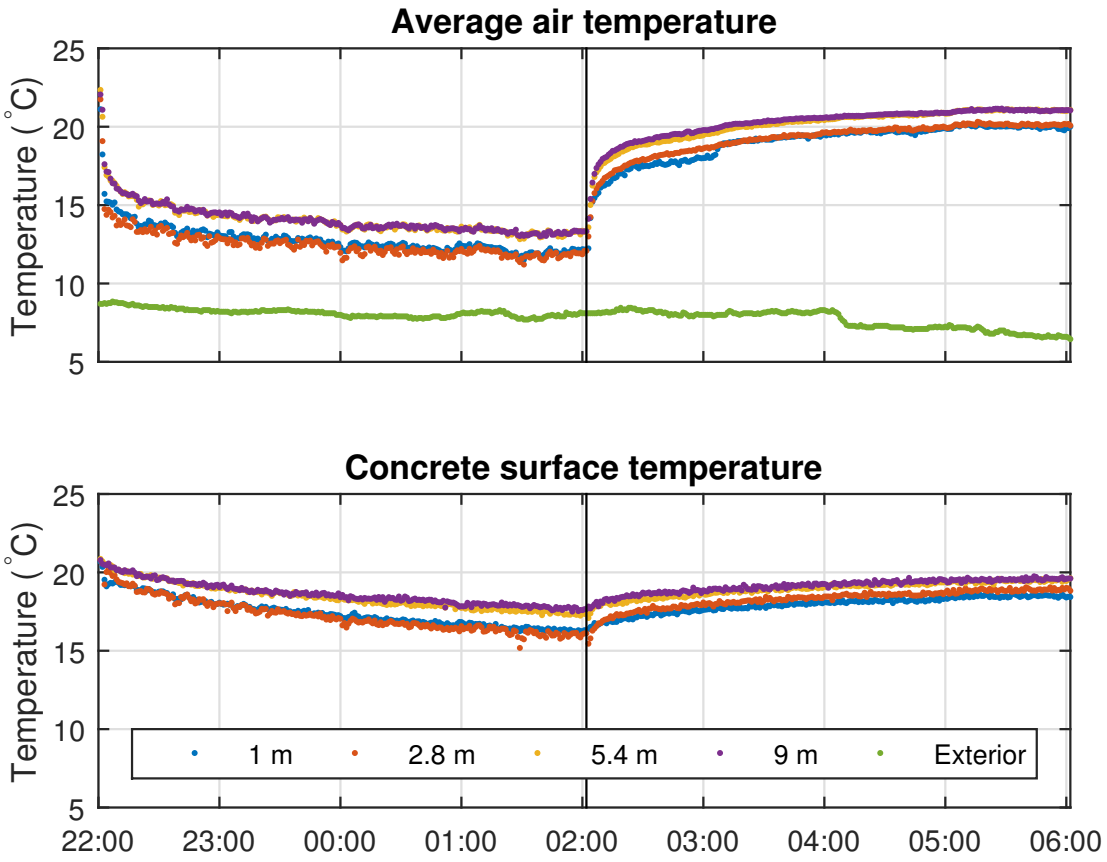

Figure 3.5: Average air and concrete temperature throughout the 2015 experiment

soon as the dampers close, and even when the exterior temperature is quite low at 8°C, it does not require more than half an hour for the air temperature to reach acceptable thermal comfort levels.

The air temperature during the night experiment of 2015 follows an exponential profile, both when the dampers are open and the temperature decreases, and when the dampers close and the temperature gets back to acceptable levels. The sensor at 2.8 meters shows a lower air temperature than that of 1 meters. The corridor can be divided into two sections: the primary, which is the first 5 meters and the secondary, which is the second 5 meters. The reason for that is that the measurements of the first and second sensors are clearly separated from the ones of the third and fourth [1]. During the 4 hours the concrete surface temperature of the primary region reached as low as 15.7°C and of the secondary 17.3°C. The

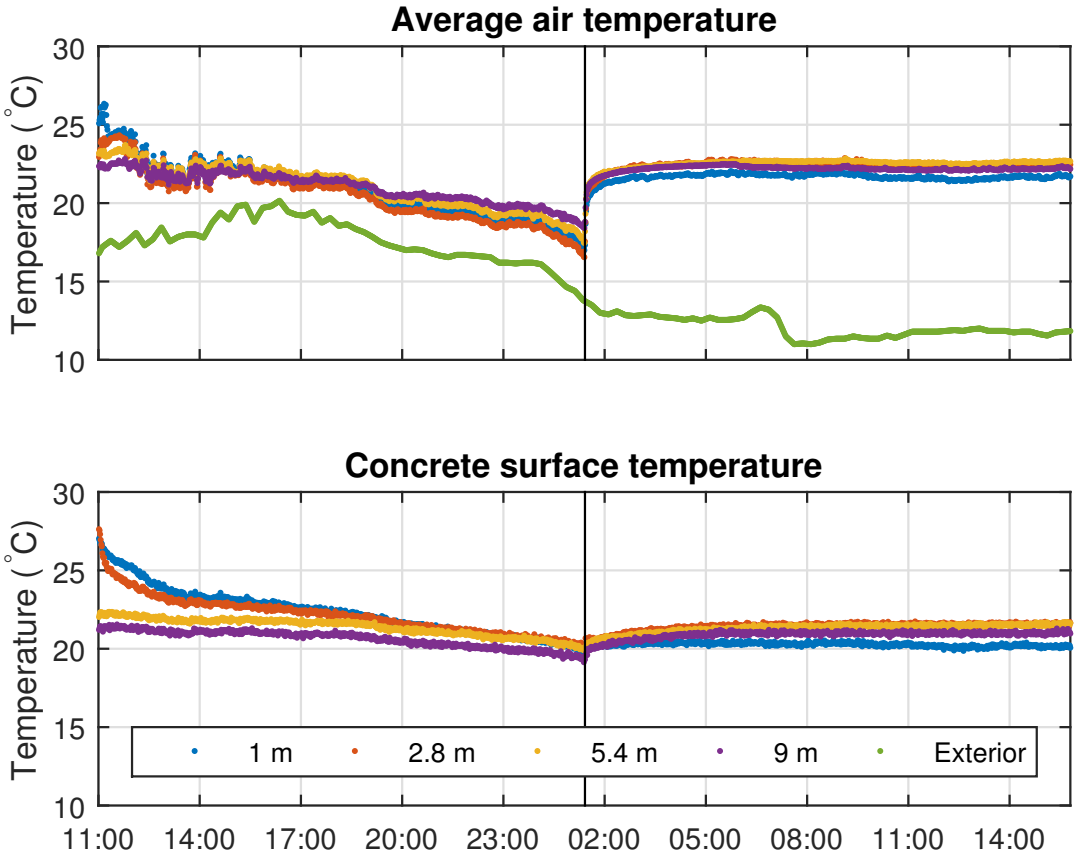

Figure 3.6: Average air and concrete temperature throughout the 2017 experiment

air temperature of the primary region is lower than the one of the secondary, suggesting that the heat transfer rate is higher. This is to be expected, because the temperature difference between the incoming and the interior air is higher. Yuan [1] argues that this difference in average air temperature between the primary and secondary region can be attributed to the placement of the sensors, since the ones in the secondary region are not on the main expected airflow path (further discussed in Section 4.1). However, the author believes that that they are indicative, since the cooling effect can be also seen in the concrete surface temperature, which is measured on the whole surface area with the infrared sensors.

The second experiment, in 2017, shows the thermal phenomena when the exterior temperature is above 15°C and solar radiation hits the façade. The air temperature is still decreasing exponentially, but there are more intense fluctuations because the temperature difference be-

tween the indoor and incoming air is not high. The first day was sunny (solar radiation is shown in Figure 3.7) and as a result the temperature of concrete surface at 1 m and 2.8 m is high when the experiment starts because of the direct solar gains. When there is no solar radiation, however, the air temperature has the same behavior as in the 2015 experiment, with the temperature at 2.8 m being the lowest. The concrete surface temperature though does not follow a similar pattern. When the dampers are open, the surface temperature of the sensors follows a reversed distribution compared to the 2015 experiment. This happens because in the 2017 experiment the exterior conditions tend to heat the building, and not to cool it. The lowest temperature it reaches is around 20°C for all the sensors, except for the one at 9 m, which falls as low as 19°C. When the dampers close the concrete surface temperature increases and stays constant at around 21°C at 1 m, 21.5°C at 2.8 m and 5.4 m and 20°C at 9 m.

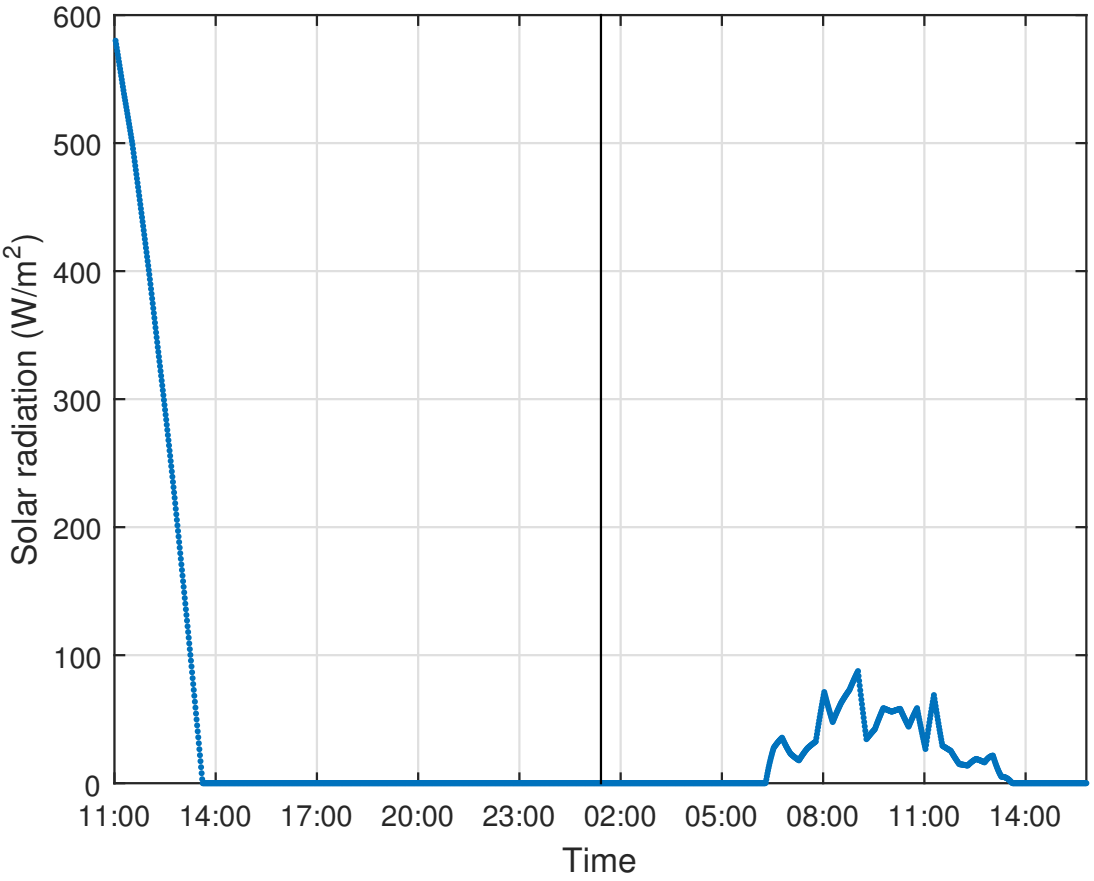

Figure 3.7: Solar radiation incident on the corridor façade throughout the 2017 experiment

3.4.2 Thermal comfort

According to ASHRAE Standard 55 [95] there are many sources of thermal discomfort that can be associated with natural or hybrid ventilation.

The first one is discomfort created from draft. The equations that estimate the discomfort from draft include the turbulence intensity of the draft, which is not known in these circumstances. Using the conservation of mass, the velocity at the inlet dampers results in an equivalent flow over the cross-section of the corridor. The maximum during the two experiments is 0.03 m/s, which is well below the discomfort limit, no matter what the turbulent intensity is.

The second source of discomfort is vertical air temperature difference. It represents the discomfort from the difference of temperatures at head level and ankle level. Thermal stratification cases, in which the air temperature at head level is cooler than the ankle level do not cause discomfort according to the standard. If the temperature at head level is warmer than the ankle level, then the allowed difference is maximum 3°C. For the 2015 experiment the largest temperature difference is 1.8°C and for the 2017 one 2.1°C. In both cases the discomfort created from vertical air temperature differences was below the limit.

CHAPTER 4

MODELING

The purpose of this thesis is to create a control strategy for the natural / hybrid ventilation system, based on thermal comfort criteria. The first 10 meters of the corridor were modeled. The simulation can be ran in real time, getting inputs from the BAS and the result will be the position of the dampers, which can be fed back to the BAS as a controlled variable for the system. That way the opening of the motorized dampers will be changed automatically to ensure thermal comfort in the corridors.

At first a preliminary transient computational fluid dynamics (CFD) with ANSYS FLUENT was used to model the heat transfer phenomena. However, the large computational resources required by FLUENT make the model unsuitable. The results were used to help understand the general behavior of the air flow.

Then, a faster and simpler transient finite difference model was developed in MATLAB. The information from the CFD simulation helped to make informed decisions for the assumptions. The model was calibrated with the experimental data of the 2017 experiment and then validated on the 2015 experiment. Different parameters were used for cooling (dampers open) and different for heating (dampers closed).

4.1 Preliminary analysis

The 10-meters long and 3-meters high corridor was modeled in FLUENT. The measured data were the boundary conditions to the model and a k-ω scheme was used to simulate the air flow.

Figure 4.1 shows the estimated air flow in the corridor. The air flows close to the left wall, then at approximately 3 meters from the inlet it crosses the corridor and hugs the right wall until the end of the corridor.

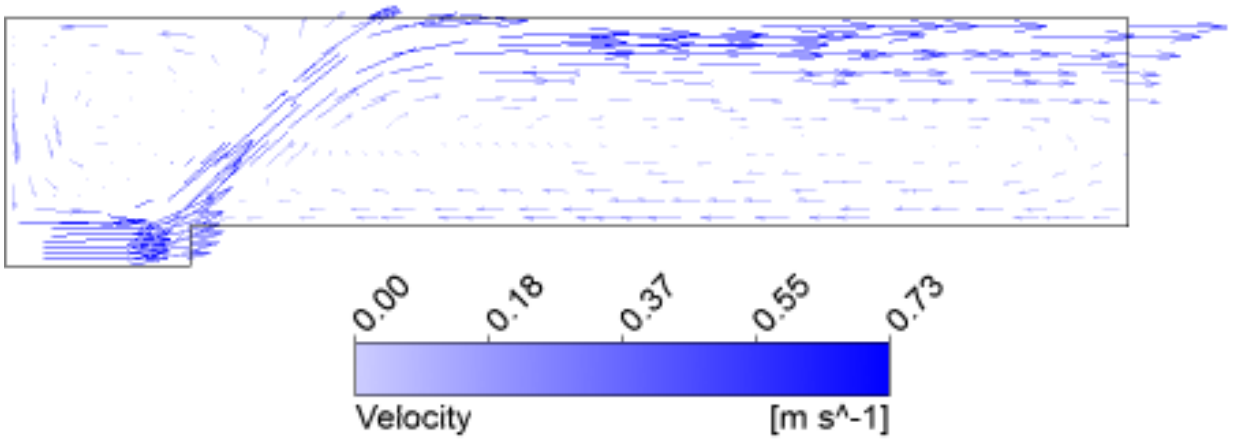

Figure 4.1: Plan view of the estimated air flow path from CFD simulation

There are two main regions of recirculation. The smaller one is close to the inlet and the bigger one on the left side of the corridor close to the end. This recirculation results in lower air velocities (below 0.2 m/s) than the main air flow, where the velocity is around 0.6 m/s. Therefore the heat transfer is expected to be higher on the main airflow path.

4.2 Model description

Since using the detailed airflow model from FLUENT was unsuitable, a simpler, faster model was created in MATLAB. This sections presents that model and the assumptions it is based on.

4.2.1 Geometry

The model emphasizes on the first 10 meters after the inlet of the air into the building. The difference of temperatures between the interior and exterior air will be highest there, and thermal comfort is more likely to be compromised. If thermal comfort is ensured there, then the occupants will feel comfortable everywhere. For this reason just the corridor is modeled, not the whole building.

To simplify the model the bend of the corridor at approximately 3 meters is not considered. The corridor is assumed to be a rectangular prism with dimensions 10 m x 1.8 m x 3 m. The floor is modeled as a 40-cm thick concrete slab.

Then the corridor was discretized into 4 control volumes along its length, as Figure 4.2 shows. The first control volume has length of 1.5 meters, the second and the third 3 meters each and the last one 2.5. The regions closer to the façade are smaller because the heat transfer is expected to be higher there.

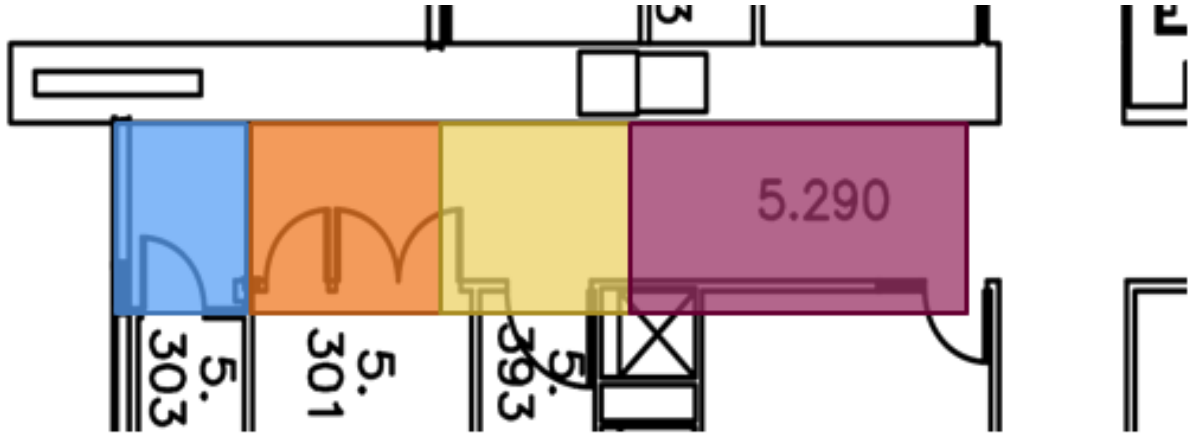

Figure 4.2: The corridor is discretized into 4 control volumes

The concrete is discretized into 10 layers, with thicknesses of 0.5 cm, 1.5 cm, 3 cm, 5 cm, 10 cm, 10 cm, 5 cm, 3 cm, 1.5 cm and 0.5 cm. This way the layers that are close to the surface have a small enough dimension, that their Biot number is low enough to satisfy the criterion for the lumped solid approximation, discussed in Section 2.1.2. If h is the convective heat transfer coefficient (W/m^2K), L the characteristic length (m) and k the thermal conductivity

(W/mK), then according to Equation (2.5) for concrete:

$$Bi = \frac{hL_c}{k} < 0.1 \Rightarrow h < \frac{0.1k}{L_c} \Rightarrow h < 34\,W/m^2K \tag{4.1}$$

From Equation (4.1) the approximation is valid if the convective heat transfer coefficient between the concrete and the air is less than 34 W/m^{2}K and the error is lower the smaller the number is. Figure 4.3 shows the discretization of the concrete slab.

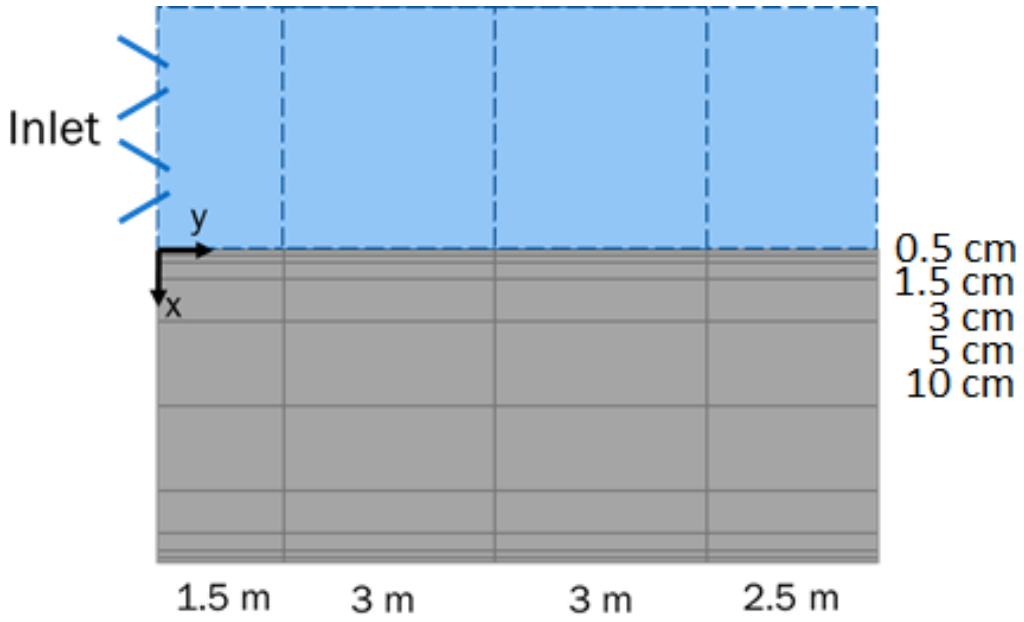

Figure 4.3: The concrete slab is discretized into layers. The layers are thicker in the middle. Courtesy of Sophie Yuan.

4.2.2 Estimation of air inlet temperature

In order to reduce the amount of sensors required for the operation and control of the hybrid ventilation system, the air inlet temperature was correlated to the temperature of the weather station. That can be done for any floor of the building, giving robustness to the model. The equation used is Equation (4.2), with a Root Mean Squared Error (RMSE) of 0.532 °C and a coefficient of determination (R^2) of 0.986. T_{inlet} is the inlet air temperature (°C), T_{ws} is the temperature measured at the weather station (°C), t is the time the dampers

are open (min) and S is the solar radiation incident on the façade of the corridor (W/m^2). More information about the procedure and the uncertainty can be found in Appendix D.1.

$$T_{inlet} = 1.0515T_{ws} - 0.42222(T_{ws} - 21)t^{-0.49935} + 0.0088051S + 2.1573 \tag{4.2}$$

4.2.3 Estimation of air inlet velocity

The weather station measures wind speed and direction. However, the inlet air velocity was not found to be correlated to them, either because not enough data were available, or because of the local effects from the nearby buildings and roads. The air inlet velocity for the two experiments is shown in Figure 4.4. It is observed that no matter the reading of the weather station (which ranged from 0.1 m/s to 6.5 m/s), the air inlet velocity is fluctuating between 0.2 m/s and 0.5 m/s, even though the weather conditions during the two experiments were significantly different. For this reason it is assumed that it follows a Gaussian distribution around the mean value of the measured data. From both experiments the mean value is $0.360 \pm 0.003\, m/s$ and the standard deviation $0.053 \pm 0.002\, m/s$.

4.2.4 Estimation of effective surface temperature

In order to simplify the model and keep the number of nodes (and sensors needed) to the minimum, the vertical walls and the suspended ceiling are combined to one effective temperature based on their area, according to Equation (4.3).

$$T_{sfc} = \frac{T_{left\,wall}A_w + T_{right\,wall}A_w + T_{ceil}A_{ceil}}{2A_w + A_{ceil}} \tag{4.3}$$

Then this temperature is correlated to the concrete surface temperature T_c (°C), the inlet air temperature T_{inlet} (°C), the time the dampers are open t (min) and the solar radiation S (W/m^2) when the dampers are open and just the concrete surface temperature T_c (°C) and the time the dampers have been closed t (min) when the dampers are closed. The equations are shown in Equation (4.4) and Equation (4.5). The RMSEs are between 0.1 °C and 0.39 °C, with the lowest R^2 being 0.87. The assumption that when the dampers are closed the temperature of the combined surfaces is not affected by the air inlet temperature T_{inlet} (°C)

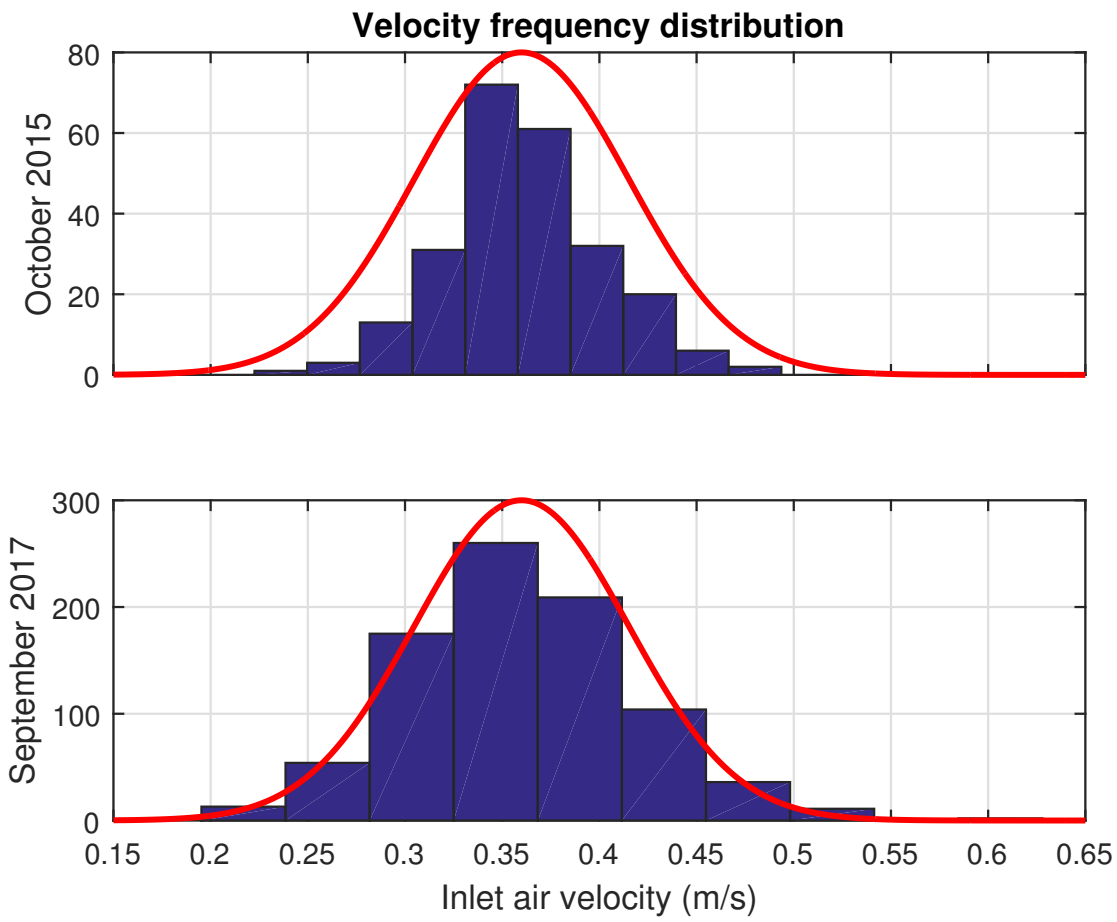

Figure 4.4: Air inlet velocity frequency distribution during the two experiments

is accurate, since there is no air flow from the outside, so the effect will be minimal. However, there will be an effect from the solar radiation S, especially on the first control volume. The day that the dampers were closed was a rainy day and there are not enough data available for the correlation. More information can be about the procedure and the uncertainty can be found in Appendix D.2.

$$T_{sfc} = \alpha T_c + \beta(T_{inlet} - 21)t^{\gamma} + \delta T_{inlet} + \epsilon S + \zeta \tag{4.4}$$

$$T_{sfc} = \alpha T_c + \beta t^{\gamma} + \delta \tag{4.5}$$

4.2.5 Equations and thermal network

The heat transfer equations were solved with an implicit finite difference method. The second order spatial derivatives are discretized as second-order central differences and the temporal derivative as a backward difference. The general equation for node i is shown in Equation (4.6).

$$\sum_{j=0}^{NJ}\left(U_{ij}^{n+1}(T_j^{n+1}-T_j)\right)-\frac{C}{\Delta t}T_j^{n+1}=-\dot{Q}_i^{n+1}-\frac{C}{\Delta t}T_i^n \tag{4.6}$$

where:

U_{ij} (W/K), conductance between nodes i and j. For conductance equal to $\frac{2Ak}{dx}$ and for convection $h_{conv}A$;

T_i^n (°C), temperature of node i at timestep n;

C (J/K), capacitance of the node, equal to $\rho AC_p dx$;

$\dot{Q}_i$ (W), heat flow into node i;

Δt (s), timestep;

NJ, total amount of nodes.

If Equation (4.6) is written in a matrix form it results to Equation (4.7). N is the number of thermal nodes and M is the number of thermal nodes that have a specified temperature:

$$\mathbf{UT}^{n+1}=\mathbf{Q} \tag{4.7}$$

where

$$\mathbf{U}=\begin{bmatrix} (\sum_i^N U_{1N}+\sum_i^M U_{1M}+\frac{C_1}{\Delta t}) & -U_{12} & \cdots & -U_{1N} \\ -U_{21} & (\sum_i^N U_{2N}+\sum_i^M U_{2M}+\frac{C_2}{\Delta t}) & \cdots & -U_{2N} \\ \vdots & \vdots & \ddots & \vdots \\ -U_{N1} & -U_{N2} & \cdots & (\sum_i^N U_{NN}+\sum_i^M U_{NM}+\frac{C_1}{\Delta t}) \end{bmatrix}$$

$$\mathbf{T} = \begin{bmatrix} T_1 \\ T_2 \\ \vdots \\ T_N \end{bmatrix}$$

$$\mathbf{Q} = \begin{bmatrix} \dot{Q}_1 + \sum_M U_{1M} T_M + \frac{C_1}{\Delta t} T_1^n \\ \dot{Q}_2 + \sum_M U_{2M} T_M + \frac{C_2}{\Delta t} T_2^n \\ \vdots \\ \dot{Q}_N + \sum_M U_{NM} T_M + \frac{C_N}{\Delta t} T_N^n \end{bmatrix}$$

The equivalent thermal network of the corridor is shown in Figure 4.5.

4.2.6 Air velocity factors, effective heat transfer coefficients and power output

As explained in Section 4.1 there is recirculation of air throughout the 4 control volumes. For this reason correction factors were applied to the velocity of the air. The correction factors were calibrated with the 2017 experiment. Inlet velocity when the dampers are closed is 0.

The radiation between the surfaces is not considered directly. Instead, an effective heat transfer coefficient is used to account for the convection and the radiation. It represents the effect of the heat from luminaires as well. These coefficients were calibrated with at the same time with the air velocity factors.

The model parameters were fit by minimizing the least squares error. The function `lsqcurvefit` is a non-linear optimization technique in MATLAB that minimizes the sum of the squares of absolute differences between the estimated temperatures and the measured ones. Different values were used when the dampers are open and different when they are closed, since the air flow will change, affecting the heat transfer to and from surfaces. The confidence intervals were computed with MATLAB function `nlparci`. Appendix E explains how the command computes the confidence intervals.

The results of the fitting for open dampers are presented in Table 4.1.

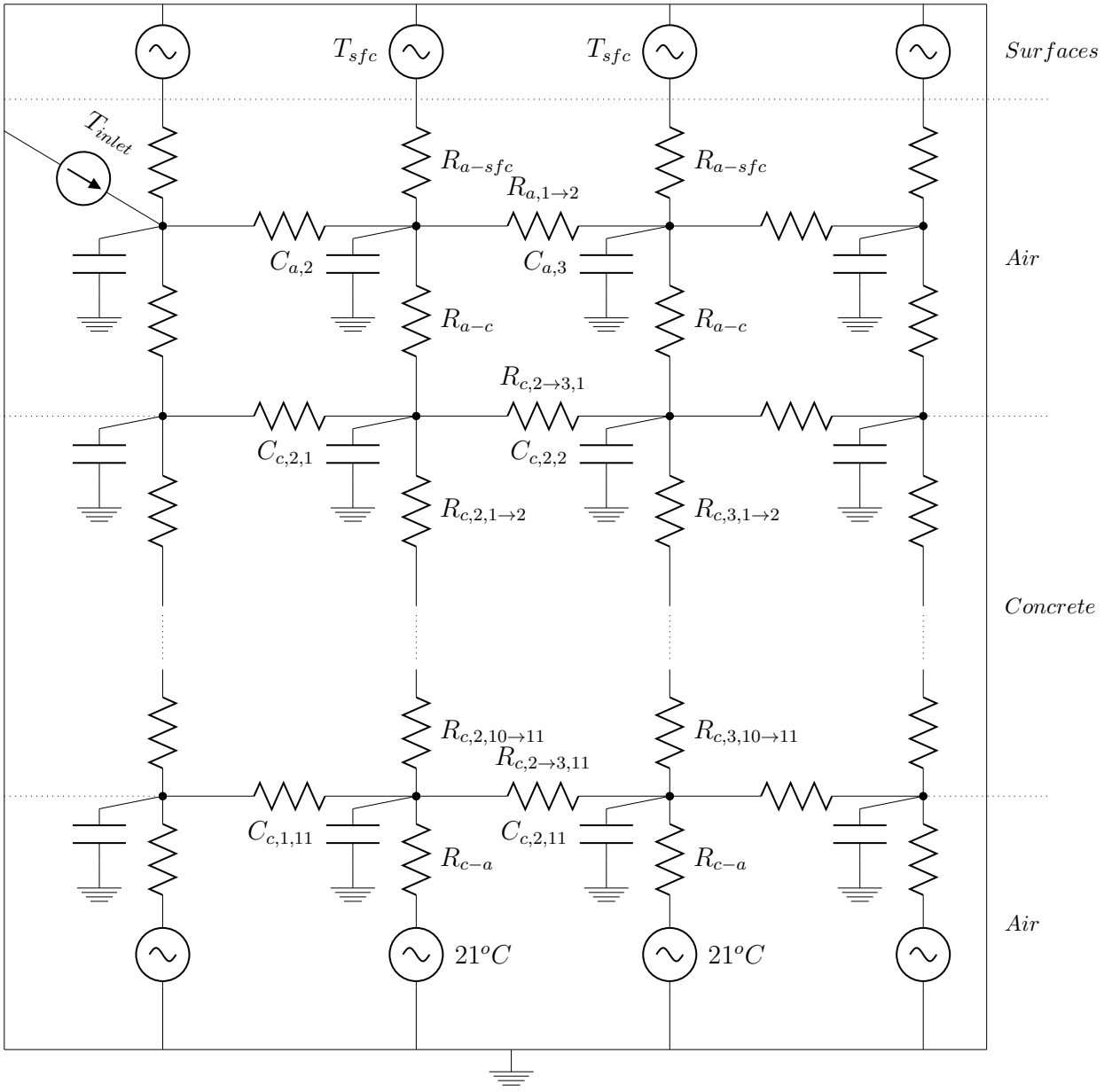

Figure 4.5: Thermal network of the modeled corridor. The first subscript expresses the object (a for air, sfc for combined surfaces and c for conrete), the second subscript the control volume of the corridor and the third the node of the layers of the concrete (1 being the concrete surface and 11 the surface of the roof of the floor underneath)

It can be observed that the heat transfer coefficients between the air and the combined surfaces have a confidence interval that includes 0. This translates to the fact that these coefficients are not proven to be significantly different from 0. This does not mean that they *are* 0; it means that it cannot be proven that they are *not*, or at least that this cannot be

Table 4.1: Air velocity correction factors f_v to account for recirculation of the air in the corridor and effective heat transfer coefficients between air and concrete $h_{a\text{-}c}$ and air and combined surfaces $h_{a\text{-}sfc}$ when the dampers are open. The index represents the control volume

Variable	Bounds	Value	95% confidence interval
$f_{v,1}$	[0,1]	1.00	[0.564, 1.437]
$f_{v,2}$	[0,1]	1.00	[0.237, 1.763]
$f_{v,3}$	[0.1,1]	0.100	[0.0816, 0.118]
$f_{v,4}$	[0.1,1]	0.100	[0.0540, 0.146]
$h_{a\text{-}c,1}$ (W/m^{2}K)	[1,25]	17.73	[16.63, 18.82]
$h_{a\text{-}c,2}$ (W/m^{2}K)	[1,25]	23.91	[22.33, 25.48]
$h_{a\text{-}c,3}$ (W/m^{2}K)	[1,25]	10.09	[8.697, 11.49]
$h_{a\text{-}c,4}$ (W/m^{2}K)	[1,25]	11.52	[9.871, 13.17]
$h_{a\text{-}sfc,1}$ (W/m^{2}K)	[1,15]	1.00	[-118, 120]
$h_{a\text{-}sfc,2}$ (W/m^{2}K)	[1,15]	1.00	[-34.3, 36.3]
$h_{a\text{-}sfc,3}$ (W/m^{2}K)	[1,15]	1.00	[-1.84, 3.84]
$h_{a\text{-}sfc,4}$ (W/m^{2}K)	[1,15]	1.00	[-5.33, 7.33]

captured with the specific data. This model is a physics-based model however, and in that aspect it is impossible that no heat exchange happens between the vertical walls and the air or the ceiling and the air. It is likely, though, that this heat exchange is so small that was not accurately captured in the available data. For this reason, until more data become available, these coefficients will be considered to be 1 W/m^{2}K.

The results of the fitting for closed dampers are presented in Table 4.2. The heating output of the HVAC system was modeled to be controlled by a typical PI controller and through the fitting, the maximum output was defined.

When the dampers are closed the dominant heat transfer is between air and combined surfaces, and not so much between air and concrete, except for control volume 4. The maximum power output is the same for both heating and cooling modes.

Table 4.2: Maximum power output to each control volume Q, effective heat transfer coefficients between air and concrete $h_{closed,a\text{-}c}$ and air and combined surfaces $h_{closed,a\text{-}sfc}$ when the dampers are closed. The index represents the control volume

Variable	Bounds	Value	95% confidence interval
Q_1 (W)	[0,500]	149.6	[118.6, 180.5]
Q_2 (W)	[0,500]	254.8	[235.0, 274.7]
Q_3 (W)	[0,500]	143.6	[131.9, 155.2]
Q_4 (W)	[0,500]	79.61	[71.69, 87.52]
$h_{closed,a\text{-}c,1}$ (W/m^2K)	[1,25]	2.000	[1.827, 2.173]
$h_{closed,a\text{-}c,2}$ (W/m^2K)	[1,25]	8.238	[7.918, 8.558]
$h_{closed,a\text{-}c,3}$ (W/m^2K)	[1,25]	6.550	[6.339, 6.760]
$h_{closed,a\text{-}c,4}$ (W/m^2K)	[1,25]	5.393	[5.210, 5.577]
$h_{closed,a\text{-}sfc,1}$ (W/m^2K)	[1,15]	12.47	[10.27, 14.67]
$h_{closed,a\text{-}sfc,2}$ (W/m^2K)	[1,15]	9.005	[5.721, 12.289]
$h_{closed,a\text{-}sfc,3}$ (W/m^2K)	[1,15]	14.99	[11.69, 18.29]
$h_{closed,a\text{-}sfc,4}$ (W/m^2K)	[1,15]	1.473	[-1.895, 4.841]

4.2.7 Summary of assumptions

- The geometry is simplified (Section 4.2.1).
- The corridor is divided into 4 control volumes, each represented by one node for the air, one for the surface of the concrete and one for the rest of combined surfaces (Section 4.2.1).
- The solar radiation is indirectly taken into account. The direct solar heat gains on the concrete are not considered, but the effect on the air inlet temperature is (Section 4.2.2).
- Radiation between the surfaces is considered indirectly, using a combined heat transfer coefficient. The values are calibrated with the measurements of the 2017 experiment (Section 4.2.6).
- The properties of air and concrete used in this study are considered to be constant and

the same as in previous studies [1, 155, 158] (Table 4.3).

Table 4.3: Properties of concrete and air

Property	Concrete	Air
Density ρ (kg/m^3)	1700	1.2
Specific heat capacity C_p (J/kgK)	800	1005
Thermal conductivity k (W/mK)	1.7	-

- To account for the recirculation of the air, correction factors are applied to air velocity at each control volume (Section 4.2.6).
- The air inlet temperature is correlated to the weather station temperature and the solar radiation (Section 4.2.2).
- The air inlet velocity is assumed to follow a Gaussian distribution with the mean value and the standard deviation of the measurements (Section 4.2.3).
- When the dampers are closed the heating of the corridor is modeled as an air heater with a PI controller. The values of this PI controller were calibrated using the measurements of the 2017 experiment.

4.3 Evaluation of performance

To evaluate the performance of the model, the two experiments were simulated. A good performance is expected on the 2017 experiment, since this was the one used to calibrate all the parameters of the model. Then the model estimates the temperatures for the 2015, the data of which it has never "seen" before. Goodness of fit is computed for each one, along with the confidence interval of each prediction using MATLAB and its built-in function `nlpredci`, which computes the confidence interval. Appendix E explains how this command computes the confidence interval.

4.3.1 Open dampers

For each experiment there are 8 sets of measured data – 4 for average air temperature and 4 for concrete surface temperature – that need to be compared with the predicted values. Because of the high number of lines, the figures are shown in Appendix E, where the 95% confidence interval for each line is also shown. All the measured temperatures are within the confidence interval computed by the model, except for the concrete surface of control volume 1 and 2 of the 2015 data. The model underpredicts the temperature and the measured values are just above the confidence interval. Table 4.4 shows the root mean squared error (RMSE) and the coefficient of variation of the root mean squared error (CVRMSE) for concrete surface temperature and average air temperature, for the two experiments.

Table 4.4: Goodness of fit for open dampers

	Metric	Control Volume	1	2	3	4
2017	RMSE (°C)	Average air	0.64	1.00	0.59	0.58
		Concrete surface	0.23	0.52	0.32	0.84
	CVRMSE (%)	Average air	3.01	4.68	2.76	2.72
		Concrete surface	1.02	2.31	1.45	3.94
2015	RMSE (°C)	Average air	0.96	0.36	0.26	1.02
		Concrete surface	1.46	1.66	0.17	0.22
	CVRMSE (%)	Average air	8.05	2.91	1.80	6.77
		Concrete surface	9.08	10.59	0.90	1.18

The model simulates the 2017 data with good accuracy, since the RMSE is less than 1 °C and the CVRMSE is below 5 %. When the 2015 data are presented, which the model has not "seen" before, the performance is worse than with the 2015 data, which is expected. The accuracy is still acceptable, with the maximum RMSE being approximately 1.7 °C and the maximum CVRMSE 10.6 %.

The model also predicts the total cooling achieved with the hybrid ventilation system. The concrete slab is "discharged" without the HVAC system operating. A total of $-0.23 \pm 0.01\, kWh/m^2$ are dissipated from the concrete slab (the minus sign indicates

that the heat is being extracted from the slab) during the 2015 experiment and a total of $-0.18 \pm 0.05\, kWh/m^2$. Although the 2017 experiment was significantly longer than the 2015, the temperature difference between the interior and exterior temperature was smaller, and this is reflected in the amount of cooling stored in the concrete slab.

This is not the only form of cooling happening during the operation of the hybrid ventilation system. When the air reaches the end of the corridor it is cooler than the interior air, suggesting that it will provide more cooling as it moves towards the interior of the building. Assuming that the interior of the building is at 21°C, this extra cooling was $-0.063 \pm 0.003\, kWh/m^2$ (the minus sign indicates that heat is being extracted from the core of the building) during the 2015 experiment and $0.017 \pm 0.005\, kWh/m^2$ during the 2017 experiment. This indicates that the air coming in during the 2017 experiment tended to heat the building more after passing through the corridor. It still "discharged" the concrete of the corridor though.

4.3.2 Closed dampers

Similarly the model was tested for when the dampers are closed, using the data from the experiments. Most of the measured temperatures are within the confidence interval. The concrete surface of the first control volume of the 2017 data is slightly overpredicted by the model. Similarly, the air temperature of the first and third control volume and the concrete surface temperature of the fourth control volume of the 2015 data are underpredicted by the model. Table 4.5 shows the root mean squared error (RMSE) and the coefficient of variation of the root mean squared error (CVRMSE) for concrete surface temperature and average air temperature, for the two experiments.

All the RMSEs are less than 0.75 °C and the maximum CVRMSE is about 2.2 %, suggesting that the model predicts the temperatures well.

4.4 Estimation of thermal comfort

To estimate thermal comfort Fanger's model was used, shown in Equation (4.8).

Table 4.5: Goodness of fit for closed dampers

	Metric	Control Volume	1	2	3	4
2017	RMSE (°C)	Average air	0.21	0.33	0.51	0.52
		Concrete surface	0.44	0.15	0.12	0.21
	CVRMSE (%)	Average air	0.98	1.50	1.17	1.06
		Concrete surface	2.15	0.71	0.55	1.03
2015	RMSE (°C)	Average air	0.73	0.28	0.70	0.61
		Concrete surface	0.34	0.37	0.37	0.38
	CVRMSE (%)	Average air	3.99	1.49	3.57	3.11
		Concrete surface	1.94	2.08	1.99	2.00

$$\begin{aligned} PMV = (0.303e^{-0036M} + 0.028)\Big\{&(M-W) - 3.05\cdot 10^{-3}\Big[5733 - 6.99(M-W) - p_{v,a}\Big] \\ &- 0.42\Big[(M-W) - 58.15\Big] - 1.72\cdot 10^{-5} M\Big[5876 - p_{v,a}\Big] - 1.4\cdot 10^{-3} M(34 - T_a) \\ &- 3.95\cdot 10^{-8} f_{cloth}\Big[(T_{cloth}+273.15)^4 - (T_{mrt}+273.15)^4\Big] - f_{cloth} h_{conv}(T_{cloth} - T_a)\Big\} \end{aligned} \tag{4.8}$$

where

M (W/m^2), metabolic activity. In this case equal to 115 W/m^2 for casual walking [52];

W (W/m^2), rate of mechanical work accomplished. It is assumed to be zero for most cases [52];

$p_{v,a}$ (Pa), partial pressure of water vapor in ambient air [96]. It is calculated from the available weather data with basic psychometric equations explained in Appendix C;

T_a (°C), ambient air temperature;

f_{cloth}, clothing area factor, equal to $1.05+0.1I_{cl}$, where I_{cl} (clo) is the clothing insulation. In this case for trousers and long-sleeved shirt it is 0.6 [91];

T_{mrt} (°C), mean radiant temperature. For a standing person it can be estimated as

$$T_{mrt} = \frac{0.08(T_{pr}(up) + T_{pr}(dn)) + 0.23(T_{pr}(r) + T_{pr}(l)) + 0.35(T_{pr}(fr) + T_{pr}(b))}{1.32}$$

where T_{pr} is the plane radiant temperature [91];

h_{conv} (W/m^{2}K), convective heat transfer coefficient between the person and the air. It can be estimated as

$$h_{conv} = \begin{cases} 2.38(T_{cl} - T_a)^{0.25}, & \text{if } 2.38(T_{cl} - T_a)^{0.25} > 12.1\sqrt{V} \\ 12.1\sqrt{V}, & \text{if } 2.38(T_{cl} - T_a)^{0.25} < 12.1\sqrt{V} \end{cases}$$

where V (m/s) is the air velocity;

T_{cloth} (°C), clothing temperature that can be estimated by [96]:

$$\begin{aligned} T_{cloth} =& 35.7 - 0.028(M - W) - 0.155 I_{cloth} \cdot \\ & \Big\{ (M - W) - 3.05 \cdot 10^{-3} \Big[5733 - 6.99(M - W) - p_{v,a} \Big] \\ & - 0.42 \Big[(M - W) - 58.15 \Big] - 1.72 \cdot 10^{-5} M \Big[5876 - p_{v,a} \Big] \\ & - 1.4 \cdot 10^{-3} M (34 - T_a) \Big\} \end{aligned}$$

To use the PMV index for non steady-state conditions, the average PMV of an hourly period is used [113].

To evaluate the adaptive PMV Equation (2.6) is used, which is repeated here for reference.

$$aPMV = (PMV^{-1} + \beta)^{-1}$$

From the PMV or the aPMV the PPD is estimated from Equation (2.7), which is repeated here.

$$PPD = 100 - 95 e^{-0.03353 PMV^4 - 0.2179 PMV^2} \tag{4.9}$$

According to [119] the PMV limit in corridors can be extended to [-1.5,1.5], which translates to PPD < 50 %.

CHAPTER 5

CONTROL STRATEGIES OF HYBRID VENTILATION SYSTEMS

In this chapter different control strategies are applied to the model, to see their effect on thermal comfort and energy savings.

At first the discomfort and energy savings of the current control strategy are evaluated. Then a proper adaptive comfort model is chosen and a control strategy with thermal comfort as the criterion is presented. The last part of this chapter presents various predictive control algorithms and studies the effect of the control and prediction horizon, of weighting discomfort against energy savings, of night precooling and of modulated control of the motorized dampers.

5.1 Current control strategy (reference case)

To test the performance of different control strategies the first step is to choose appropriate days to simulate. The days of 13^{th}–24^{th} May, 2016 include exterior temperatures of down to 3 °C and up to 30 °C. This range covers cases of temperatures that are too high or too low for the hybrid ventilation system and some days that are ideal. Figure 5.1 shows the temperature, the solar radiation and the humidity content.

As discussed in Section 3.1 the system works based on temperature and humidity content

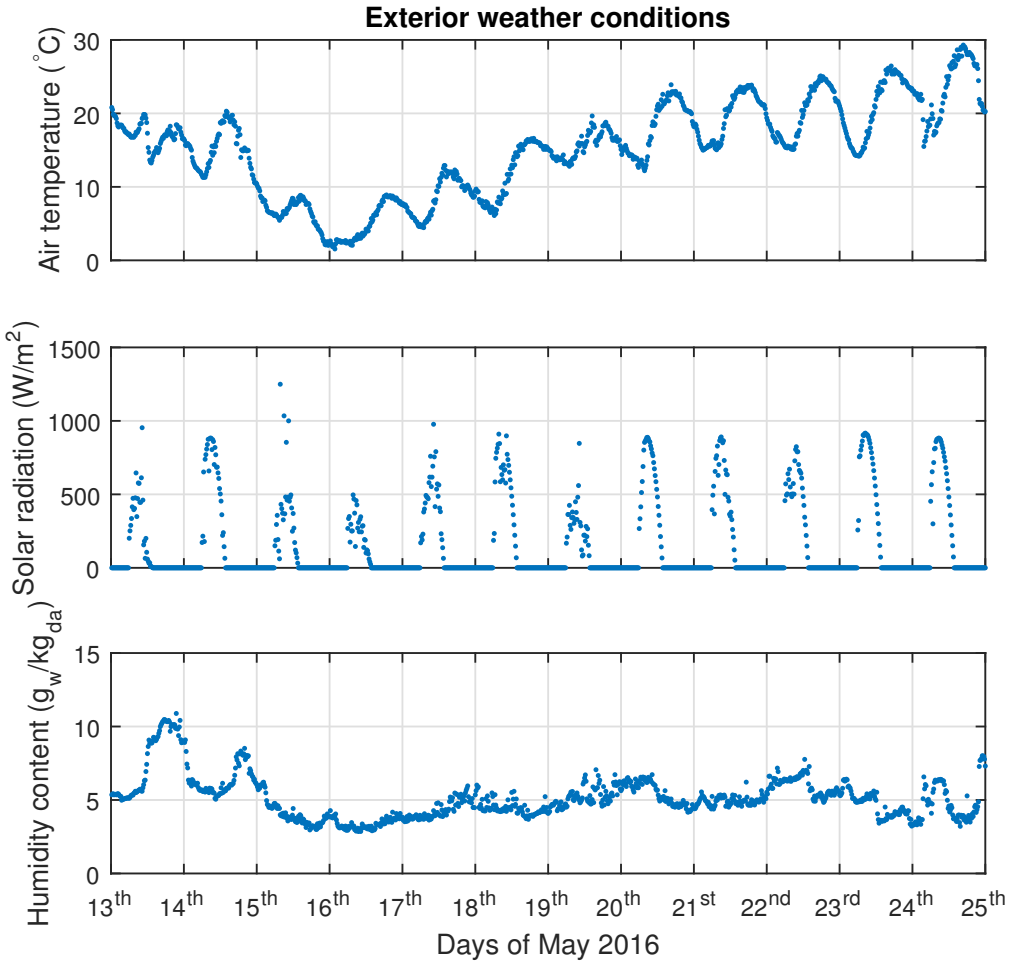

Figure 5.1: Weather station air temperature, solar radiation incident on the corridor façade and air humidity content

setpoint deadbands. The low temperature deadband is 14–15 °C, the high temperature deadband is 22–23 °C and the humidity content deadband is 9–9.5 g_{water}/kg_{dry_air}. This case will serve as the reference case to which the rest of the simulation results will be compared.

To assess how this control strategy affects thermal comfort the PPD index is computed with as an hourly average. Thermal comfort is only of interest at the last 2 control volumes. Close to the dampers there is only a fire escape staircase, and people are not expected to pass by. However, close to the end of the corridor, at about 6 meters, there is a conference room, where people are bound to stand or pass by. For this reason only at the last 2 control volumes is the PPD index computed and compared to the limit, which is 50 % (Section 4.4).

The discomfort is presented in PPD-hours, which is the product of the discomfort above the limit (as a PPD percentage) and its respective time length. 1 PPD-hour can mean that the PPD is above the 50 % limit by 1 % (51 % PPD total) for one hour, or above the limit by 12 % (62 % PPD total) for five minutes, or above the limit by 0.1 % (50.1 % PPD total) for 10 hours. The reason for that is that just by reporting the hours the PPD index was above the limit does not reflect the intensity of the discomfort.

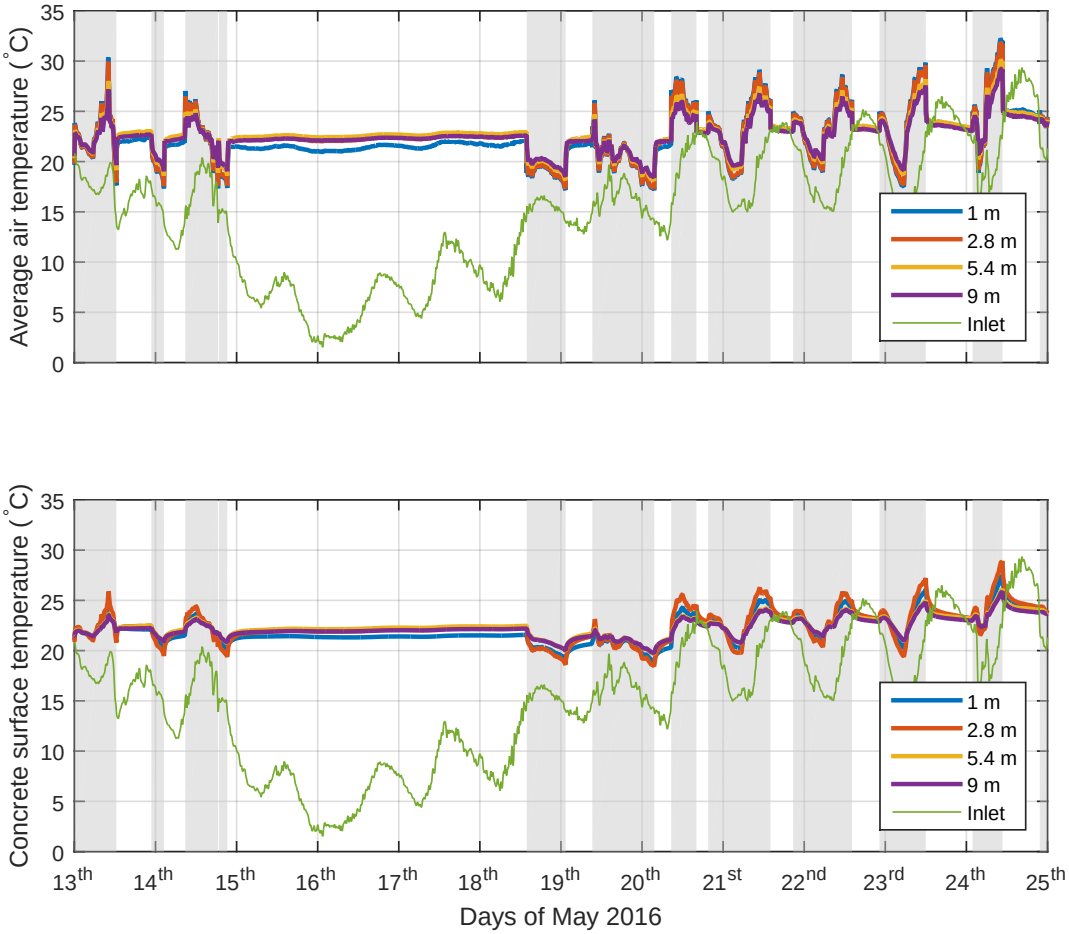

Figure 5.2: Predicted average air and concrete surface for reference control strategy. The grey area indicates that the hybrid ventilation is on

Figure 5.2 shows the average air and concrete surface temperature, as predicted by the model. The grey area shows that the hybrid ventilation is working. On the 13th the system stops working because the humidity content is too high. Between the 15th and the 18th the

exterior temperature is too low for the dampers to open, and for the 21st to 25th the system is operating during the night hours and is closed during the day because the temperature is too high.

The hybrid ventilation system is operating for 126.3 hours, or 43.9% of the time. The air temperature never falls below 17°C in any of the zones and the concrete surface lowest temperature is 18.5°. The difference between the weather temperature temperature and the air inlet temperature results in the system operating when the latter is too high. It reaches 32°C at its maximum, while that overheats the concrete slab as well, which reaches up to 29°C.

As a result the PPD index was above the 50 % limit for approximately 50 hours or 17.5 % of the time that was simulated (40 % of the time the hybrid ventilation system was working). The average discomfort in control volume 3 and 4 is shown in Figure 5.3. The high discomfort is the result of high temperatures and gets higher towards the last days of the simulation. When the discomfort is above the limit, it exceeds it by a lot, resulting in a total of 892 PPD-hours. In terms of energy savings potential, the concrete slab was cooled a total of -1.00 kWh/m^2 and the potential energy from the air was -0.45 kWh/m^2. The total energy inserted into the space (heating and cooling) is 3.35 kWh/m^2, suggesting that more energy is used to condition the corridor from the mechanical ventilation, than from the hybrid ventilation system. This does not include the energy from the fans for the recirculation of the air.

Despite the algorithm indicating that the discomfort exceeds the limit for 17.5% of the time, there were no complains during the operation of the hybrid ventilation during the last two summers. Most of the discomfort, according to Figure 5.3 comes from air temperature being too high. This proves what was presented in the literature review (in Section 2.1.3), that the PMV model does not apply to naturally ventilated spaces, since it overestimates the discomfort when the conditions are warm [114].

5.1.1 Adaptive thermal comfort

For this reason different adaptive models from the literature review were tested. The discomfort was evaluated and compared to the reference case, which was calculated with the

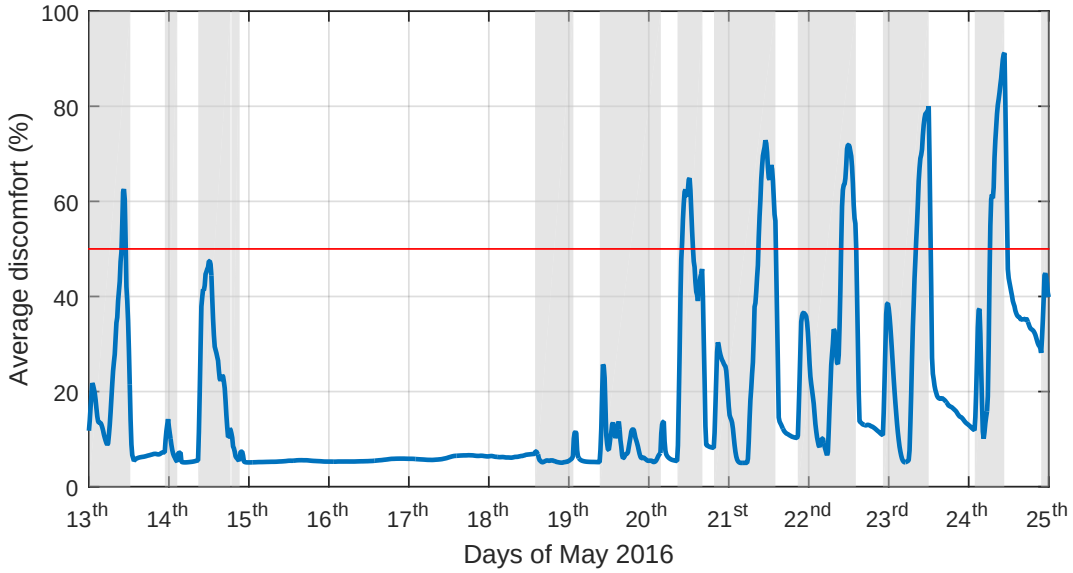

Figure 5.3: Average PPD index for reference case. The grey area indicates that the hybrid ventilation is on

standard Fanger's model.

Parameter β for the adaptive PMV model is taken from Table 2.1. The table is repeated here for reference.

Table 5.1 shows the results for the various β coefficients in Table 2.1. The obvious limitation when using these adaptive models is the fact that they were created for different environments and climates: Chongqing (China), Xian (China), Beijing (China) and Seoul (South Korea). The ideal action would be to perform a comfort study using questionnaires in the corridors of the EV building when the hybrid ventilation system is in operation and then use the results to calibrate the β value. According to the available information, there have been no complaints about the conditions of the corridors. The closest simulation result to that is using the β values suggested by Yao et al. [108]. For this reason the following simulations use those values.

Table 2.1: Coefficient β for equation (2.6) based on various studies

Author and reference	β
Yao et al. [108]	0.293 for warm (22–38 °C) -0.125 for cool (8–18 °C)
Gao et al. [109]	0.029 for indoor air velocity 0–0.2 m/s 0.167 for 0.2–0.8 m/s
Xu et al. [110]	0.285 for warm (30–34 °C) and indoor air velocity 0.3–0.6 m/s -0.136 for cool (8–15 °C)and 0.1–0.2 m/s
Kim et al. [111]	-1.40 warm (25–32 °C) -5.74 cool (14–24 °C)
Song et al. [112]	0.64 in HHE, -0.06 in CE and PMV<0 1.07 in CE and PM>0, -0.37 in CDE

5.2 Thermal comfort as control variable

In order to maximize the energy saved through the concrete slab, the first step is to form a control strategy that always keeps the hybrid ventilation system open, unless the PPD index is violated. The motorized dampers change position every 15 minutes to prevent excessive noise and damage on the actuators. For this reason, a control strategy was tested, according to which the system checks every 15 minutes the discomfort index of the past hour, and if it is at all times less than the limit, then the dampers are kept open. If thermal comfort criteria are not met, then the dampers close. This model is reactive, which means that all the information needed to make a decision is based on past data and no prediction is made for the future. Figure 5.4 shows the average air and concrete surface temperatures for this control strategy.

Comparing Figure 5.4 to Figure 5.2, the two most obvious differences are that in Figure 5.4 the system is operating for a greater time than in Figure 5.2 and that the dampers open and close often when the exterior temeprature is too high or too low, which leads to big oscillations in temperature.

Figure 5.5 shows the discomfort throughout the simulation. When the exterior temperature is too high or too low the system starts operating for a short amount of time, then

Table 5.1: Performance of various adaptive models

Author and reference	Discomfort > 50 %		
	hours	% of operation time	PPD-hours
Reference case	50.25	39.8%	892
Yao et al. [108]	2.25	1.8%	11
Gao et al. [109]	42.25	33.4%	695
Xu et al. [110]	47.25	37.41%	728
Kim et al. [111]	13	10.3%	134

the discomfort exceeds the limit and the dampers close. As soon as an hour passes with comfortable conditions, the system will start operating again, exceeding the discomfort limit almost immediately, because the outdoor air is temperature is too low. This is the result of the reactive nature of the control. Consequently, the minimum air temperature is 6.5 °C and the minimum concrete surface temperature is 12.5 °C. When the exterior temperature is high, the air temperature reaches up to 33 °C and the concrete surface up to 28.5 °C.

There is a big difference in the concrete surface temperature between Figure 5.2 and Figure 5.4. In the former, the dampers are kept close the whole time the exterior temperature is low, resulting in a concrete surface temperature of about 21 °C when the days started being warmer (May 21 $^{\text{th}}$). On the other hand, in the latter, the concrete surface temperature is oscillating around 16.5 °C the days that the exterior temperature is low, and when the warmer days come, the concrete is ready to absorb part of the heat, so that no active cooling would be needed.

The system is operating for 238.75 hours, or 82.9% of the total time simulated, which is more than double than that of the reference case (126.3 hours). The PPD index is above the 50% limit for 80.25 hours, which is the 27.9% of the total time (33.6% of the time the hybrid ventilation system is working). The total PPD-hours are 1033, compared to the 11 of the reference case. Even though the energy savings potential is greatly increased to -2.41 kWh/m^2 for the concrete slab and -4.50 kWh/m^2 for the air, the control of the system fails to maintain a comfortable environment. The total energy for mechanical heating and cooling of the place is less than in the reference case, dropping to 1.25 kWh/m^2.

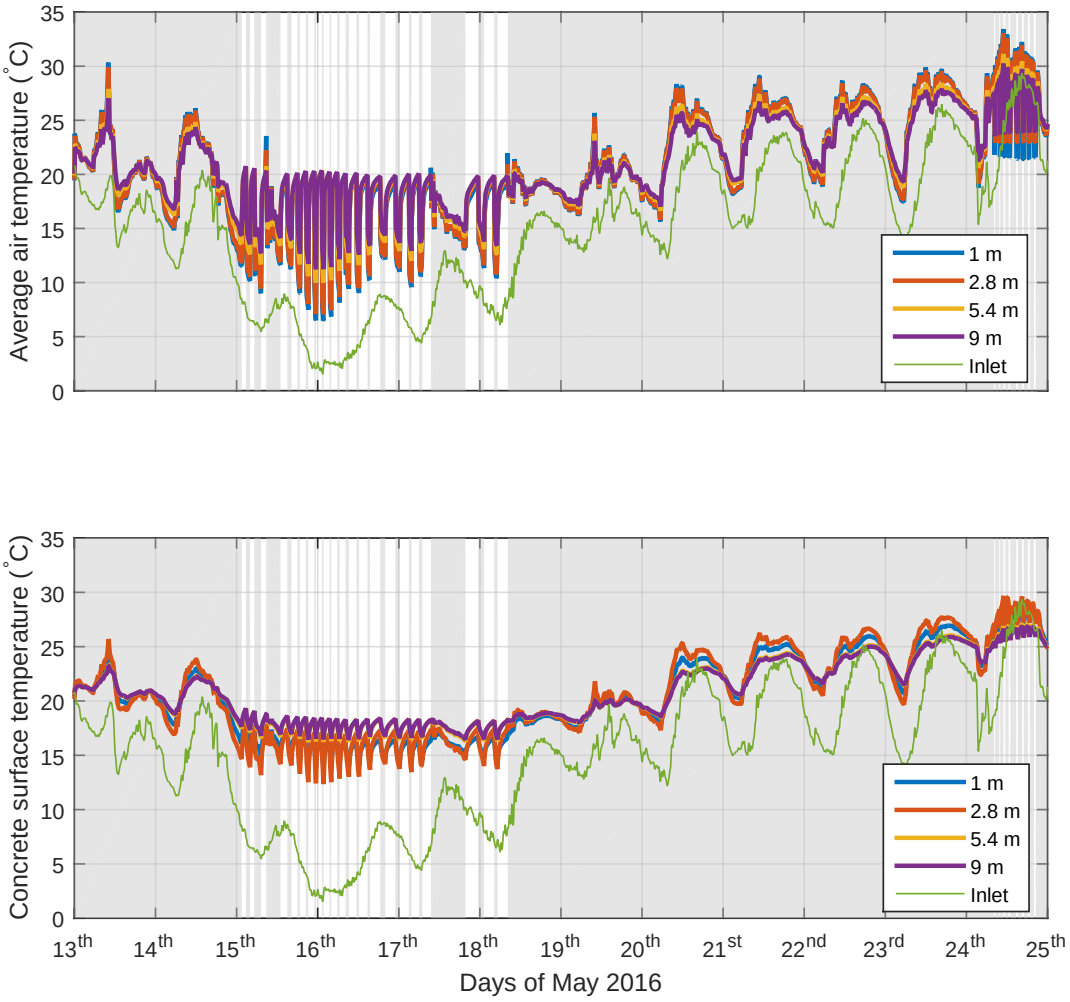

Figure 5.4: Predicted average air and concrete surface for reactive control strategy. The grey area indicates that the hybrid ventilation is on

5.3 Predictive control

Operating the system in a predictive manner can help minimize discomfort. The algorithm estimates the future response of the system, and the changes in the control anticipate discrepancies and keep the conditions comfortable.

5.3.1 On/off control

The algorithm uses the data of the next hour to make a decision, meaning that the prediction horizon is one hour. The dampers change position every 15 minutes. If the

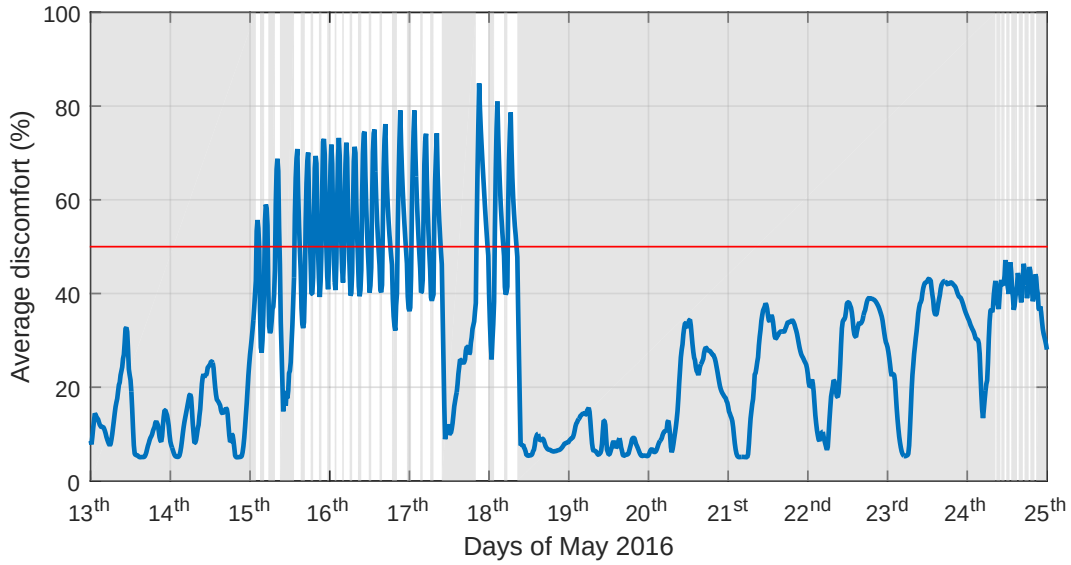

Figure 5.5: Average PPD index for reactive control. The grey area indicates that the hybrid ventilation is on

dampers can only assume two positions (open or closed), for every prediction horizon there are 16 possible combinations. The algorithm tests those and picks the one that keeps the discomfort as high as possible without exceeding the limit at any moment. It applies that position for the next 15 minutes, which is called the control horizon.

Figure 5.6 shows the average air and concrete surface temperatures for the predictive control strategy. Figure 5.6 shows that the oscillations are more frequent than in Figure 5.4. The system opens and closes often, but this time not when the discomfort limit is violated. The dampers close in time for the thermal comfort to be in an acceptable range.

This is shown in Figure 5.7. The discomfort oscillates a lot below the 50 % limit, but does not exceed it almost at all. The times that are above the limit could be avoided if the prediction horizon was longer.

The maximum and minimum temperatures, both for air and concrete surface, are the same as in the reactive control. They last for a shorter period of time and this is why they do not cause as much of a discomfort as in the reactive strategy. The concrete surface temperature is at average kept between 16 and 19 °C. When the days become warmer the system can handle better the heating loads, because the thermal mass is “discharged”.

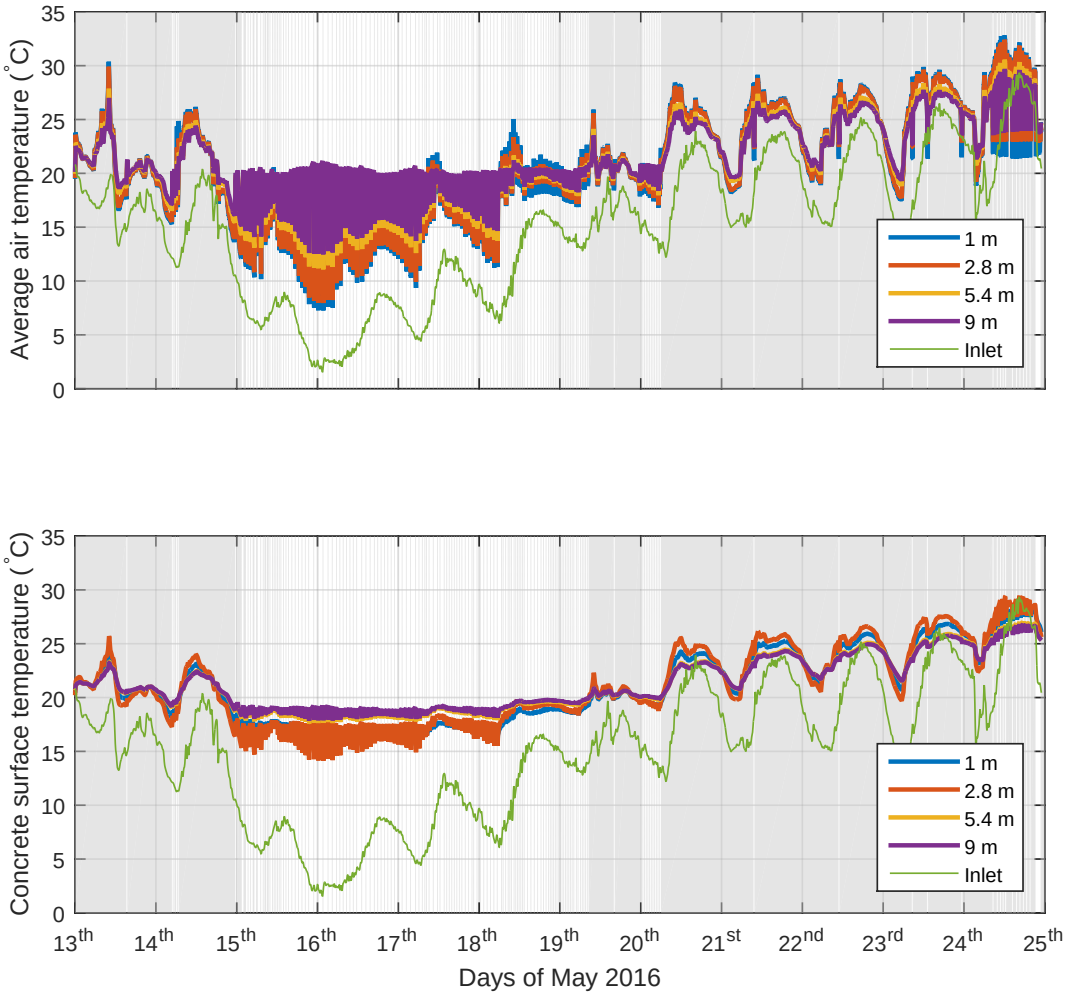

Figure 5.6: Predicted average air and concrete surface for predictive control strategy. The grey area indicates that the hybrid ventilation is on

The system operates for 206.25 hours, or 71.6% of the total simulated. The PPD index is above the limit only for 2.25 hours, or 0.8 % of the total time. The total PPD-hours are 6, which is the same order of magnitude with the reference case. The energy savings potential of the concrete floor is -2.12 kWh/m^2 (compared to -2.41 kWh/m^2 with the reactive strategy) and the potential of the air is -2.83 kWh/m^2 (compared to -4.50 kWh/m^2). The energy for mechanical heating and cooling is 1.73 kWh/m^2 (compared to 1.25 kWh/m^2). That shows that the constant closing and opening of the dampers does not increase the heating loads so much that the energy spent exceeds the free energy from the hybrid ventilation system.

The results show that with the predictive control strategy combines the advantages of the

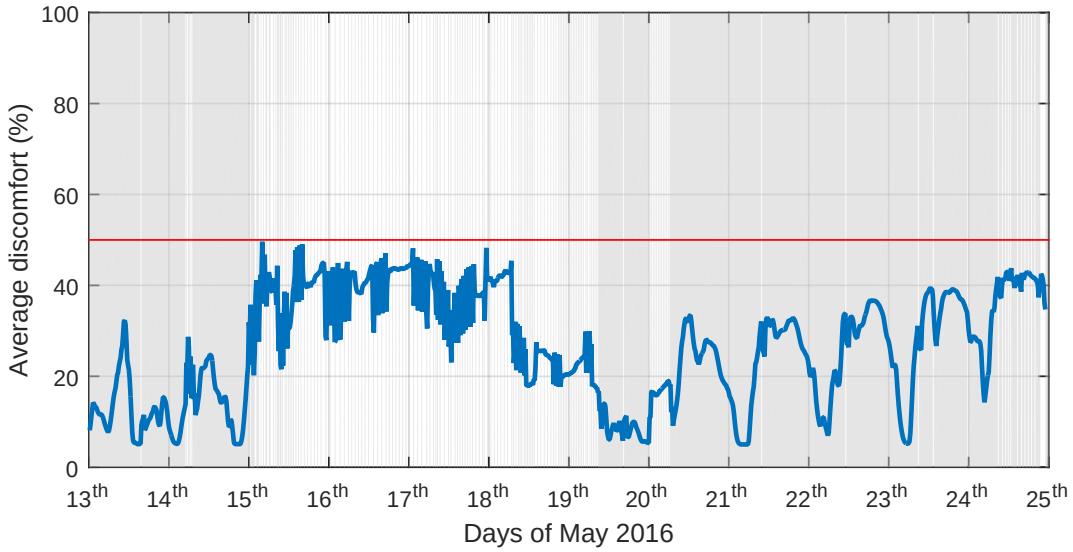

Figure 5.7: Average PPD index for the predictive control strategy. The grey area indicates that the hybrid ventilation is on

current control strategy (the reference case) and the reactive one presented. The discomfort levels are as low as the reference case, but at the same time the energy savings potential is greatly increased to the levels of the reactive strategy.

5.3.2 Prediction and control horizon

In this section the effect of the prediction and the control horizon will be examined. The smaller the control horizon, the more often the dampers will change position. This makes the system more resilient, since it can react to the weather changes faster, but it can be too sensitive and change positions too frequently, resulting in damage on the actuators and discomfort due to noise. On the other hand, if the control horizon is too large, the system will not react in time to the weather changes and the discomfort will be high.

If the prediction horizon is large, then the model has more information to prepare for the upcoming weather conditions and performs better. The limitation is that if it becomes too large, then the immediate thermal comfort needs will not be met, since the building is adjusting to something that will happen too long into the future. Obviously, the prediction horizon is also restricted by the ability to forecast with accuracy. Weather temperature

is easy to predict accurately for a day or two, but the prediction accuracy of wind speed, precipitation or solar radiation reduces a lot with time.

Table 5.2 shows the discomfort and the energy savings potential for various control and prediction horizons. The small differences between the results are not significant. The shortest possible control horizon is 15 minutes, because this is the shorter time the dampers are allowed to change position.

Table 5.2: Discomfort and energy savings potential for different control horizons (CH) and prediction horizons (PH)

CH (mins)	PH (mins)	Discomfort > 50 %			Energy savings (kWh/m^2)		
		hours	% of operation time	PPD-hours	Concrete	Air	HVAC
15	60	2.25	0.8 %	6	-2.12	-2.83	1.73
15	120	2.5	0.9 %	6	-2.10	-2.83	1.74
30	60	2.75	1.0 %	5	-2.16	-2.86	1.75
30	120	3	1.0 %	5	-2.14	-2.86	1.74

5.3.3 Weighing thermal comfort against energy savings

To study what is the effect of energy savings potential as a control variable on the predictive control strategy, a weighting factor α is introduced. This factor weighs the energy savings potential against thermal comfort, as shown in Equation (5.1). To be of the same units and magnitude, both discomfort and energy savings potential are normalized against the difference of their maximum and minimum values [160]. In this case the energy potential both from the concrete floor and the air at the end of the corridor are used, because the air will cool the thermal mass of the rest of the building, before being exhausted at the rooftop. The energy used from the HVAC system to condition the corridor is also taken into account, but the same does not apply to the energy of the fans for the recirculation of the air when the dampers are closed.

$$CF = \alpha D_n + (1 - \alpha) En_n \tag{5.1}$$

where

CF, cost function for the optimization;

D_n, normalized PPD;

En_n, normalized energy savings potential;

α, weighting factor.

It is obvious that as the weighting factor decreases, the control strategy considers energy savings potential more, and the thermal comfort is easier to be compromised.

Figure 5.8 shows the PPD index for three cases, when α is 1, 0.7 and 0.5. In general the discomfort follows the exact same profile when it is low. However, when it is close to the limit, the discomfort keeps the same pattern, but it shifts upwards, exceeding the limit more and more as α decreases.

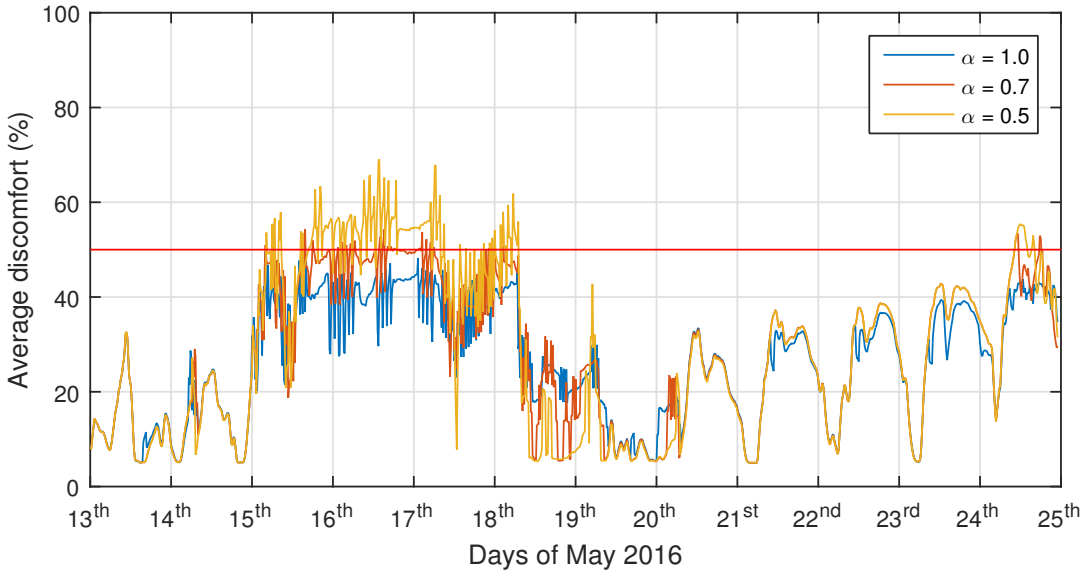

Figure 5.8: Effect of weighting parameter α on discomfort

Table 5.3 shows the discomfort indexes and the energy savings potential as α changes. The first observation, is that even if in some cases the time that the discomfort is above the limit does not increase a lot, the PPD-hours do; that indicates that the time may be close, but the feeling of discomfort becomes more intense. Another observation is that the energy savings potential from the concrete floor does not increase a lot, meaning that the corridor

has achieved a limit on the heat exchange with the air. This results to a lower air temperature at the end of the corridor, which increases the energy potential of the air towards the rest of the building. In all cases the energy for heating and cooling from the HVAC system is lower than the energy potential gained from the concrete.

Table 5.3: Discomfort and energy savings potential for different values of α

α	Discomfort > 50 %			Energy savings (kWh/m^2)		
	hours	% of operation time	PPD-hours	Concrete	Air	HVAC
1.0	2.25	0.8 %	6	-2.12	-2.83	1.73
0.9	25.25	8.8 %	35	-2.15	-2.99	1.78
0.8	40.75	14.2 %	107	-2.16	-3.14	1.63
0.7	57.75	20.1 %	221	-2.19	-3.31	1.52
0.6	65.25	22.7 %	412	-2.21	-3.56	1.34
0.5	86.25	30.0 %	663	-2.23	-3.81	1.23

By introducing this weighting factor, different levels of importance can be given to thermal comfort for various situations. One example is weighting thermal comfort more when the building is occupied and less when it is unoccupied. This strategy is explored in the next section.

5.3.4 Night precooling

As much as thermal comfort is the most important factor in institutional buildings, their occupancy schedule is usually well–defined. Excluding office hours, most institutional building can be assumed to be unoccupied. In addition, the corridors are transition spaces, which provides a lot of flexibility for thermal comfort criteria, and as a result energy efficiency. Some people may still be in the building, but they will only be a few and they will be working in their offices or labs. The amount of time that they would spend in the corridors – and especially the ones that serve as inlets to the hybrid ventilation – would be minimal. For this reason, in this section the simple assumption of an day – night occupancy schedule is

explored.

The building is considered to be occupied 8:00 am to 5:00 pm. During those times the predictive control strategy works considering only the thermal comfort of the occupants ($\alpha = 1$). When the building is not occupied though, the weighting factor α can be lowered to give more emphasis on energy savings. Yuan in her thesis [1] suggested a night ventilation schedule, starting at 20:00 pm and stopping at 07:00 am. This period of time is simulated with a α of 0.5.

The resulting air and concrete surface temperatures follow the same profile as in Figure 5.6, with the same maximum and minimum temperatures. Figure 5.9 presents the discomfort and the weighting factor α throughout the simulation. Although there are times that the discomfort is above the limit, it is clear that the majority happens when the weighting factor is 0.5, indicating that it is night and the building is unoccupied.

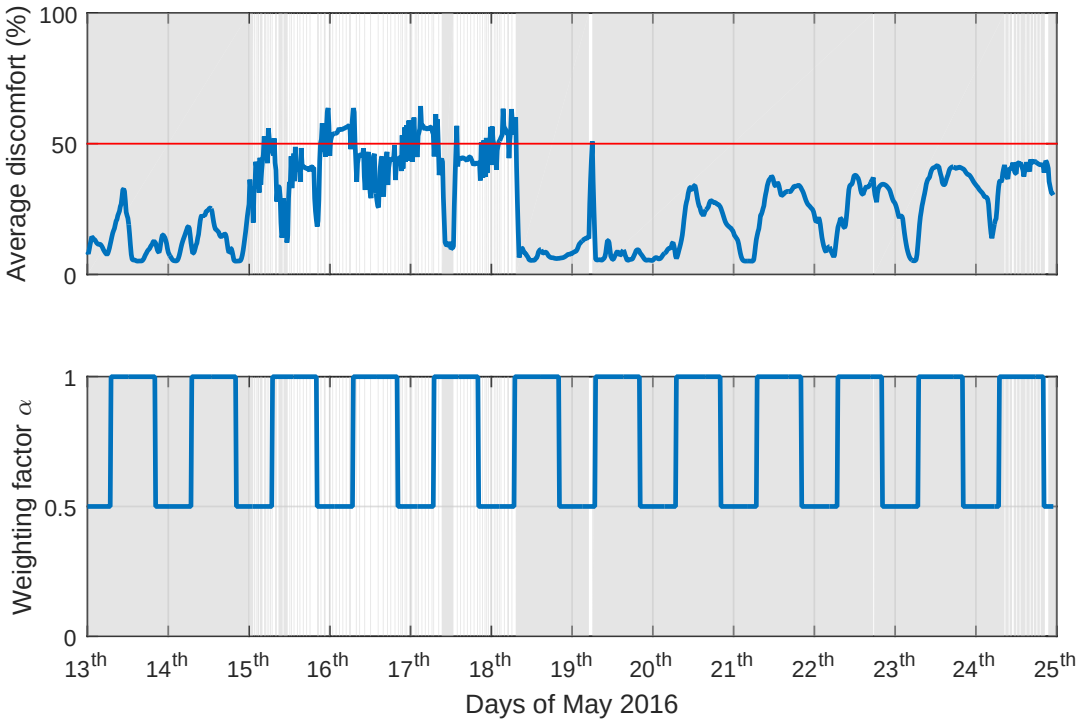

Figure 5.9: Average PPD index and weighting factor α for predictive control with occupancy schedule. The grey area indicates that the hybrid ventilation is on

The system operates for a total of 231.5 hours, or 80.0 % of the time. The PPD index

is above the limit for 47.75 hours, but only 4.5 hours are during the occupancy hours of the building. This is 1.6 % of the total time, with 37 PPD–hours. The energy savings potential of the concrete floor is -2.24 kWh/m^2 and of the air -3.76 kWh/m^2. The mechanical system has a consumption of 1.12 kWh/m^2.

The energy savings now are as much as running the hybrid ventilation system with α 0.5, higher than any other case simulated (except for the reactive control), but the total PPD-hours of interest (during the occupied hours) are only 37.

5.3.5 Modulated damper opening

All the control strategies discussed until assume that the dampers can only assume two positions. The motorized inlet dampers of the EV building give the opportunity to modulate the inlet to a percentage, to better control the inlet velocity. The percentage of the dampers opening is correlated exponentially to the percentage of the flow that passes through them.

In this study the dampers can assume 5 positions, so that they the velocity percentage is 0, 0.25, 0.5, 0.75 and 1. This positions, according to the manuals available from Concorida's facilities management, are 0, 70, 82, 92 and 100 % opening of the dampers respectively.

The weighting factor was kept constant at 1 for the whole simulation. Figure 5.10 shows the discomfort and the percentage of the flow.

When the discomfort is well below the limit the dampers open fully to allow as much of the exterior air into the building. When the exterior conditions push the discomfort close to the limit either because it is too cold or too hot, the dampers only open to allow 25 % or 50 % of the flow. It is observed that the dampers never stay at the 75 % position. Instead they choose to close completely, even for a small amount of time and then reopen (as they do between the 21st and the 22nd.

The system operates for a total of 223.75 hours, or 77.7 % of the time. The PPD index is above the limit for 5.5 hours, or 1.9 % of the time, with 6 PPD-hours. The PPD-hours and the energy savings potential of the concrete floor, which is -2.23 kWh/m^2, may be the same with the on/off predictive control strategy, but the energy savings of the air increases greatly yo 3.44 kWh/m^2. The energy consumption of the HVAC system is 1.25 kWh/m^2

If a night setback is set for the weighting factor, as in Section 5.3.4, the hours above

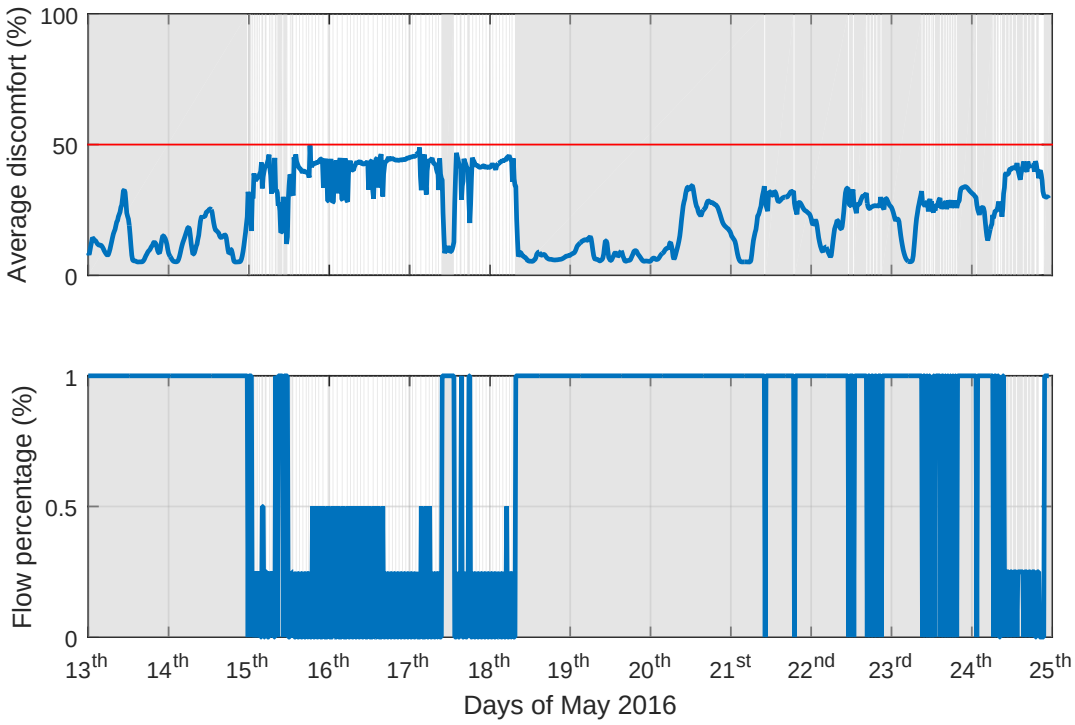

Figure 5.10: Average PPD index and percentage of flow for predictive control with modulated dampers opening. The grey area indicates that the hybrid ventilation is on

the limit fall to 2.75, or 1 % of the total time, but the PPD–hours 10. The energy savings potential increases to -2.27 kWh/m^2 for the concrete floor and to -3.67 kWh/m^2 for the air, but so does the energy consumption of the HVAC system, which increases to 1.28 kWh/m^2.

This strategy seems to be the one that maximizes energy savings potential, without compromising the thermal comfort of the people when the building is occupied. The energy savings are a bit less than the on/off night setback, but the thermal discomfort is reduced from 37 to 10 PPD–hours.

5.3.6 Summary

Table 5.4 shows a summary of all the control strategies that were simulated and their results on discomfort and energy savings potential. Unless otherwise indicated, α is 1, control horizon is 15 minutes and prediction horizon is 60 minutes.

It is obvious that some of the control strategies used have similar results, and picking

Table 5.4

Control strategy	Discomfort > 50 %			Energy savings (kWh/m^2)			
	hours	% of operation time	PPD-hours	Concrete	Air	HVAC	Net
Reference	2.25	1.8 %	11	-1.00	-0.45	3.35	1.9
Reactive	80.25	27.9 %	1033	-2.41	-4.50	1.25	-5.66
Predictive	2.25	0.8 %	6	-2.12	-2.83	1.73	-3.22
Predictive, CH=15, PH=120	2.5	0.9 %	6	-2.10	-2.83	1.74	-3.19
Predictive, CH=30, PH=60	2.75	1.0 %	5	-2.16	-2.86	1.75	-3.27
Predictive, CH=30, PH=120	3	1.0 %	5	-2.14	-2.86	1.74	-3.26
Predictive, α=0.9	25.25	8.8 %	35	-2.15	-2.99	1.78	-3.36
Predictive, α=0.8	40.75	14.2 %	107	-2.16	-3.14	1.63	-3.67
Predictive, α=0.7	57.75	20.1 %	221	-2.19	-3.31	1.52	-3.98
Predictive, α=0.6	65.25	22.7 %	412	-2.21	-3.56	1.34	-4.43
Predictive, α=0.5	86.25	30.0 %	663	-2.23	-3.81	1.23	-4.81
Predictive, night setback	4.5	1.6 %	37	-2.24	-3.76	1.12	-4.88
Predictive, modular	5.5	1.9 %	6	-2.23	-3.44	1.25	-4.42
Predictive, modular, night setback	2.75	1 %	10	-2.27	-3.67	1.28	-4.66

a single one is not easy, because they may have a slightly different behavior for days of different weather conditions. The difference between the reference case, the reactive and the predictive nature of the control is apparent, proving why predictive control is superior. It achieves almost as much energy savings as reactive control, but the PPD–hours are 2 orders of magnitude less.

CHAPTER 6

CONCLUSION

This thesis presents and evaluates various control strategies to improve the operation of the novel hybrid ventilation system of Concordia's EV building by developing control strategies that minimize discomfort and cooling energy consumption. This building is a representative high rise office building that benefits from a significant buoyancy effect due to its height, fan assistance when necessary and motorized inlet dampers that can be modulated individually.

Hybrid ventilation can be beneficial in multiple ways to an institutional building. It reduces the present cooling loads of the building and it can reduce the cooling loads of the following day by precooling the thermal mass during the night. It can improve thermal comfort, if the exterior conditions are appropriate. The air inflow reduces the amount of air recirculated mechanically in the building and this reduces the energy the fans consume.

One of the most challenging and at the same time most important decisions when operating a hybrid ventilation system is choosing the minimum exterior air temperature that the air should be allowed into the building, through the motorized dampers and into the corridors. Many researchers have proposed setpoints for various parameters, such as exterior or interior temperature, wind speed, relative humidity or humidity content, etc.

Instead of a single setpoint or deadband, this study explains the procedure to develop a model, calibrate it with full–scale measurements and evaluate predictive control strategies. The model takes as inputs the air temperature and relative humidity and the solar radiation,

measured at the weather station at the roof of the EV building. It estimates the thermal discomfort and the energy savings potential form the cool air entering the space. The model was applied on 12 real days with data taken from the station.

Right now the system operates with a simple IF–THEN–ELSE structure, with setpoints based on heuristic control. That creates a comfortable environment, but is rather conservative towards energy savings. A reactive type of control can result into almost 4 times more energy savings, but it creates an uncomfortable environment for 28 % of the time. On the other hand, a predictive type of control can minimize discomfort to less than 1 % of the time, while yielding more than 3 times the energy savings of the heuristic control.

The control horizon and the prediction horizon did not prove to affect the result significantly, because the minimum control horizon is 15 minutes (to avoid noise and overworking the actuators), which means that the system "sees" enough into the future to "know" what kind of weather conditions to prepare for and also has time to react to them. A prediction horizon of days could be tested as part of the future work, to see how the system would react.

The algorithm weighted thermal comfort against energy savings and as expected showed that the larger the energy savings potential, the more thermal comfort was compromised. The concrete floor energy savings potential was similar in all the cases, suggesting that the heat exchange between the floor and the incoming air had achieved a limit.

Different weighting factors for different occupancy schedules can increase energy savings potential, without compromising thermal comfort. The fact that the inlet air enters the building from a corridor, which is a transition space, increases the flexibility of the building towards thermal comfort and, as a result, energy savings. The first 5 meters of the inlet contain only a fire escape stairway. When the air reaches the 5 meters its temperature rises significantly. The experiments show that even when the exterior air temperature is as low as 7 °C, when the air reaches the 5 meters, the temperature is 14 °C.

The building is an office building and therefore has a well–defined occupancy schedule, allowing to only consider discomfort during the day (7 am to 8 pm) and weigh discomfort to energy savings potential during the night (8 pm to 7 am).

The motorized inlets allow for a modulated opening, controlling the air inflow better. This provides a finer control of the system, further reducing thermal discomfort.

6.1 Limitations and future work

The model of the corridor can be enhanced by performing more experiments to better calibrate it for different weather conditions. The direct solar heat gains can be considered to make the model more accurate.

Predictive control is as good as the least accurate forecast. In order for the control strategy presented in this study to be successful, the weather conditions forecast of the next hour is necessary. There have already been some studies on short–term weather forecasts for the weather station placed on the roof of the EV building. In most cases the results were satisfactory when correlated to more than one nearby weather stations.

An interesting study would be to use predictive control with a prediction horizon of a few days, so that the building conditions for the weather of the next day, not just an hour. Even though the accuracy of the forecast will be lower and so will the accuracy of the model, the building will be in a better condition to accept the cooling loads of the next day. Using a large prediction horizon during the night can help precool the building, and then a smaller one during the hours that the building will be occupied to better control and fine tune thermal comfort can increase the energy savings potential even further, without affecting thermal comfort.

In order to achieve that, the control of the mechanical ventilation needs to be adjusted. The existing strategy is that it starts operating as soon as the dampers close, which counteracts the effect of the precooling. A time lag could be introduced between the time that the dampers close and the mechanical ventilation system starts working, to allow the building to be heated passively, through the thermal mass and the internal gains.

To better control the operation of the system, the energy consumed by the fans of the HVAC system to recirculate the air needs to be considered, and in the case of the fan–assisted ventilation, their energy consumption needs to be considered too. This will improve the control of the system, allowing it to make better and well–rounded decisions.

The model does not simulate the operation of the roof fans. The added pressure difference will affect the air velocity, which is an input to the model. There is an ongoing study of the air flow and heat transfer in the whole building. That model considers the effect of the fan and

decides the opening of all the dampers in the building. Using that air flow as an input to the model presented in this work, the thermal discomfort can be evaluated. Based on thermal discomfort, a new position for the dampers can be suggested. Iteratively, the optimum position can be found for all dampers, ensuring that thermal comfort is not compromised.

The uncertainties presented in this work are the prediction uncertainties of the model, and do not consider the propagation of error, nor the uncertainty of the weather forecast. As a result the uncertainty at any given point is underpredicted. The complexity of the model renders the analytical calculation of the propagation of error too complicated. Instead, a Monte Carlo analysis can be performed. According to the Monte Carlo method, thousands or hundreds of thousands of samples of each parameter are randomly generated, according to their distribution. For each set of the randomly generated parameters, the corresponding predicted value of the model is calculated. The distribution of the simulated predicted values form the error of the end result. The disadvantage of this method is that it is computationally demanding.

BIBLIOGRAPHY

[1] S. Yuan, "A study of hybrid ventilation in an institutional building for predictive control," Master's thesis, Montreal, Canada, August 2016.

[2] N. resouces Canada, "Energy use data handbook, 1990 – 2014," 2017.

[3] K. Roth, J. Dieckmann, and J. Brodrick, "Natural and hybrid ventilation," vol. 48, pp. H37–H39, 06 2006.

[4] M. Gouda, S. Danaher, and C. Underwood, "Building thermal model reduction using nonlinear constrained optimization," *Building and Environment*, vol. 37, no. 12, pp. 1255 – 1265, 2002.

[5] S. Omrani, V. Garcia-Hansen, B. Capra, and R. Drogemuller, "Natural ventilation in multi-storey buildings: Design process and review of evaluation tools," *Building and Environment*, vol. 116, pp. 182 – 194, 2017.

[6] Q. Chen, "Ventilation performance prediction for buildings: A method overview and recent applications," *Building and Environment*, vol. 44, no. 4, pp. 848 – 858, 2009.

[7] Z. J. Zhai, M. E. Mankibi, and A. Zoubir, "Review of natural ventilation models," *Energy Procedia*, vol. 78, pp. 2700 – 2705, 2015. 6th International Building Physics Conference, IBPC 2015.

[8] C. Allocca, "Single-sided natural ventilation: Design analysis and general guidelines," Master's thesis, Massachusetts Institute of Technology, the United States of America, 2001.

[9] Z. T. Ai, C. M. Mak, and D. J. Cui, "On-site measurements of ventilation performance and indoor air quality in naturally ventilated high-rise residential buildings in Hong Kong," *Indoor and Built Environment*, vol. 24, no. 2, pp. 214–224, 2015.

[10] P. Warren, "Ventilation through openings on the one wall only," *Energy Conservation in Heating, Cooling, and Ventilation of Buildings*, vol. 1, no. 1, pp. 186–206, 1978.

[11] E. Dascalaki, M. Santamouris, A. Argiriou, C. Helmis, D. Asimakopoulos, K. Papadopoulos, and A. Soilemes, "On the combination of air velocity and flow measurements in single sided natural ventilation configurations," *Energy and Buildings*, vol. 24, no. 2, pp. 155 – 165, 1996.

[12] M. Caciolo, S. Cui, P. Stabat, and D. Marchio, "Development of a new correlation for single-sided natural ventilation adapted to leeward conditions," *Energy and Buildings*, vol. 60, pp. 372 – 382, 2013.

[13] E. Dascalaki, M. Santamouris, and D. Asimakopoulos, "On the use of deterministic and intelligent techniques to predict the air velocity distribution on external openings in single-sided natural ventilation configurations," *Solar Energy*, vol. 66, no. 3, pp. 223 – 243, 1999.

[14] T. Larsen, *Natural Ventilation Driven by Wind and Temperature Difference*. PhD thesis, Denmark, 2006.

[15] Y. Li, "Analysis of natural ventilation - a summary of existing analytical solutions," *International Energy Agency*, vol. Technical Report Annexx 35: HybVent, 2002.

[16] J. M. Holford and G. R. Hunt, "Fundamental atrium design for natural ventilation," *Building and Environment*, vol. 38, no. 3, pp. 409 – 426, 2003.

[17] R. Z. Freire, M. O. Abadie, and N. Mendes, "On the improvement of natural ventilation models," *Energy and Buildings*, vol. 62, pp. 222 – 229, 2013.

[18] Z. Ai and C. Mak, "Determination of single-sided ventilation rates in multistory buildings: Evaluation of methods," *Energy and Buildings*, vol. 69, pp. 292 – 300, 2014.

[19] S. V. Patankar, "Numerical heat transfer and fluid flow / suhas v. patankar," 08 2017.

[20] L. J. Lo, D. Banks, and A. Novoselac, "Combined wind tunnel and cfd analysis for indoor airflow prediction of wind-driven cross ventilation," *Building and Environment*, vol. 60, pp. 12 – 23, 2013.

[21] S.-W. Hong, V. Exadaktylos, I.-B. Lee, T. Amon, A. Youssef, T. Norton, and D. Berckmans, "Validation of an open source cfd code to simulate natural ventilation for agricultural buildings," *Computers and Electronics in Agriculture*, vol. 138, pp. 80 – 91, 2017.

[22] C. Baxevanou, D. Fidaros, and A. Tsangrassoulis, "Management of natural ventilation in high-rise building a cfd study," *Procedia Environmental Sciences*, vol. 38, pp. 428 – 435, 2017. Sustainable synergies from Buildings to the Urban Scale.

[23] T. G. Farea, D. R. Ossen, S. Alkaff, and H. Kotani, "Cfd modeling for natural ventilation in a lightwell connected to outdoor through horizontal voids," *Energy and Buildings*, vol. 86, pp. 502 – 513, 2015.

[24] W. Guo, X. Liu, and X. Yuan, "Study on natural ventilation design optimization based on cfd simulation for green buildings," *Procedia Engineering*, vol. 121, pp. 573 – 581, 2015. The 9th International Symposium on Heating, Ventilation and Air Conditioning (ISHVAC) joint with the 3rd International Conference on Building Energy and Environment (COBEE), 12-15 July 2015, Tianjin, China.

[25] R. Ramponi and B. Blocken, "Cfd simulation of cross-ventilation for a generic isolated building: Impact of computational parameters," *Building and Environment*, vol. 53, pp. 34 – 48, 2012.

[26] K. Visagavel and P. Srinivasan, "Analysis of single side ventilated and cross ventilated rooms by varying the width of the window opening using cfd," *Solar Energy*, vol. 83, no. 1, pp. 2 – 5, 2009.

[27] H. Awbi, "Air movement in naturally-ventilated buildings," *Renewable Energy*, vol. 8, no. 1, pp. 241 – 247, 1996. Special Issue World Renewable Energy Congress Renewable Energy, Energy Efficiency and the Environment.

[28] T. E. Jiru and G. T. Bitsuamlak, "Application of cfd in modelling wind-induced natural ventilation of buildings - a review," *International Journal of Ventilation*, vol. 9, no. 2, pp. 131–147, 2010.

[29] H. Wang and Q. Y. Chen, "Modeling of the impact of different window types on single-sided natural ventilation," *Energy Procedia*, vol. 78, pp. 1549 – 1555, 2015. 6th International Building Physics Conference, IBPC 2015.

[30] C. Ding, K. P. Lam, and N. H. Wong, "Coupled natural ventilation modeling for contextual parametric design decision support," *Procedia Engineering*, vol. 169, pp. 264 – 271, 2016. Fourth International Conference on Countermeasures to Urban Heat Island, 30-31 May and 1 June 2016.

[31] J. Song and X. Meng, "The improvement of ventilation design in school buildings using cfd simulation," *Procedia Engineering*, vol. 121, pp. 1475 – 1481, 2015. The 9th International Symposium on Heating, Ventilation and Air Conditioning (ISHVAC) joint with the 3rd International Conference on Building Energy and Environment (COBEE), 12-15 July 2015, Tianjin, China.

[32] M.-H. Johnson, Z. (John) Zhai, and M. Krarti, "Performance evaluation of network airflow models for natural ventilation," vol. 18, May 2012.

[33] J. Axley, "Multizone airflow modeling in buildings: History and theory," *HVAC&R Research*, vol. 13, no. 6, pp. 907–928, 2007.

[34] G. Tan and L. R. Glicksman, "Application of integrating multi-zone model with cfd simulation to natural ventilation prediction," *Energy and Buildings*, vol. 37, no. 10, pp. 1049 – 1057, 2005.

[35] W. Tian, T. A. Sevilla, W. Zuo, and M. D. Sohn, "Coupling fast fluid dynamics and multizone airflow models in modelica buildings library to simulate the dynamics of hvac systems," *Building and Environment*, vol. 122, pp. 269 – 286, 2017.

[36] Z. Zhang, X. Chen, S. Mazumdar, T. Zhang, and Q. Chen, "Experimental and numerical investigation of airflow and contaminant transport in an airliner cabin mockup," *Building and Environment*, vol. 44, no. 1, pp. 85 – 94, 2009.

[37] L. Shao and S. Riffat, "Tracer-gas mixing with air: Effect of tracer species," *Applied Energy*, vol. 49, no. 2, pp. 197 – 211, 1994.

[38] L. Shao, S. Sharples, and I. Ward, "Tracer gas mixing with air," *Building Services Engineering Research and Technology*, vol. 14, no. 2, pp. 43–50, 1993.

[39] O. Stathopoulou, V. Assimakopoulos, H. Flocas, and C. Helmis, "An experimental study of air quality inside large athletic halls," *Building and Environment*, vol. 43, no. 5, pp. 834 – 848, 2008.

[40] A. Wang, Y. Zhang, Y. Sun, and X. Wang, "Experimental study of ventilation effectiveness and air velocity distribution in an aircraft cabin mockup," *Building and Environment*, vol. 43, no. 3, pp. 337 – 343, 2008. Indoor Air 2005: Modeling, Assessment, and Control of Indoor Air Quality.

[41] S. Omrani, V. Garcia-Hansen, R. Drogemuller, and B. Capra, "Predicting environmental conditions at building site for natural ventilation design: Correlation of meteorological data to air speed at building openings," in *50th International Conference of the Architectural Science Association: Fifty Years Later: Revisiting the Role of Architectural Science in Design and Practice* (L. Zuo, L. Daniel, and V. Soebarto, eds.), (Adelaide, SA), pp. 1–10, The Architectural Science Association and The University of Adelaide, December 2016.

[42] L. Xu and T. Ojima, "Field experiments on natural energy utilization in a residential house with a double skin faade system," *Building and Environment*, vol. 42, no. 5, pp. 2014 – 2023, 2007.

[43] E. Hitchin and C. Wilson, "A review of experimental techniques for the investigation of natural ventilation in buildings," *Building Science*, vol. 2, no. 1, pp. 59 – 82, 1967.

[44] Y. Sun and Y. Zhang, "An overview of room air motion measurement: Technology and application," *HVAC&R Research*, vol. 13, no. 6, pp. 929–950, 2007.

[45] M. Sandberg, "Whole-field measuring methods in ventilated rooms," *HVAC&R Research*, vol. 13, no. 6, pp. 951–970, 2007.

[46] C. Gao and W. Lee, "Evaluating the influence of window types on the natural ventilation performance of residential buildings in hong kong," *International Journal of Ventilation*, vol. 10, no. 3, pp. 227–238, 2011.

[47] C. Gao and W. Lee, "Evaluating the influence of openings configuration on natural ventilation performance of residential units in hong kong," *Building and Environment*, vol. 46, no. 4, pp. 961 – 969, 2011.

[48] C. Zhou, Z. Wang, Q. Chen, Y. Jiang, and J. Pei, "Design optimization and field demonstration of natural ventilation for high-rise residential buildings," *Energy and Buildings*, vol. 82, pp. 457 – 465, 2014.

[49] Y. Jiang, D. Alexander, H. Jenkins, R. Arthur, and Q. Chen, "Natural ventilation in buildings: measurement in a wind tunnel and numerical simulation with large-eddy simulation," *Journal of Wind Engineering and Industrial Aerodynamics*, vol. 91, no. 3, pp. 331 – 353, 2003.

[50] W. Ding, Y. Hasemi, and T. Yamada, "Natural ventilation performance of a double-skin faade with a solar chimney," *Energy and Buildings*, vol. 37, no. 4, pp. 411 – 418, 2005.

[51] A. Athienitis, M. Cellura, Y. Chen, D. Véronique, P. Bourdoukan, and K. Kapsis, "Modeling and design of net zebs as integrated energy systems," in *Modeling, Design, and Optimization of Net-Zero Energy Buildings* (A. Athienitis and L. O'Brien, eds.), pp. 9–73, Wilhelm Ernst and Sohn, 2015.

[52] *2009 ASHRAE Handbook: Fundamentals*. American Society of Heating, Refrigeration and Air-Conditioning Engineers, 2009.

[53] E. Sassine, Z. Younsi, Y. Cherif, and E. Antczak, "Thermal performance evaluation of a massive brick wall under real weather conditions via the conduction transfer function method," *Case Studies in Construction Materials*, vol. 7, pp. 56 – 65, 2017.

[54] *Engineering Reference*. EnergyPlus Version 8.7 Documentation, U.S. Department of Energy, September 2016.

[55] *Mathematical Reference*. TRNSYS 16, Solar Energy Laboratory, University of Wisconsin-Madison, 2006.

[56] D. C. Hittle, *Calculating building heating and cooling loads using the frequency response of multilayered slabs*. PhD thesis, Army Construction Engineering Research Lab., Champaign, IL., 1981.

[57] G. P. Mitalas and D. G. Stephenson, "Room thermal response factors," vol. 73, January 1967.

[58] G. Myers, "Long-time solutions to heat-conduction transients with time-dependent inputs.," vol. 102, pp. 115–120, 02 1980.

[59] G. P. Mitalas and J. G. Arseneault, "Fortran iv program to calculate z-transfer functions for the calculation of transient heat transfer through walls and roofs," January 1971.

[60] D. C. Hittle and R. Bishop, "An improved root-finding procedure for use in calculating transient heat flow through multilayered slabs," *International Journal of Heat and Mass Transfer*, vol. 26, no. 11, pp. 1685 – 1693, 1983.

[61] K. Ouyang and F. Haghighat, "A procedure for calculating thermal response factors of multi-layer wallsstate space method," *Building and Environment*, vol. 26, no. 2, pp. 173 – 177, 1991.

[62] S. Wang and Y. Chen, "Transient heat flow calculation for multilayer constructions using a frequency-domain regression method," *Building and Environment*, vol. 38, no. 1, pp. 45 – 61, 2003.

[63] E. Sassine, Z. Younsi, Y. Cherif, and E. Antczak, "Frequency domain regression method to predict thermal behavior of brick wall of existing buildings," *Applied Thermal Engineering*, vol. 114, pp. 24 – 35, 2017.

[64] J. S. Prez, M. A. Chicote, F. V. Dez, and E. V. Gmez, "A new method for calculating conduction response factors for multilayer constructions based on frequencydomain spline interpolation (fdsi) and asymptotic analysis," *Energy and Buildings*, vol. 148, pp. 280 – 297, 2017.

[65] A. Athienitis, "A methodology for integrated building hvac system thermal analysis," *Building and Environment*, vol. 28, no. 4, pp. 483 – 496, 1993.

[66] Y. Chen and S. Wang, "Frequency-domain regression method for estimating ctf models of building multilayer constructions," *Applied Mathematical Modelling*, vol. 25, no. 7, pp. 579 – 592, 2001.

[67] X. Q. Li, Y. Chen, J. Spitler, and D. Fisher, "Applicability of calculation methods for conduction transfer function of building constructions," *International Journal of Thermal Sciences*, vol. 48, no. 7, pp. 1441 – 1451, 2009.

[68] J. Zhou, G. Zhang, Y. Lin, and Y. Li, "Coupling of thermal mass and natural ventilation in buildings," *Energy and Buildings*, vol. 40, no. 6, pp. 979 – 986, 2008.

[69] A. Athienitis and M. Santamouris, *Thermal Analysis and Design of Passive Solar Buildings*. BEST (Buildings, Energy and Solar Technology) Series, James & James, 2002.

[70] L. Mazzarella and M. Pasini, "Ctf vs fd based numerical methods: Accuracy, stability and computational time's comparison," *Energy Procedia*, vol. 78, pp. 2620 – 2625, 2015. 6th International Building Physics Conference, IBPC 2015.

[71] F. P. Incropera and D. P. DeWitt, *Fundamentals of Heat and Mass Transfer*. New York City, New York: John Wiley and Sons, Inc., 5th edition ed., 2001.

[72] R. Kramer, J. van Schijndel, and H. Schellen, "Simplified thermal and hygric building models: A literature review," *Frontiers of Architectural Research*, vol. 1, no. 4, pp. 318 – 325, 2012.

[73] G. Hudson and C. P. Underwood, "A simple building modelling procedure for matlab/simulink," January 1999.

[74] G. H. dos Santos and N. Mendes, "Analysis of numerical methods and simulation time step effects on the prediction of building thermal performance," *Applied Thermal Engineering*, vol. 24, no. 8, pp. 1129 – 1142, 2004. The 8th UK National Conference on Heat Transfer.

[75] M. de Wit, "Hambase : heat, air and moisture model for building and systems evaluation," January 2006.

[76] J. Penman, "Second order system identification in the thermal response of a working school," *Building and Environment*, vol. 25, no. 2, pp. 105 – 110, 1990.

[77] K. Antonopoulos and E. Koronaki, "Apparent and effective thermal capacitance of buildings," *Energy*, vol. 23, no. 3, pp. 183 – 192, 1998.

[78] G. Fraisse, C. Viardot, O. Lafabrie, and G. Achard, "Development of a simplified and accurate building model based on electrical analogy," *Energy and Buildings*, vol. 34, no. 10, pp. 1017 – 1031, 2002.

[79] T. R. Nielsen, "Simple tool to evaluate energy demand and indoor environment in the early stages of building design," *Solar Energy*, vol. 78, no. 1, pp. 73 – 83, 2005.

[80] J. H. Kmpf and D. Robinson, "A simplified thermal model to support analysis of urban resource flows," *Energy and Buildings*, vol. 39, no. 4, pp. 445 – 453, 2007.

[81] J. Vivian, A. Zarrella, G. Emmi, and M. D. Carli, "An evaluation of the suitability of lumped-capacitance models in calculating energy needs and thermal behaviour of buildings," *Energy and Buildings*, vol. 150, pp. 447 – 465, 2017.

[82] V. Dermardiros, "Modelling and experimental evaluation of an active thermal energy storage system with phase-change materials for model-based control," Master's thesis, Concordia University, Montreal, Canada, 2015.

[83] G. Mustafaraj, G. Lowry, and J. Chen, "Prediction of room temperature and relative humidity by autoregressive linear and nonlinear neural network models for an open office," *Energy and Buildings*, vol. 43, no. 6, pp. 1452 – 1460, 2011.

[84] A. Mechaqrane and M. Zouak, "A comparison of linear and neural network arx models applied to a prediction of the indoor temperature of a building," *Neural Computing & Applications*, vol. 13, pp. 32–37, Apr 2004.

[85] C. Deb, L. S. Eang, J. Yang, and M. Santamouris, "Forecasting diurnal cooling energy load for institutional buildings using artificial neural networks," *Energy and Buildings*, vol. 121, pp. 284 – 297, 2016.

[86] A. Ruano, E. Crispim, E. Conceio, and M. Lcio, "Prediction of building's temperature using neural networks models," *Energy and Buildings*, vol. 38, no. 6, pp. 682 – 694, 2006.

[87] H. U. Frausto and J. G. Pieters, "Modelling greenhouse temperature using system identification by means of neural networks," *Neurocomputing*, vol. 56, pp. 423 – 428, 2004.

[88] M. Norgaard, O. Ravn, and N. K. Poulsen, "Nnsysid and nnctrl tools for system identification and control with neural networks," *Computing Control Engineering Journal*, vol. 12, pp. 29–36, Feb 2001.

[89] A. Papachristou, "An experimental and numerical investigation of predictive control with different building-integrated thermal storage systems," Master's thesis, Montreal, Canada, October 2016.

[90] Y. Chen, *Methodology for Design and Operation of Active Building-Integrated Thermal Energy Storage Systems*. PhD thesis, Montreal, Canada, September 2013.

[91] R. American Society of Heating and A.-C. Engineers, *2007 ASHRAE Handbook: Heating, Ventilating, and Air-conditioning Applications*. ASHRAE Handbook: Heating Ventilation and Air Conditioning Applications SI, ASHRAE, 2007.

[92] J. E. Braun, "Load control using building thermal mass," *ASME Journal of Solar Engineering*, vol. 125, pp. 292–301, 08/2003 2003.

[93] D. Olsthoorn, F. Haghighat, A. Moreau, and G. Lacroix, "Abilities and limitations of thermal mass activation for thermal comfort, peak shifting and shaving: A review," *Building and Environment*, vol. 118, pp. 113 – 127, 2017.

[94] A. Reilly and O. Kinnane, "The impact of thermal mass on building energy consumption," *Applied Energy*, vol. 198, pp. 108 – 121, 2017.

[95] ASHRAE, *ANSI/ ASHRAE Standard 55-2004, Thermal Comfort Conditions for Human Occupancy*. American Society of Heating, Air-Conditioning, and Refrigeration Engineers, Inc., 2004.

[96] S. Carlucci, L. Pagliano, W. O'Brien, and K. Kapsis, "Comfort considerations in Net ZEBs: theory and design," in *Modeling, Design, and Optimization of Net-Zero Energy Buildings* (A. Athienitis and L. O'Brien, eds.), pp. 75–106, Wilhelm Ernst and Sohn, 2015.

[97] D. Enescu, "A review of thermal comfort models and indicators for indoor environments," *Renewable and Sustainable Energy Reviews*, vol. 79, pp. 1353 – 1379, 2017.

[98] J. van Hoof, M. Mazej, and J. Hensen, "Thermal comfort: Research and practice," vol. 15, pp. 765–88, January 2010.

[99] P. O. Fanger, "Thermal comfort : analysis and applications in environmental engineering," 1972. Originally presented as the author's thesis, Danmarks Tekniske Hjskole, 1970.

[100] K. Parsons, "The effects of gender, acclimation state, the opportunity to adjust clothing and physical disability on requirements for thermal comfort," *Energy and Buildings*, vol. 34, no. 6, pp. 593 – 599, 2002. Special Issue on Thermal Comfort Standards.

[101] M. A. Humphreys and J. F. Nicol, "The validity of iso-pmv for predicting comfort votes in every-day thermal environments," *Energy and Buildings*, vol. 34, no. 6, pp. 667 – 684, 2002. Special Issue on Thermal Comfort Standards.

[102] A. Paula Xavier and R. Lamberts, "Indices of thermal comfort developed from field survey in brazil," vol. 106, January 2000.

[103] D. J. Croome, G. Gan, and H. B. Awbi, "Evaluation of thermal comfort and indoor air quality in offices," *Building Research & Information*, vol. 20, no. 4, pp. 211–225, 1992.

[104] P. W. C. Howell and P. A. Kennedy, "Field validation of the fanger thermal comfort model," *Human Factors*, vol. 21, no. 2, pp. 229–239, 1979.

[105] M. A. Humphreys and M. Hancock, "Do people like to feel neutral?," *Energy and Buildings*, vol. 39, no. 7, pp. 867 – 874, 2007.

[106] J. Han, G. Zhang, Q. Zhang, J. Zhang, J. Liu, L. Tian, C. Zheng, J. Hao, J. Lin, Y. Liu, and D. J. Moschandreas, "Field study on occupants thermal comfort and residential thermal environment in a hot-humid climate of china," *Building and Environment*, vol. 42, no. 12, pp. 4043 – 4050, 2007.

[107] S. H. Hong, J. Gilbertson, T. Oreszczyn, G. Green, and I. Ridley, "A field study of thermal comfort in low-income dwellings in england before and after energy efficient refurbishment," *Building and Environment*, vol. 44, no. 6, pp. 1228 – 1236, 2009.

[108] R. Yao, B. Li, and J. Liu, "A theoretical adaptive model of thermal comfort adaptive predicted mean vote (apmv)," *Building and Environment*, vol. 44, no. 10, pp. 2089 – 2096, 2009.

[109] J. Gao, Y. Wang, and P. Wargocki, "Comparative analysis of modified pmv models and set models to predict human thermal sensation in naturally ventilated buildings," *Building and Environment*, vol. 92, pp. 200 – 208, 2015.

[110] W. Xu, X. Chen, and J. Zhao, "An adaptive predicted mean vote (apmv) model in office," in *2010 International Conference on Mechanic Automation and Control Engineering*, pp. 1887–1891, June 2010.

[111] J. T. Kim, J. H. Lim, S. H. Cho, and G. Y. Yun, "Development of the adaptive pmv model for improving prediction performances," *Energy and Buildings*, vol. 98, pp. 100 – 105, 2015. Renewable Energy Sources and Healthy Buildings.

[112] X. Song, L. Yang, W. Zheng, Y. Ren, and Y. Lin, "Analysis on human adaptive levels in different kinds of indoor thermal environment," *Procedia Engineering*, vol. 121, pp. 151 – 157, 2015. The 9th International Symposium on Heating, Ventilation and Air Conditioning (ISHVAC) joint with the 3rd International Conference on Building Energy and Environment (COBEE), 12-15 July 2015, Tianjin, China.

[113] ISO 7730:2005, *Ergonomics of the thermal environment - Analytical determination and interpretation of heat stress using calculation of the predicted heat strain.* International standard, ISO, 2005.

[114] C. Chun, A. Kwok, and A. Tamura, "Thermal comfort in transitional spacesbasic concepts: literature review and trial measurement," *Building and Environment*, vol. 39, no. 10, pp. 1187 – 1192, 2004.

[115] Q. Kwong, S. Tang, and N. Adam, "Thermal comfort evaluation of the enclosed transitional space in tropical buildings: Subjective response and computational fluid dynamics simulation," *Journal of Applied Sciences*, vol. 9, no. 19, pp. 3480–3490, 2009.

[116] R.-L. Hwang, K.-H. Yang, C.-P. Chen, and S.-T. Wang, "Subjective responses and comfort reception in transitional spaces for guests versus staff," *Building and Environment*, vol. 43, no. 12, pp. 2013 – 2021, 2008.

[117] N. Ghaddar, K. Ghali, and S. Chehaitly, "Assessing thermal comfort of active people in transitional spaces in presence of air movement," *Energy and Buildings*, vol. 43, no. 10, pp. 2832 – 2842, 2011.

[118] Y.-C. Wu and A. Mahdavi, "Assessment of thermal comfort under transitional conditions," *Building and Environment*, vol. 76, pp. 30 – 36, 2014.

[119] A. Pitts, "Thermal comfort in transition spaces," *Buildings*, vol. 3, no. 1, pp. 122–142, 2013.

[120] J. Hensen, "Modelling coupled heat and air flow: Ping-pong vs onions," 1998.

[121] J. Hensen, M. Bartk, and D. Frantisek, "Modeling and simulation of a double-skin facade system," vol. 1, January 2007.

[122] P. Sahlin, "On the effects of decoupling air flow and heat balance in building simulation models," 08 2017.

[123] Z. J. Zhai, M.-H. Johnson, and M. Krarti, "Assessment of natural and hybrid ventilation models in whole-building energy simulations," *Energy and Buildings*, vol. 43, no. 9, pp. 2251 – 2261, 2011.

[124] Z. Zhai, Q. Chen, J. H. Klems, and P. Haves, "Strategies for coupling energy simulation programs and computational fluid dynamics programs," in *Building Sim 2001*, vol. 1, (Rio de Janeiro, Brazil), pp. 59–66, August 2001.

[125] G. C. da Graa, Q. Chen, L. Glicksman, and L. Norford, "Simulation of wind-driven ventilative cooling systems for an apartment building in beijing and shanghai," *Energy and Buildings*, vol. 34, no. 1, pp. 1 – 11, 2002.

[126] L. Wang, Z. Yan, S. Qiao, G. M. Lu, and Y. Huang, "Structural and morphological transformations of mesostructured titanium phosphate through hydrothermal treatment," *Journal of Colloid and Interface Science*, vol. 316, no. 2, pp. 954 – 961, 2007.

[127] F. Muhsin, W. F. M. Yusoff, M. F. Mohamed, and A. R. Sapian, "Cfd modeling of natural ventilation in a void connected to the living units of multi-storey housing for thermal comfort," *Energy and Buildings*, vol. 144, pp. 1 – 16, 2017.

[128] V. Vitale and G. Salerno, "A numerical prediction of the passive cooling effects on thermal comfort for a historical building in rome," *Energy and Buildings*, 2017.

[129] S. Hussain and P. H. Oosthuizen, "Numerical investigations of buoyancy-driven natural ventilation in a simple atrium building and its effect on the thermal comfort conditions," *Applied Thermal Engineering*, vol. 40, pp. 358 – 372, 2012.

[130] H. Boyer, A. Lauret, L. Adelard, and T. Mara, "Building ventilation: a pressure airflow model computer generation and elements of validation," *Energy and Buildings*, vol. 29, no. 3, pp. 283 – 292, 1999.

[131] A. Delsante and T. A. Vik, "Hybrid ventilation - state of the art review," *IEA Energy in Buildings and Community Systems Programme*, 2001. Hybrid ventilation and new and retrofitted office buildings.

[132] M. Kolokotroni and P. Heiselberg, "Ventilative cooling - state of the art review," *IEA Energy in Buildings and Community Systems Programme*, 2015.

[133] B. Chenari, J. D. Carrilho, and M. G. da Silva, "Towards sustainable, energy-efficient and healthy ventilation strategies in buildings: A review," *Renewable and Sustainable Energy Reviews*, vol. 59, pp. 1426 – 1447, 2016.

[134] T. Schulze and U. Eicker, "Controlled natural ventilation for energy efficient buildings," *Energy and Buildings*, vol. 56, pp. 221 – 232, 2013.

[135] P. S. Curtiss, J. F. Kreider, and M. J. Brandemuehl, "Local and global control of commercial building hvac systems using artificial neural networks," in *American Control Conference, 1994*, vol. 3, pp. 3029–3044 vol.3, June 1994.

[136] A. I. Dounis, M. Bruant, M. Santamouris, G. Guarracino, and P. Michel, "Comparison of conventional and fuzzy control of indoor air quality in buildings.," *Journal of Intelligent and Fuzzy Systems*, vol. 4, no. 2, pp. 131–140, 1996.

[137] A. Dounis, M. Bruant, G. Guarracino, P. Michel, and M. Santamouris, "Indoor air-quality control by a fuzzy-reasoning machine in naturally ventilated buildings," *Applied Energy*, vol. 54, no. 1, pp. 11 – 28, 1996.

[138] A. Preglej, J. Rehrl, D. Schwingshackl, I. Steiner, M. Horn, and I. krjanc, "Energy-efficient fuzzy model-based multivariable predictive control of a hvac system," *Energy and Buildings*, vol. 82, pp. 520 – 533, 2014.

[139] L. Marjanovic and M. Eftekhari, "Design and simulation of a fuzzy controller for naturally ventilated buildings," *Building Services Engineering Research and Technology*, vol. 25, no. 1, pp. 33–53, 2004.

[140] H. C. Spindler and L. K. Norford, "Naturally ventilated and mixed-mode buildingspart i: Thermal modeling," *Building and Environment*, vol. 44, no. 4, pp. 736 – 749, 2009.

[141] H. C. Spindler and L. K. Norford, "Naturally ventilated and mixed-mode buildingspart ii: Optimal control," *Building and Environment*, vol. 44, no. 4, pp. 750 – 761, 2009.

[142] A. Mahdavi and C. Prglhf, "A model-based approach to natural ventilation," *Building and Environment*, vol. 43, no. 4, pp. 620 – 627, 2008.

[143] X. Li and J. Wen, "Review of building energy modeling for control and operation," *Renewable and Sustainable Energy Reviews*, vol. 37, pp. 517 – 537, 2014.

[144] A. Afram and F. Janabi-Sharifi, "Theory and applications of hvac control systems a review of model predictive control (mpc)," *Building and Environment*, vol. 72, pp. 343 – 355, 2014.

[145] M. Avci, M. Erkoc, A. Rahmani, and S. Asfour, "Model predictive hvac load control in buildings using real-time electricity pricing," *Energy and Buildings*, vol. 60, pp. 199 – 209, 2013.

[146] F. Oldewurtel, A. Parisio, C. N. Jones, D. Gyalistras, M. Gwerder, V. Stauch, B. Lehmann, and M. Morari, "Use of model predictive control and weather forecasts for energy efficient building climate control," *Energy and Buildings*, vol. 45, pp. 15 – 27, 2012.

[147] P. May-Ostendorp, G. P. Henze, C. D. Corbin, B. Rajagopalan, and C. Felsmann, "Model-predictive control of mixed-mode buildings with rule extraction," *Building and Environment*, vol. 46, no. 2, pp. 428 – 437, 2011.

[148] S. Prvara, J. Cigler, Z. Va, F. Oldewurtel, C. Sagerschnig, and E. ekov, "Building modeling as a crucial part for building predictive control," *Energy and Buildings*, vol. 56, pp. 8 – 22, 2013.

[149] J. Hu and P. Karava, "Model predictive control strategies for buildings with mixed-mode cooling," *Building and Environment*, vol. 71, pp. 233 – 244, 2014.

[150] J. Hu and P. Karava, "A state-space modeling approach and multi-level optimization algorithm for predictive control of multi-zone buildings with mixed-mode cooling," *Building and Environment*, vol. 80, pp. 259 – 273, 2014.

[151] M. Kolokotroni and A. Aronis, "Cooling-energy reduction in air-conditioned offices by using night ventilation," *Applied Energy*, vol. 63, no. 4, pp. 241 – 253, 1999.

[152] J. Pfafferott, S. Herkel, and M. Jschke, "Design of passive cooling by night ventilation: evaluation of a parametric model and building simulation with measurements," *Energy and Buildings*, vol. 35, no. 11, pp. 1129 – 1143, 2003.

[153] N. Artmann, H. Manz, and P. Heiselberg, "Parameter study on performance of building cooling by night-time ventilation," *Renewable Energy*, vol. 33, no. 12, pp. 2589 – 2598, 2008.

[154] P. Prajongsan and S. Sharples, "Enhancing natural ventilation, thermal comfort and energy savings in high-rise residential buildings in bangkok through the use of ventilation shafts," *Building and Environment*, vol. 50, pp. 104 – 113, 2012.

[155] P. Karava, A. Athienitis, T. Stathopoulos, and E. Mouriki, "Experimental study of the thermal performance of a large institutional building with mixed-mode cooling and hybrid ventilation," *Building and Environment*, vol. 57, pp. 313 – 326, 2012.

[156] A. Tzempelikos, A. K. Athienitis, and P. Karava, "Simulation of faade and envelope design options for a new institutional building," *Solar Energy*, vol. 81, no. 9, pp. 1088 – 1103, 2007.

[157] S. Yuan, A. Athienitis, Y. Chen, J. Rao, and C. Vallianos, "An experimental and simulation study of night cooling in a building with hybrid ventilation," in *Proceedings of CLIMA 2016 - 12th REHVA World Congress*, vol. 5, Aalborg, Denmark, May 2016.

[158] C. Vallianos, S. Yuan, A. Athienitis, and J. Rao, "Experimental and simulation study to improve operation of a hybrid ventilation system in an institutional building," in *Proceedings of 15th International Conference of IBPSA*, Aug. 2017.

[159] J. Cheng, D. Qi, L. Wang, and A. Athienitis, "Whole-building simulation of hybrid ventilation based on full-scale measurements in an institutional high-rise building for predictive control," in *Proceedings of 15th International Conference of IBPSA*, Aug. 2017.

[160] F. Sakellariou, "Model Predictive Control for Thermally Activated Building Systems," Master's thesis, Eindhoven University of Technology, the Netherlands, 2011.

APPENDIX A

SENSORS INFORMATION

Table A.1 shows details for the various sensors used in the experiments.

Table A.1: Details of various sensors

Type of sensor	name	Accuracy
Anemometer (one-directional)	SENSOR HT-415	± 0.03 m/s
Thermocouples	type T	± 1°C
Infrared sensors	OMEGA OS151-LT	± 1°C
Temperature (weather station)	Vaisala HMT337	± 0.4°C
Temperature (weather station)	Vaisala HMP155	± 0.4°C
Pyranometer	Kipp and Zonen SMP11-A-L	± 1%

APPENDIX B

SOLAR RADIATION CALCULATIONS

The weather station provides information about the total horizontal solar radiation, but not about which part is direct, diffused or reflected. Since no other information is available, using the total horizontal radiation the one incident on the façade of the corridor is estimated and is considered to be the total.

At first the solar time is calculated based on equation (B.1). AST (min) is the apparent solar time, LST (min) is the local standard time, ET (deg) is the equation of time, given by equation (B.2), LSM (deg)is the local standard meridian and LON is the longitude. For Montreal LSM = 75° and LON = 74°. In equation (B.2) n is the day of the year (1–365).

$$AST = LST + ET + 4(LSM - LON) \tag{B.1}$$

$$ET(n) = 9.87sin\left(4\pi\frac{n-81}{364}\right) - 7.53cos\left(2\pi\frac{n-81}{364}\right) - 1.5sin\left(2\pi\frac{n-81}{364}\right) \tag{B.2}$$

The solar declination angle δ (deg) is calculated with equation (B.3).

$$\delta = 23.45sin\left(360\frac{284+n}{365}\right) \tag{B.3}$$

The hour angle h (deg) in equation (B.4) expresses the number of minutes away from the

local solar noon.

$$h = 0.25(AST - 1440) \tag{B.4}$$

The solar altitude α (deg) is the angle between the sun rays and the horizontal, as shown in equation (B.5).

$$\alpha = asin\big(cos(L)cos(\delta)cos(h) + sin(L)sin(\delta)\big) \tag{B.5}$$

The solar azimuth φ (deg) is the angle between the horizontal projection of the sun rays and due south. It is given by equation (B.6) and it is positive in the afternoon.

$$\phi = acos\left(\frac{sin(\alpha)sin(L) - sin(\delta)}{cos(\alpha)cos(L)}\right)\frac{h}{|h|} \tag{B.6}$$

Equation (B.7) calculates the surface solar azimuth γ (deg), which is the angle between the horizontal projection of the sun rays and the normal of the surface on the horizontal plane. ψ (deg) is the angle between the projection of the normal to the surface on a horizontal plane and due south. It is negative to the east. In this case ψ = -55° because the façade of the corridor faces 55° east of south.

$$\gamma = \phi - \psi \tag{B.7}$$

The angle of incidence ϑ (deg) is the angle between the solar rays and a line normal to the surface and is calculated by equation (B.8). β (deg) is the tilt angle (slope) of the surface and the horizontal.

$$\theta = acos\big(cos(\alpha)cos(|\gamma|)sin(\beta) + sin(\alpha)cos(\beta)\big) \tag{B.8}$$

Finally the solar radiation incident on the surface S_{sur} results from equation (B.9). The total horizontal radiation measured at the weather station and the estimated on the façade of the corridor are shown in figure B.1.

$$S_{sur} = S_{hor}\frac{cos(\theta)}{sin(\alpha)} \tag{B.9}$$

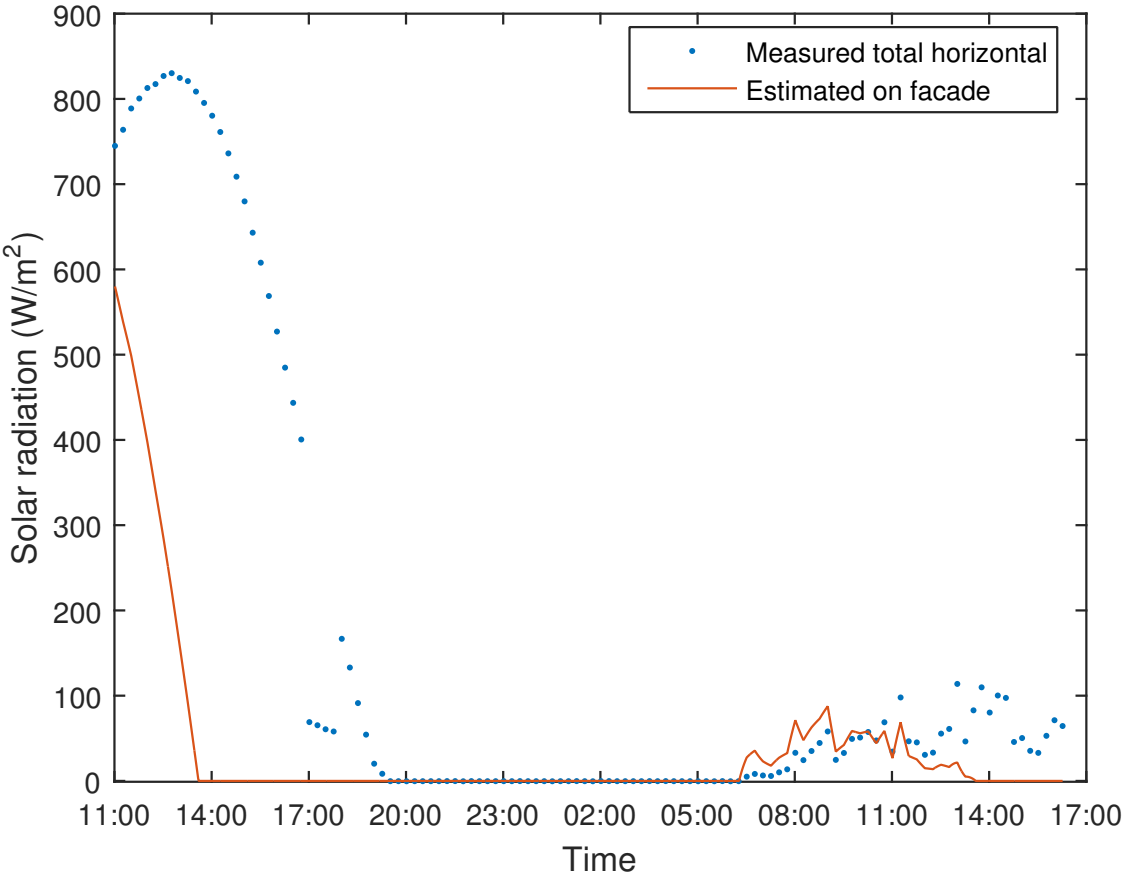

Figure B.1: Measured total horizontal solar radiation and estimated solar radiation incident on the façade of the corridor

APPENDIX C

HUMIDITY CONTENT EQUATIONS

From the weather station the dry-bulb temperature T_{db} and the relative humidity φ are available. From ASHRAE Fundamentals [52] the saturation pressure p_{ws} is given by Equation (C.1).

$$ln(p_{ws}) = \frac{C_1}{T_{db}} + C_2 + C_3 T_{db} + C_4 T_{db}^2 + C_5 T_{db}^3 + C_6 ln(T_{db}) \tag{C.1}$$

where

$C_1 = -5.800220 \cdot 10^6$;

$C_2 = 1.3914993$;

$C_3 = -4.8680239 \cdot 10^{-2}$;

$C_4 = 4.1764768 \cdot 10^{-5}$;

$C_5 = -1.4452093 \cdot 10^{-8}$;

$C_6 = 6.5459673$

Then the partial pressure of water vapor p_v can be estimated from Equation (C.2), using the saturation pressure p_{ws} and the relative humidity φ.

$$p_v = \phi p_{ws} \tag{C.2}$$

Assuming that the air is at atmospheric pressure, the humidity content W is given by Equation (C.3).

$$W = 0.621945 \frac{p_{ws}}{101325 - p_{ws}} \tag{C.3}$$

APPENDIX D

CORRELATIONS

The temperature of the inlet air and effective surface temperature were correlated to other variables, so that their constant monitoring would not be required. This procedure is the same as in [158] using only the data from the 2015 experiment. However, when they were used to predict the temperatures of the 2017 experiment the error was high, underestimating the temperature greatly. This happens because the data used were not robust enough and as a result the correlations had high accuracy for the specific weather conditions, but low accuracy otherwise. For this reason the correlations were reviewed, taking into account the measurements of the 2017 experiment as well. Because these measurements differ significantly from the previous ones, they cover adequately the various weather conditions and further recalibration should not be necessary.

D.1 Air inlet temperature

The air inlet temperature was correlated to the temperature of the weather station (T_{ws}), the time after the dampers open (t) and the solar radiation (S). The exact relation is equation (D.1).

$$T_{inlet} = \alpha T_{ws} + \beta(T_{ws} - 21)t^{\gamma} + \delta S + \epsilon \tag{D.1}$$

The method used was nonlinear regression using MATLAB function fitnlm to fit param-

eters α-ε to the experimental data. Table D.1 shows the parameters with the respective intervals for confidence level of 95%. The Root Mean Squared Error is 0.532 °C. Coefficient of determination (R^2) is 0.986 indicating that the model is fitting the data reasonably well.

Table D.1: Goodness of fit of inlet air temperature to the temperature of the weather station

Parameter	Value	Interval for 95%
α	1.0515	± 0.0216
β	-0.42222	± 0.04681
γ	-0.49935	± 0.10082
δ	0.0088051	± 0.0002861
ε	2.1573	± 0.4155

D.2 Temperature of effective surfaces

Equation (D.2) shows the correlation of the temperature of the combined surfaces for open dampers. The independent variables used were the concrete surface temperature (T_c), the inlet air temperature (T_{inlet}), the time the dampers have been in the same state (t) and the solar radiation (S). Equation (D.3) shows the one for closed dampers. In this case the inlet air temperature and the solar radiation are not taken into account. It is expected that the solar radiation will affect the first one or two control volumes even when the dampers are closed, but the data come from a rainy day, when the solar radiation was low and the relation cannot be determined.

$$T_{sfc} = \alpha T_c + \beta(T_{inlet} - 21)t^{\gamma} + \delta T_{inlet} + \epsilon S + \zeta \tag{D.2}$$

$$T_{sfc} = \alpha T_c + \beta t^{\gamma} + \delta \tag{D.3}$$

Table D.2 and table D.3 show details for the fits. The RMSEs are between 0.1°C and 0.39°C, with the lowest R^2 being 0.87. It is obvious that the correlations are the least accurate at the last control volume.

Table D.2: Goodness of fit of effective surface temperature when the dampers are closed

CV	RMSE (°C)	R^2	Parameter	Value	Interval for 95%
1	0.157	0.995	α	1.5873	± 0.0109
			β	-9.7852	± 0.4219
			γ	-0.12699	± 0.01098
			δ	-4.5375	± 0.5877
2	0.235	0.983	α	1.0394	± 0.0139
			β	-5.3547	± 0.1887
			γ	-0.25262	± 0.02411
			δ	1.7709	± 0.4221
3	0.203	0.98	α	1.1986	± 0.0166
			β	-2.9826	± 0.1609
			γ	-0.42101	± 0.04213
			δ	-2.3055	± 0.3928
4	0.346	0.871	α	1.1173	± 0.0332
			β	-0.92543	± 0.32423
			γ	-1.7192	± 0.8020
			δ	-1.6454	± 0.6966

Table D.3: Goodness of fit of effective surface temperature when the dampers are open

CV	RMSE (°C)	R^2	Parameter	Value	Interval for 95%
1	0.146	0.998	α	0.50437	± 0.03114
			β	-0.88972	± 0.02516
			γ	-0.34084	± 0.02782
			δ	0.74056	± 0.03781
			ε	0.0021350	± 0.0001680
			ζ	-5.3440	± 0.6595
2	0.119	0.998	α	0.39840	±0.02641
			β	-1.0126	± 0.02533
			γ	-0.27081	± 0.01994
			δ	0.74417	± 0.04138
			ε	0.0019857	± 0.0001041
			ζ	-2.8708	± 0.4867
3	0.253	0.99	α	1.0288	± 0.1133
			β	-0.71695	± 0.09210
			γ	-0.25972	± 0.06665
			δ	0.44497	± 0.11861
			ε	0.0015529	± 0.0001445
			ζ	-9.2830	± 1.0837
4	0.382	0.943	α	-0.44530	± 0.1873
			β	-1.0526	± 0.2338
			γ	-0.20456	± 0.07831
			δ	0.86317	± 0.26593
			ε	-0.00071163	± 0.00024258
			ζ	13.178	± 2.830

APPENDIX E

PREDICTED TEMPERATURES WITH CONFIDENCE INTERVALS

To compute the confidence intervals of the coefficients of fits MATLAB command `nlparci` was used and to compute the confidence interval of predicted values `nlpredci` was used. Equation (E.1) explains how `nlparci` computes the interval for the coefficients and Equation (E.2) how `nlpredci` computes the interval for the predictions.

$$C = b \pm t\sqrt{S} = b \pm t\sqrt{(X^T X)^{-1} s^2} \tag{E.1}$$

where

C are the coefficient bounds;

b is the value of the coefficient by the fit;

t is the the Student's t cumulative distribution function and it depends on the confidence level;

S is a vector of the diagonal elements from the estimated covariance matrix of the coefficient estimates, equal to $(X^T X)^{-1} s^2$, where for a non-linear fit X is the Jacobian of the fitted values with respect to the coefficients and s^2 is the mean squared error.

$$CI = y \pm t\sqrt{s^2 + xSx^T} \tag{E.2}$$

where

CI are the coefficient bounds;

y is the value of the prediction;

t is the the Student's t cumulative distribution function and it depends on the confidence level;

s^2 is the mean squared error;

S is a vector of the diagonal elements from the estimated covariance matrix of the coefficient estimates, equal to $(X^T X)^{-1} s^2$, where for a non-linear fit X is the Jacobian of the fitted values with respect to the coefficients and s^2 is the mean squared error;

x is a row vector of the design matrix or Jacobian evaluated at a specified predictor value.

Figures E.1 to E.4 show the average air and concrete surface temperature for each control volume for the two experiments, for open dampers. Figures E.5 to E.8 show the confidence interval for average air and concrete surface temperatures for the two experiments for open dampers. The model predicts the temperatures well for all situations and control volumes, except for the concrete surface temperature of the first two control volumes for the 2015 experiment. It underpredicts the temperature and the points are just outside the confidence interval. The concrete surface temperatures are predicted accurately for the third and fourth control volume.

Figures E.9 to E.12 show the average air and concrete surface temperature for each control volume for the two experiments, for closed dampers. Figures E.13 to E.15 and **??** show the confidence interval for average air and concrete surface temperatures for the two experiments for closed dampers. The model predicts the temperatures well for most of the situations and control volumes. It overpredicts the concrete surface temperature of the first control volume for the 2015 data and the points are just outside the confidence interval. The concrete surface

temperatures are predicted accurately for the second, third and fourth control volume. It also underpredicts the air temperature of the first and third control volume and the concrete surface temperature of the fourth control volume for the 2015 data. In general, even when the data are in the confidence interval, they are slightly underpredicted by the model.

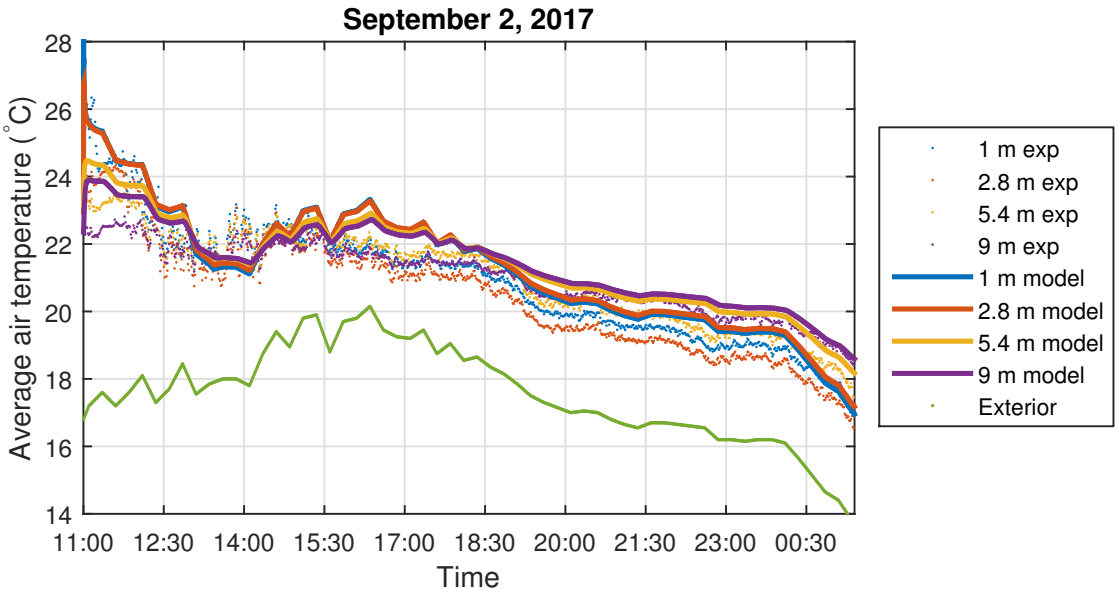

Figure E.1: Experimental and predicted average air temperature for open dampers for the experiment of September 2nd, 2017

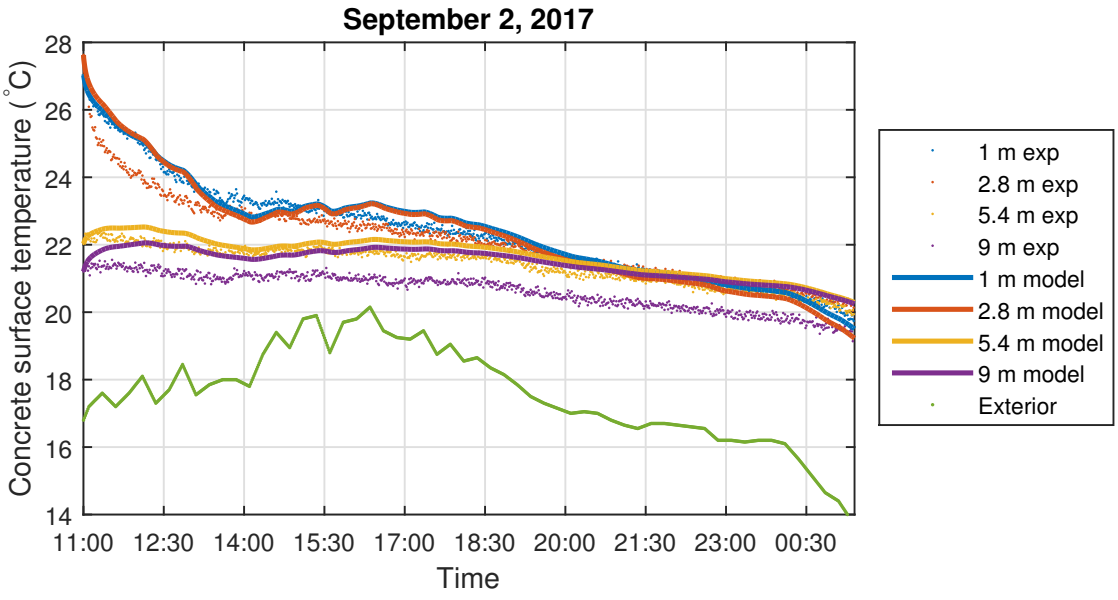

Figure E.2: Experimental and predicted concrete surface temperature for open dampers for the experiment of September 2nd, 2017

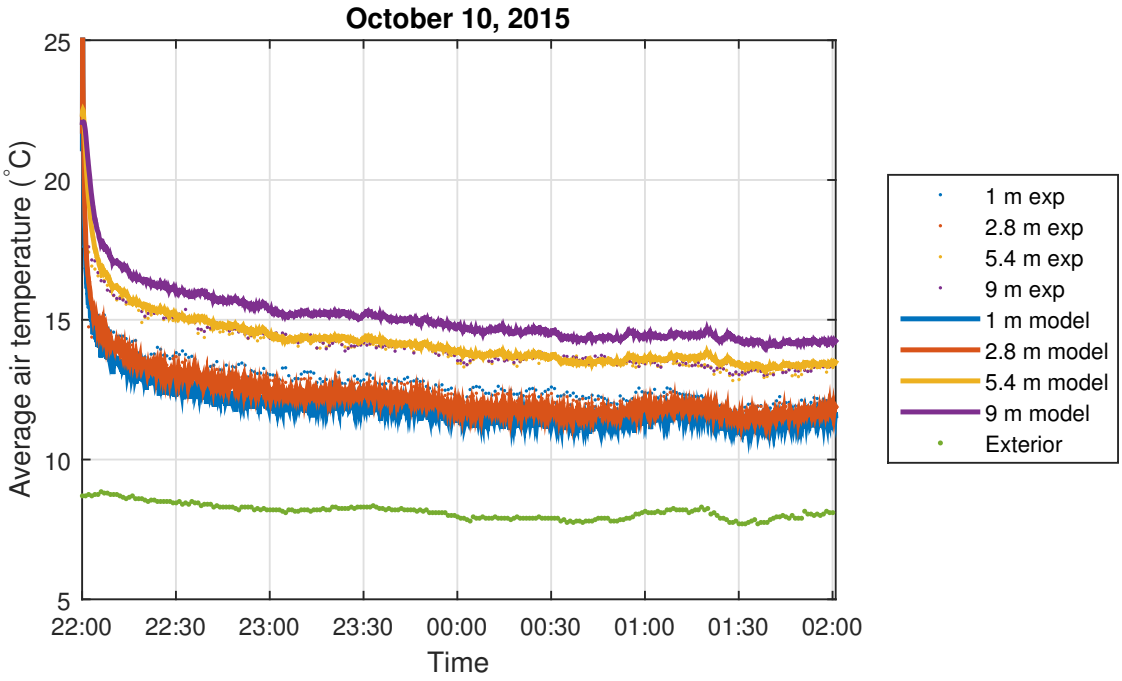

Figure E.3: Experimental and predicted average air temperature for open dampers for the experiment of October 10th, 2015

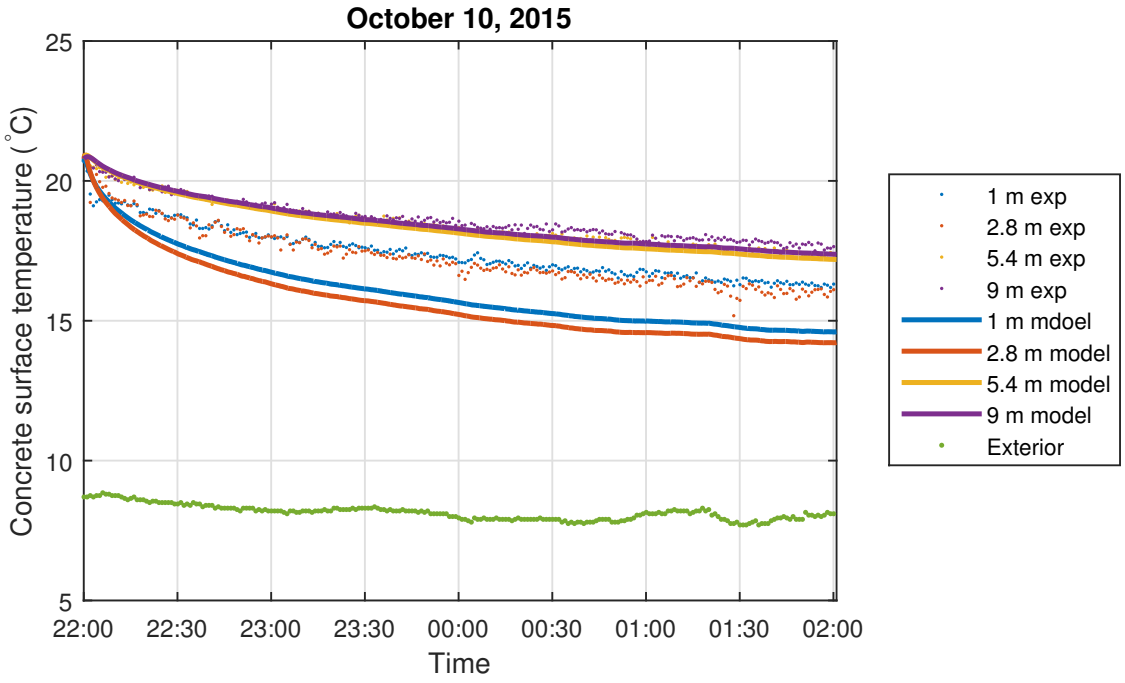

Figure E.4: Experimental and predicted concrete surface temperature for open dampers for the experiment of October 10^{th}, 2015

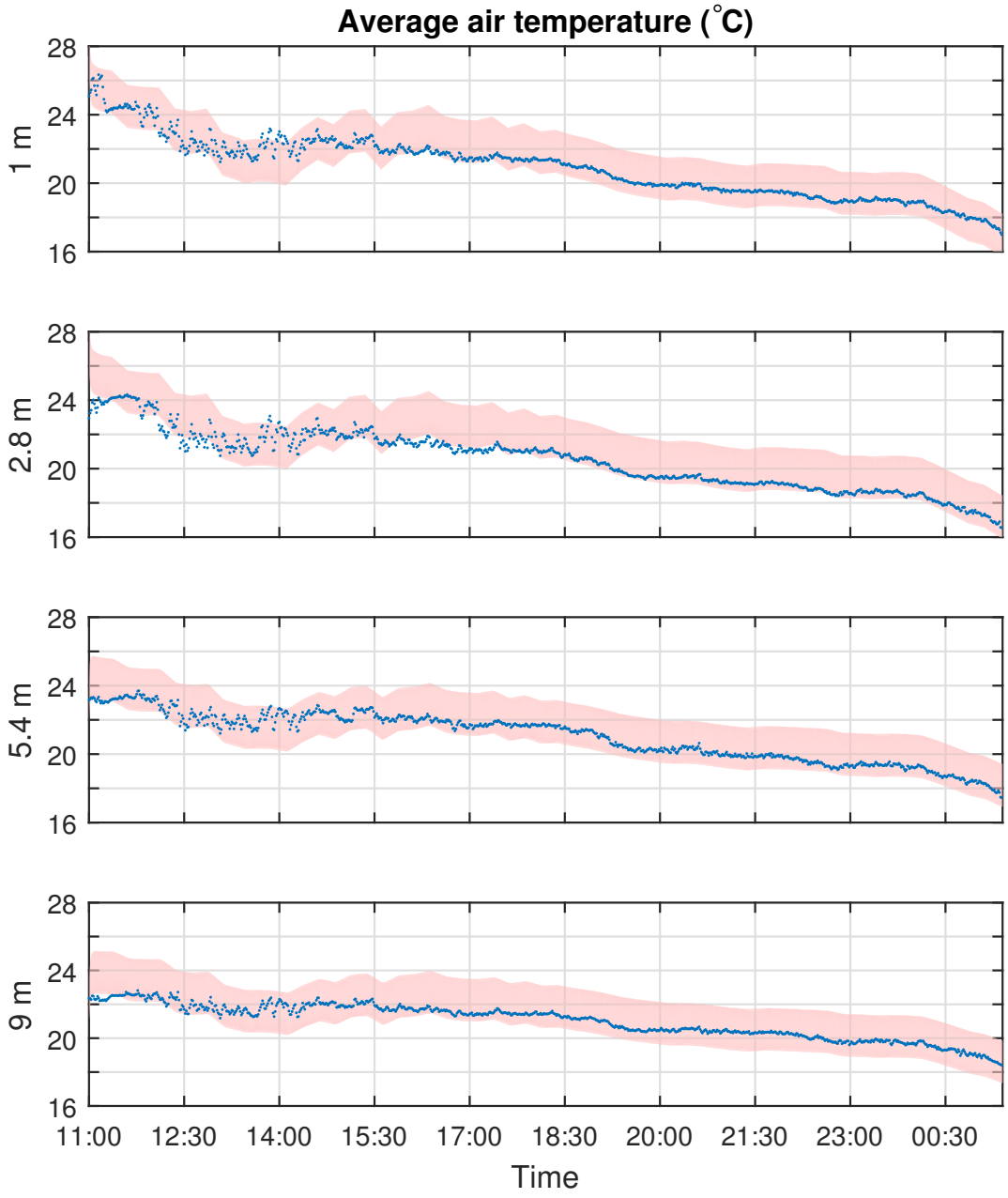

Figure E.5: 95% confidence interval for average air temperature when dampers are open for the 2017 experiment. Blue points are the measured values and the transparent red band is the confidence interval

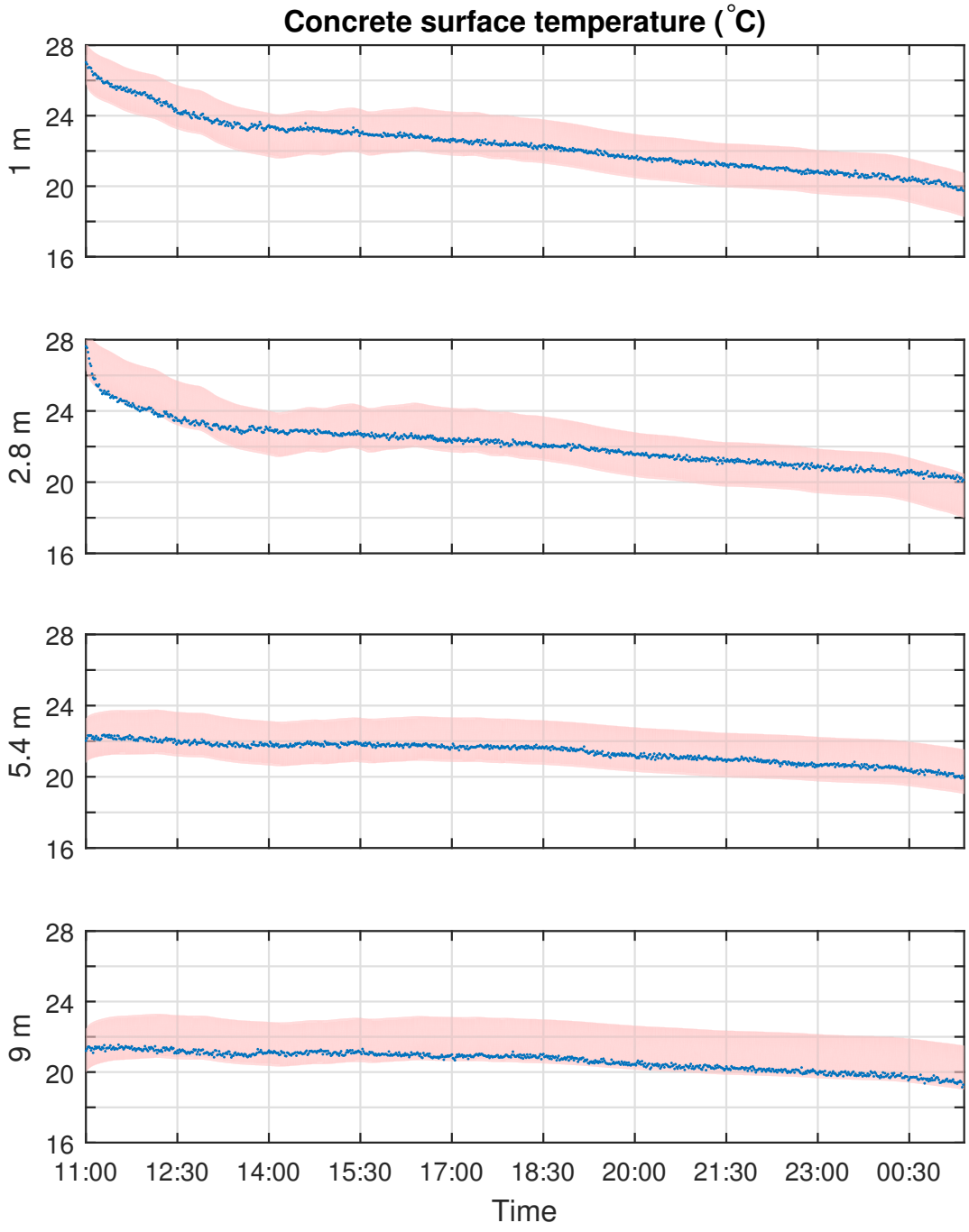

Figure E.6: 95% confidence interval for concrete surface temperature when dampers are open for the 2017 experiment. Blue points are the measured values and the transparent red band is the confidence interval

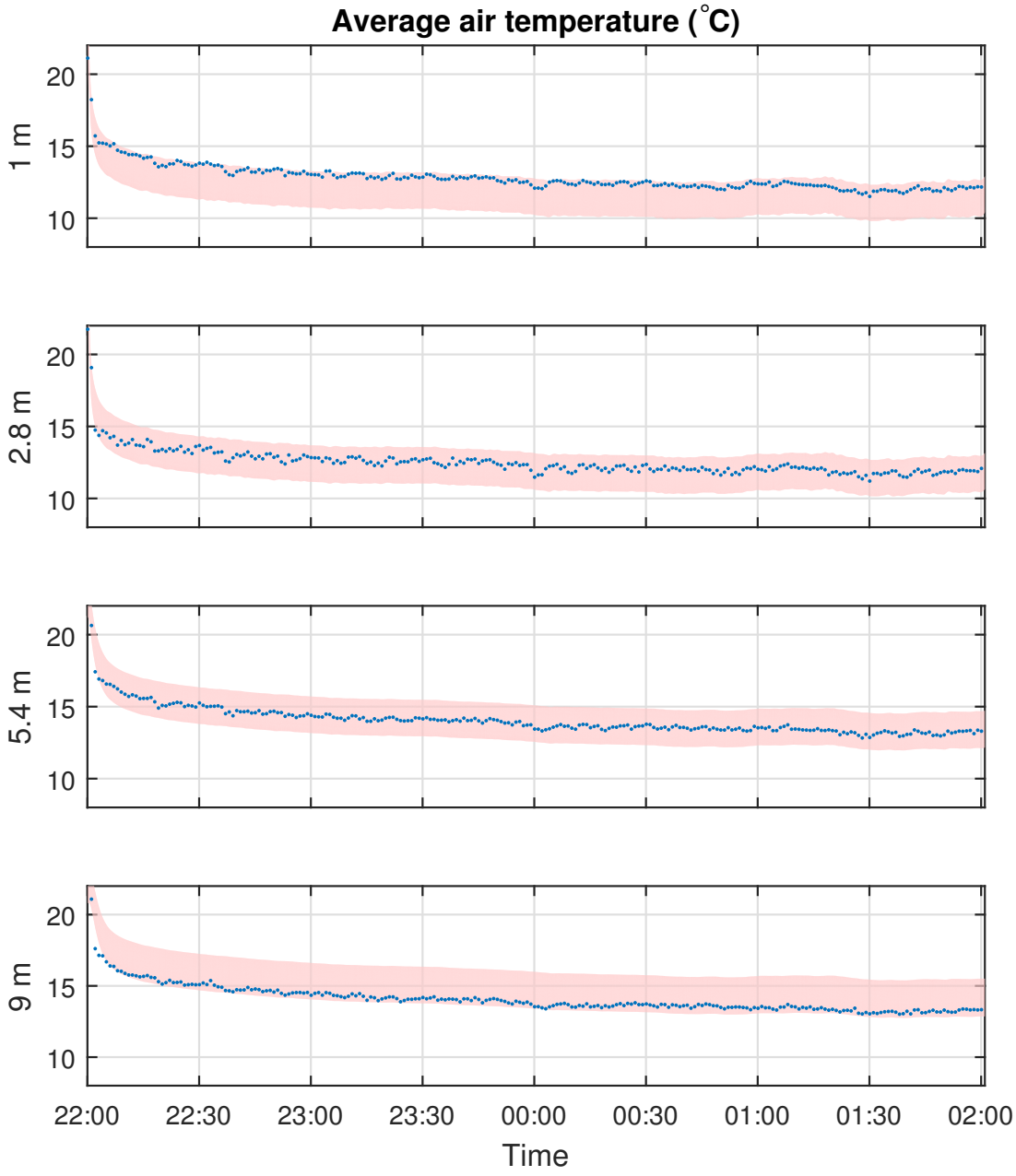

Figure E.7: 95% confidence interval for average air temperature when dampers are open for the 2015 experiment. Blue points are the measured values and the transparent red band is the confidence interval

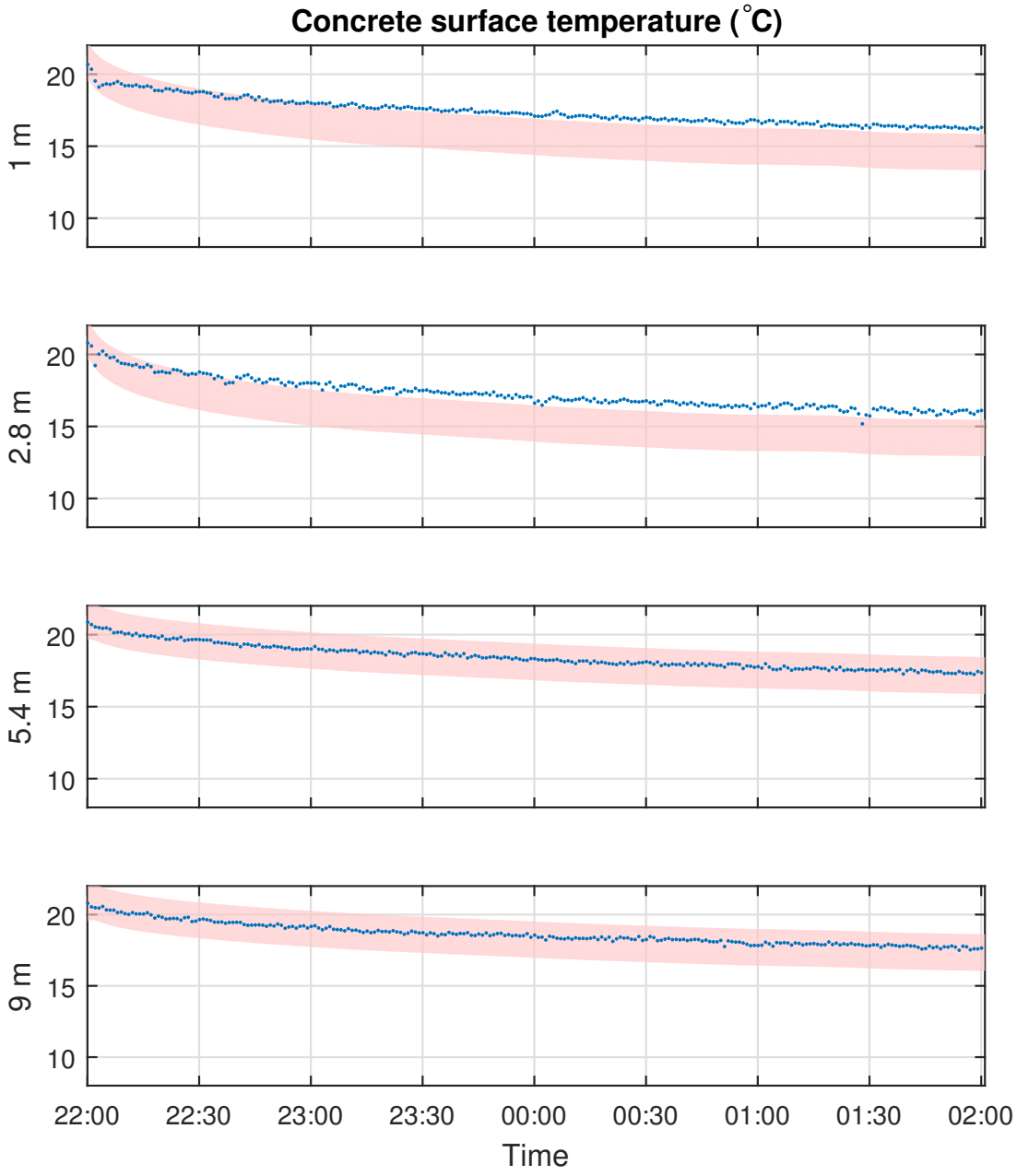

Figure E.8: 95% confidence interval for concrete surface temperature when dampers are open for the 2015 experiment. Blue points are the measured values and the transparent red band is the confidence interval

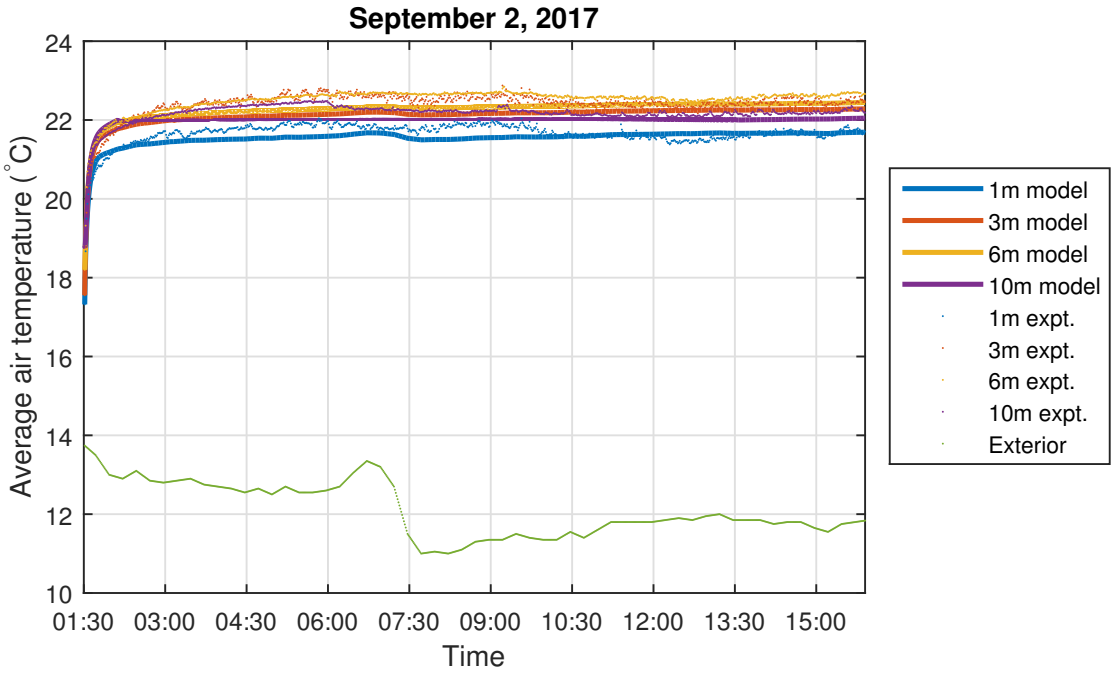

Figure E.9: Experimental and predicted average air temperature for closed dampers for the experiment of September 2nd, 2017

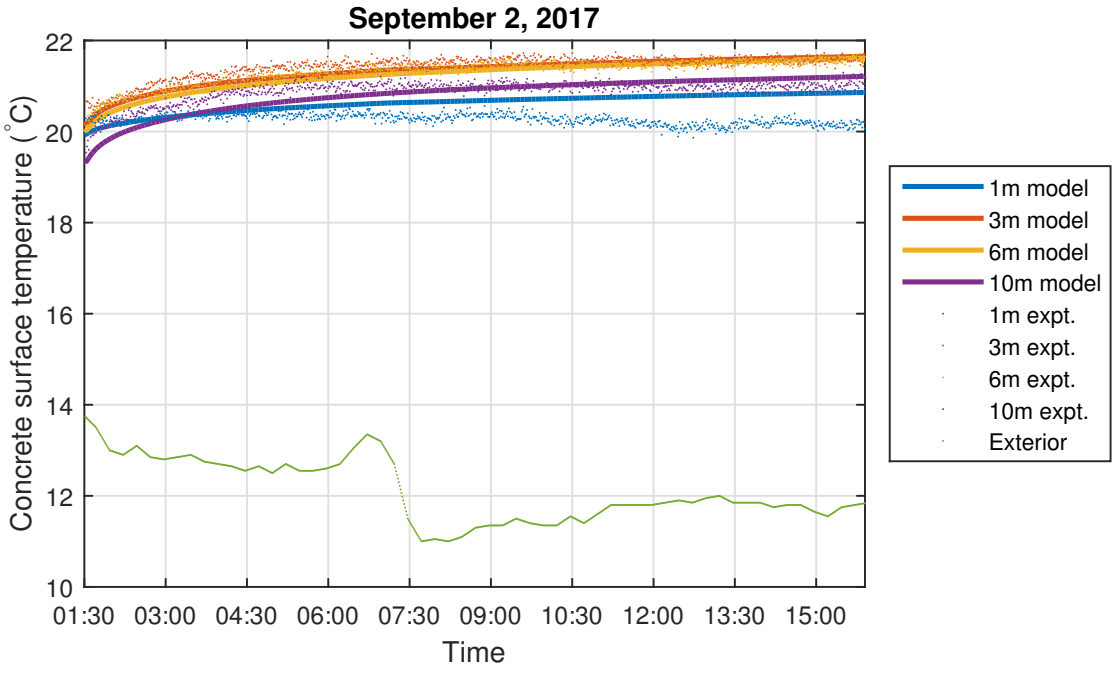

Figure E.10: Experimental and predicted concrete surface temperature for closed dampers for the experiment of September 2nd, 2017

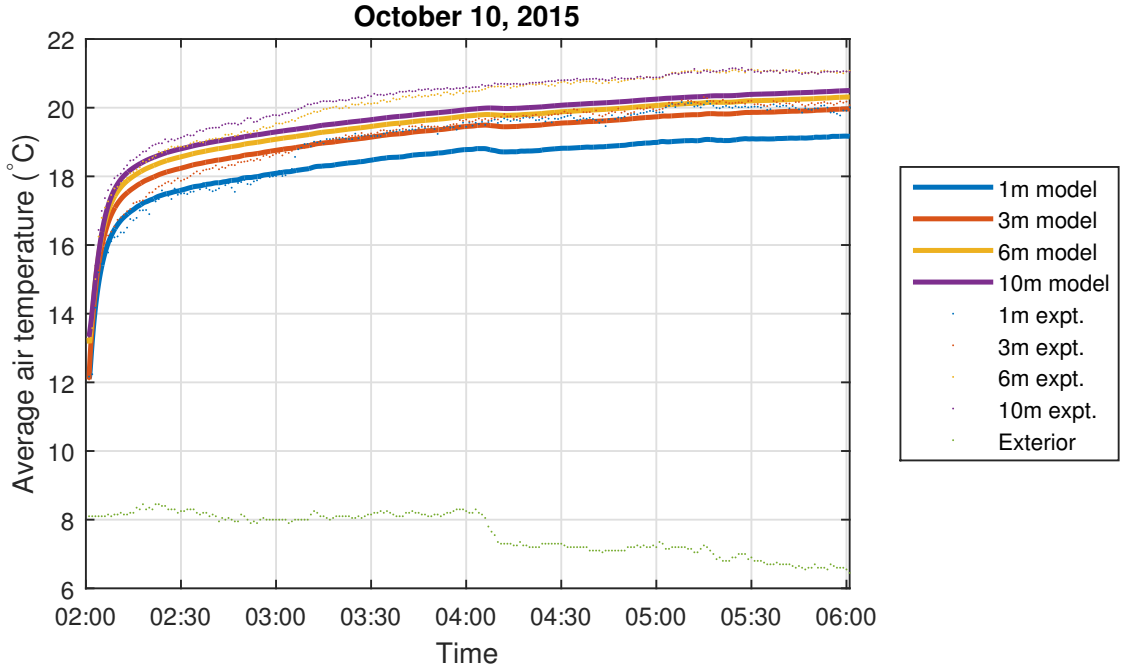

Figure E.11: Experimental and predicted average air temperature for closed dampers for the experiment of October 10$^{\text{th}}$, 2015

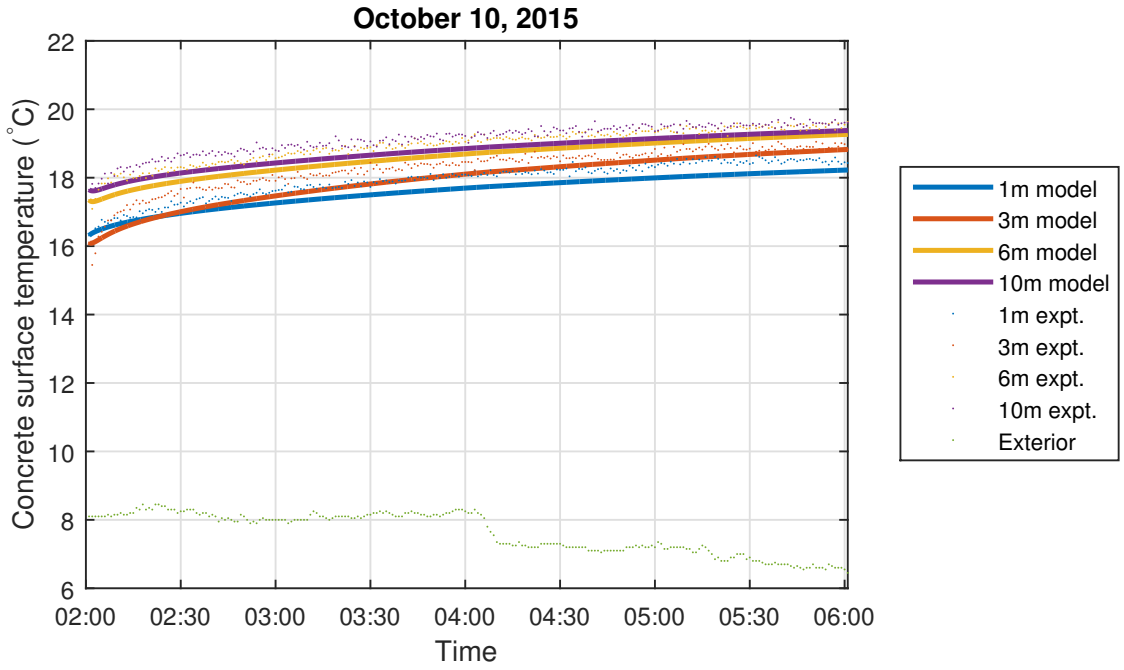

Figure E.12: Experimental and predicted concrete surface temperature for closed dampers for the experiment of October 10$^{\text{th}}$, 2015

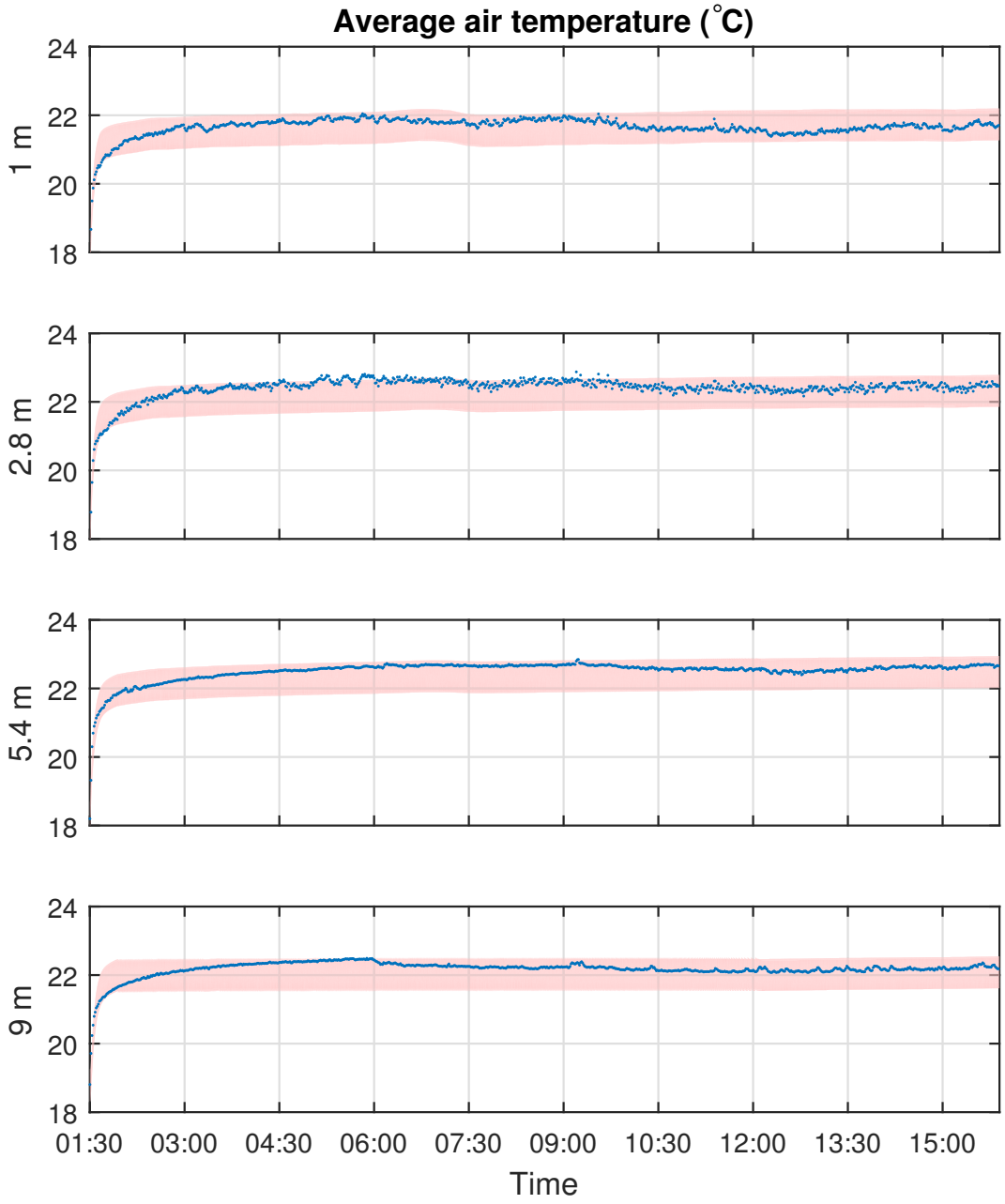

Figure E.13: 95% confidence interval for average air temperature when dampers are closed for the 2017 experiment. Blue points are the measured values and the transparent red band is the confidence interval

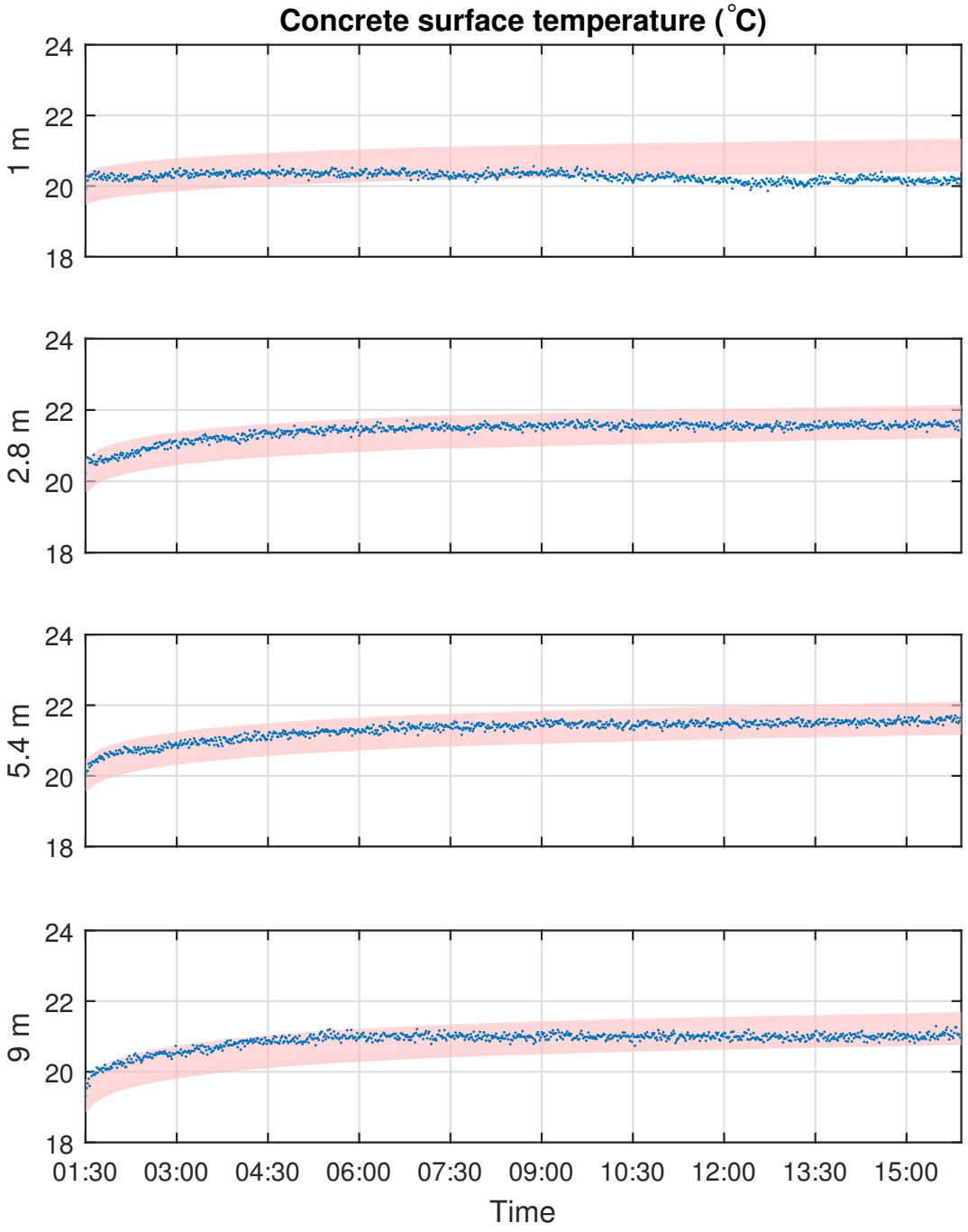

Figure E.14: 95% confidence interval for concrete surface temperature when dampers are closed for the 2017 experiment. Blue points are the measured values and the transparent red band is the confidence interval

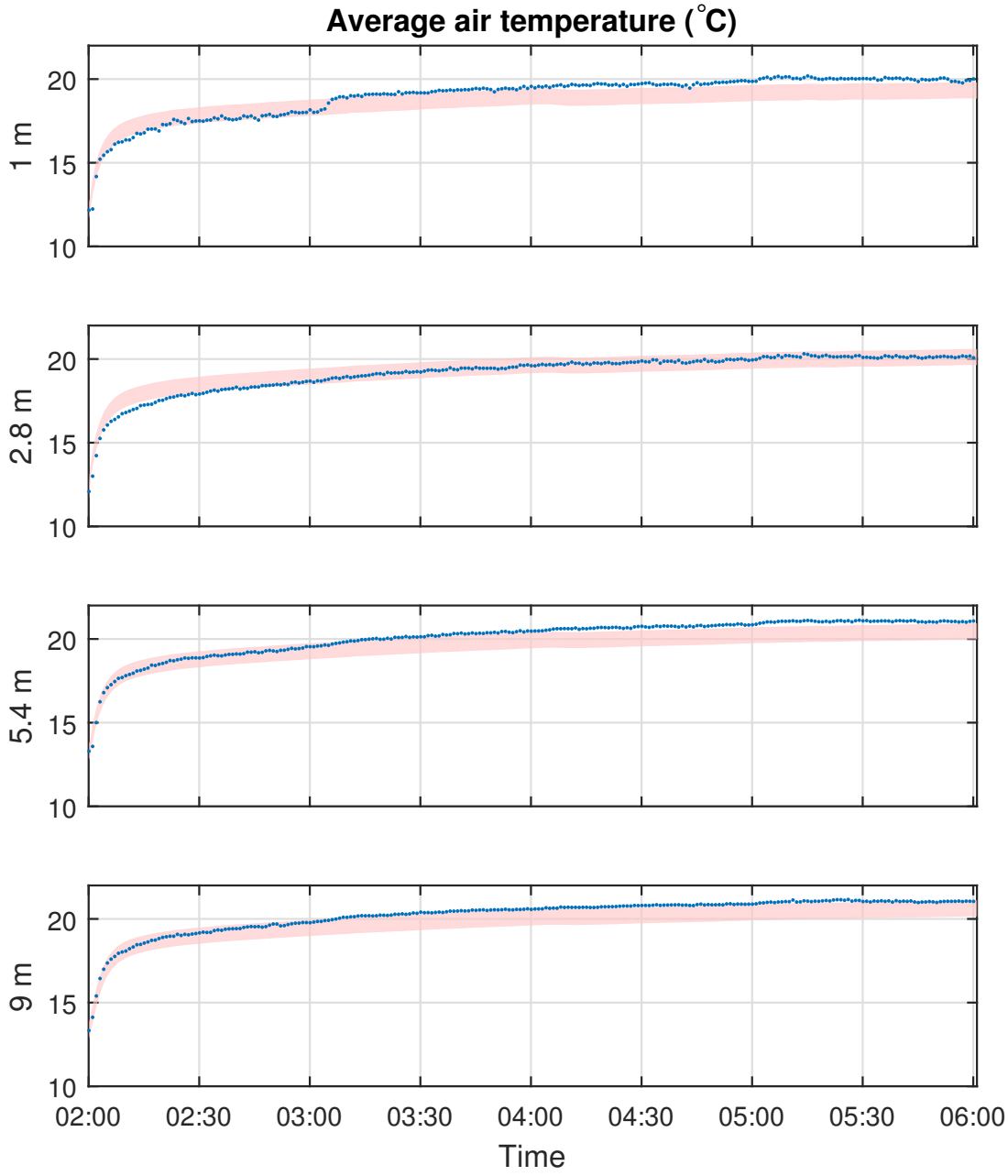

Figure E.15: 95% confidence interval for average air temperature when dampers are closed for the 2015 experiment. Blue points are the measured values and the transparent red band is the confidence interval

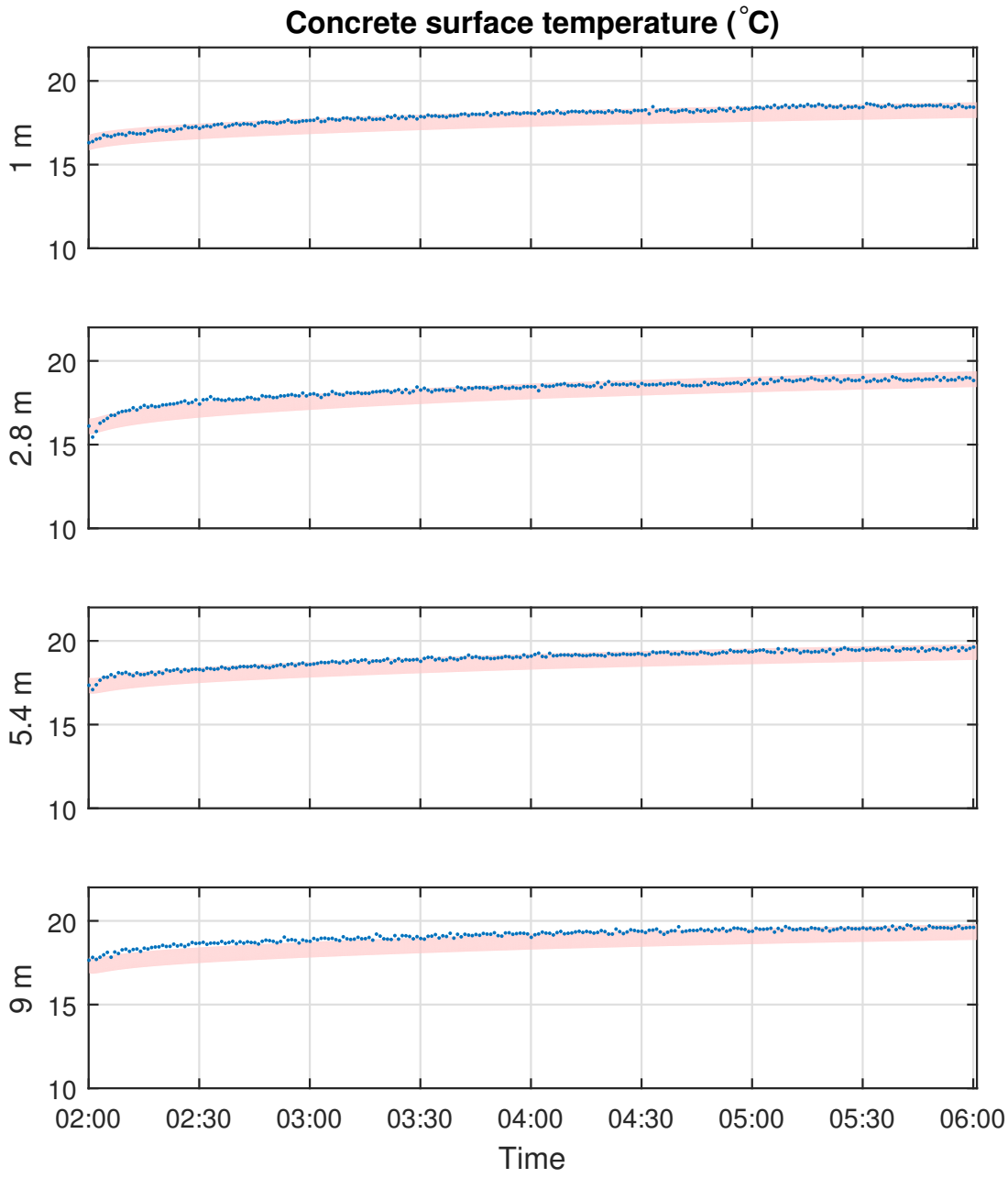

Figure E.16: 95% confidence interval for concrete surface temperature when dampers are closed for the 2015 experiment. Blue points are the measured values and the transparent red band is the confidence interval